2011

Fully integrated microsystem for bacterial genotyping

Hui-Wen Chen
Louisiana State University and Agricultural and Mechanical College

FULLY INTEGRATED MICROSYSTEM FOR BACTERIAL GENOTYPING

A Dissertation

Submitted to the Graduate Faculty of the
Louisiana State University and
Agricultural and Mechanical College
in partial fulfillment of the
requirements for the Degree of
Doctor of Philosophy

in

The Department of Chemistry

by
Hui-Wen Chen
B.S. Chung Yuan Christian University, 1998
M.S. National of Chung-Hsing University, 2000
December 2011

ACKNOWLEDGEMENTS

First and all, I would like to express my gratitude towards my advisor, Prof. Steven A. Soper for his constant patience, expertise and encouragement, and also for his invaluable advice, guidance and support throughout the course of my graduate studies at LSU. You are an inspiration to many and a mentor whom I can always count on. I wish also to thank Prof. Patrick K. Bollich, Prof. Bill Crowe, Prof. Randall W. Hall and Prof. Kermit K. Murray for their interest in my research and for taking time to serve in my dissertation committee.

I am thankful to Dr. Wieslaw Stryjewski and Donald Patterson for software and hardware, Dr. Proyag Datta and Jason Guy for hot-embossing and micromachining as well as Dr. Mateusz Hupert and Hong Wang for microfluidic design and technical support. I reserve my special thanks to Prof. Diana L. Willams and Tana Pittman from School Veterinary Medicine for Mtb sample culture. I would like extend my thanks to Drs. Subramanian Balamurugan, Malgorzata Witek and Irina Nesterova for their suggestions in completing my research and dissertation. I would also like to thank the former and current Soper group members, including Andre, Annie, Catherine, Jason, John, Paul, Sinville, Wonbae, Brandon, Brandy, Jerry, Joyce, Franklin, Katrina, Kumuditha, Michael, Nyote, Pratap, Samuel, Sudha, Swathi and Udara, for the moments we shared as colleagues and friends. Thank you all for your unselfish and timely help.

Last but not least, I am grateful for my families for their understanding and encouragement, and also for standing behind me throughout every challenge during my Ph.D. program. I am greatly thankful to my husband, Cheng-Kun Hsu, for standing by me through the hard times and encouraging me pursuing a Ph.D. degree abroad, too.

TABLE OF CONTENTS

LIST OF TABLES

LIST OF FIGURES

LIST OF SCHEMES

ABBREVIATIONS AND ACRONYMS

AOM	- aluminum oxide membranes
BPU	- biochemical processing unit
BSA	- bovine serum albumin
CAE	- capillary array electrophoresis
CA-MRSA	- community-acquired MRSA
CF LDR	- continuous flow ligase detection reaction
cfu	- colony forming units
CNS	- coagulase-negative *Staphylococci*
COC	- cyclic olefin copolymer
CTCs	- circulating tumor cells
ddNTPs	- dideoxynucleotide triphosphates
dNTPs	- deoxynucleotide triphosphates
DMD	- Duchenne Muscular Dystrophy
DNA	- deoxyribonucleotide acid
DRIE	- deep reactive ion etching
DST	- drug susceptibility testing
EDC	- 1-ethyl-3-(3-dimethylaminopropyl) carbodiimide hydrochloride
FDB	- fluid distribution board
FPCs	- flexible printed circuits
gDNA	- genomic DNA
HA-MRSA	- hospital-acquired MRSA
HGP	- human genome project
ICU	- instrument control unit
ITO	- indium-tin oxide
LDR	- ligase detection reaction
LIF	- laser-induced fluorescence
LOD	- limit-of-detection
MDR-TB	- multi-drug resistant tuberculosis
MES	- 2-(N-morpholino)ethanesulfonic acid
MHD-	- magneto-hydrodynamic
micro-PCR	- microfluidic polymerase chain reactors
MRSA	- methicillin-resistant *Staphylococcus aureus*
MR-CNS	- methicillin-resistance *S. epidermidis*
MSSA	- methicillin-susceptible *S. aureus*
MS-CNS	- methicillin-susceptible *S. epidermidis*
Mtb	- *Mycobacterium tuberculosis*
NAATs	- nucleic acid amplification tests
NHS	- *N*-hydroxysuccinimide
PC	- polycarbonate
PCR	- polymerase chain reaction
PCTE	- polycarbonate track etched membranes
PDMS	- polydimethylsiloxane
PEG	- polyethylene glycol
PI	- polyimide
PID	- percentage/integrator/differentiator

PMMA	- poly(methyl methacrylate)
PPC	- photoactivated polycarbonate
PVL	- Panton-Valentine leukocidin
RNA	- ribonucleic acid
RRDR	- rifampin-resistance determining region
RTD	- resistance temperature detector
RT-PCR	- reverse transcription polymerase chain reaction
SDS	- sodium dodecyl sulfate
SEM	- scanning electron microscopy
SPE	- solid phase extraction
STRs	- short tandem repeats
TE	- thermoelectric
XPS	- X-ray photoelectron spectroscopy
µCE	- microcapillary electrophoresis
µ-DAAD	- micro-DNA amplification and analysis device
µTAS	- micro-total analysis systems

ABSTRACT

Methods for bacterial detection and identification has garnered renewed interest in recent years due to the infections they may cause and the antimicrobial resistances they can develop, the potential for bioterrorism threats and possible contamination of food/water supplies. Therefore, the rapid, specific and accurate detection of pathogens is crucial for the prevention of pathogen-related disease outbreaks and facilitating disease management as well as the containment of suspected contaminated food and/or water supplies. In this dissertation an integrated modular-based microfluidic system composed of a fluidic cartridge and a control instrument has been developed for bacterial pathogen detection. The integrated system can directly carry out the entire molecular processing pipeline in a single disposable fluidic cartridge and can detect sequence variations in selected genes to allow for the identification of the bacterial species and even its strain. The unique aspect of this fluidic cartridge is its modular format with a task-specific module interconnected to a fluidic motherboard to permit the selection of a material appropriate for the given processing step(s). In addition, to minimize the amount of finishing steps for assembling the fluidic cartridge, many of the functional components were produced during the polymer molding step used to create the fluidic network. The operation of the fluidic cartridge was provided by electronic, mechanical, optical and hydraulic controls located off-chip and assembled into a small footprint instrument. The fluidic cartridge was capable of performing cell lysis, solid-phase extraction of genomic DNA from the whole cell lysate, continuous flow PCR amplification of specific gene fragments, continuous flow ligase detection reaction to discriminate sequence variations and universal DNA array readout, which consisted of DNA probes patterned onto a planar polymer waveguide for evanescent excitation. The

performance of the fluidic system was demonstrated through its successful application to the genetic detection of bacterial pathogens, such as *Escherichia coli* O157:H7, *Salmonella*, methicillin-resistant *Staphylococcus aureus* and multi-drug resistant *Mycobacterium tuberculosis*, which are major threats for global heath. The integrated system, which could successfully identify several strains of bacteria in <40 min with minimal human intervention and also perform strain identification, represents a significant contribution to pathogen detection.

CHAPTER 1 INTEGRATED MICROFLUIDIC SYSTEMS FOR DNA ANALYSIS*

1.1 Introduction

The potential utility of genome-related research in terms of evolving basic discoveries in biology has generated widespread use of DNA diagnostics and DNA forensics and driven the accelerated development of fully integrated microfluidic systems for genome processing. To produce a microsystem with favorable performance characteristics for genetic-based analyses, several key operational elements must be strategically chosen, including device substrate material, temperature control, fluidic control, and reaction product readout. As a matter of definition, a microdevice is a chip composed of a single processing step, for example microchip electrophoresis. Several microdevices can be integrated to a single wafer or combined on a control board as separate devices to form a microsystem. A microsystem is defined as a chip composed of at least two microdevices. Among the many documented analytical microdevices, those focused on the ability to perform the polymerase chain reaction (PCR) have been reported extensively due to the importance of this processing step in most genetic-based assays. Other microdevices that have been detailed in the literature include those for solid-phase extractions, microchip electrophoresis, and devices composed of DNA microarrays used for interrogating DNA primary structure. Great progress has also been made in the areas of chip fabrication, bonding and sealing to enclose fluidic networks, evaluation of different chip substrate materials, surface chemistries, and the architecture of reaction conduits for basic processing steps such as mixing. Other important elements that have been developed to realize functional systems include miniaturized readout formats comprising optical or electrochemical transduction and

* Reproduced with Permission from Springer

interconnect technologies. These discoveries have led to the development of fully autonomous and functional integrated systems for genome processing that can supply "sample in/answer out" capabilities. In this chapter, we focus on microfluidic systems that are composed of two or more microdevices directed toward DNA analyses. Our discussions will primarily be focused on the integration of various processing steps with microarrays. The advantages afforded by fully integrated microfluidic systems to enable challenging applications, such as single-copy DNA sequencing, single-cell gene expression analysis, pathogen detection, and forensic DNA analysis in formats that provide high throughput and point-of-analysis capabilities will be discussed as well.

1.1.1 The Human Genome Project

The completion of the human genome sequence in 2003 was one of the most important scientific accomplishments in human history[1] and marked a significant milestone for the Human Genome Project (HGP). This achievement has led to compelling genomic and proteomic research discoveries with unprecedented impacts in areas such as forensic DNA analysis,[2-5] medical diagnostics,[6, 7] infectious disease management,[8-11] and chemical and biological sciences.[12, 13] Some of the important tools for DNA processing include solid-phase extraction (SPE) and purification of DNA, PCR or other thermally induced amplification strategies, electrophoresis, and DNA microarrays. Although many conventional bench-top tools currently exist to process DNA samples, efforts are being heavily invested into further automating the processing strategy, reducing the cost of performing the assay, and increasing the sample throughput. In this chapter, we will discuss the use of microfluidics, in particular integrated systems, for processing a variety of DNA samples.

1.1.2 Molecular Processing Pipeline for DNA Analyses

Complete nucleic acid analyses (RNA or DNA) for a variety of applications can be accomplished using commercial bench-top instruments, and typically consists of several molecular processing steps including: (1) lysis of cells to release the nucleic acids of interest; (2) purification and isolation of the nucleic acids from other cellular components (e.g. cell debris and proteins); (3) amplification of trace amounts of nucleic acids to generate sufficient copy numbers for detection; and (4) analysis of unique regions within the genetic material using a combination of techniques. To complete an entire assay, a well-equipped laboratory and significant technical expertise are commonly required, with intervention at several stages of the processing pipeline to manipulate samples and/or reagents. In addition, the total time required for sample processing can be several hours to several days.

Derived from the concept of micro-total analysis systems or lab-on-a-chip platforms first proposed by Manz *et al.*[14] in the early 1990s, integrated microfluidic systems have emerged that incorporate several molecular processing steps into a single platform with sample-to-answer capabilities. These systems are particularly compelling for DNA/RNA analyses. To create such a system, a series of discrete devices performing specific molecular functions such as cell lysis, nucleic acid extraction and purification, nucleic acid amplification, and other supporting analysis techniques (e.g. capillary electrophoresis, microarrays) must be interconnected with minimal dead volumes due to the ultrasmall samples processed (picoliters to nanoliters). Fluids are manipulated using on-chip or off-chip components, such as micropumps, microvalves, and micromixers (see **Figure 1.1**). As noted previously, microsystems are composed of 2 or more microdevices and, in many cases, microdevices consist of components such as on-chip

valves, mixers, and/or pumps. In most cases, DNA/RNA processing requires multiple processing steps and therefore devices need to be combined, either in a single wafer format or a modular format, to form the system targeted for a given genetic analysis (see **Figure 1.1**).

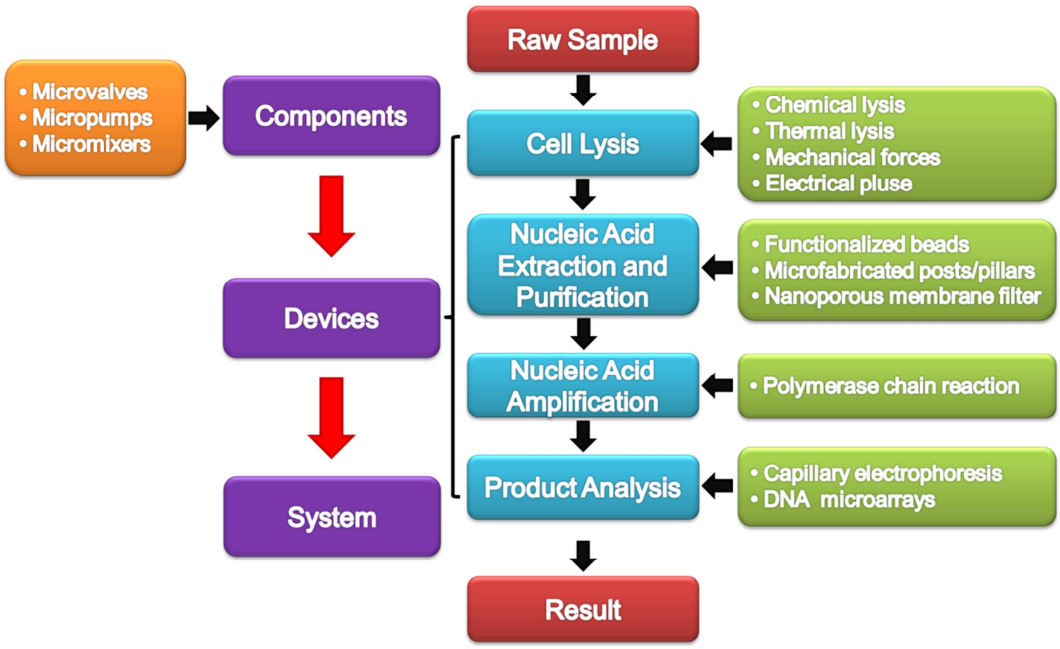

Figure 1.1 Flow diagram showing the molecular processing steps required for analyzing nucleic acids. The main steps include cell lysis, nucleic acid extraction and purification, PCR amplification, and analysis methods for identifying the resultant products. For each of the processing steps shown, a device will have poised on it a component of one of these functional steps, and each device may be comprised of various components (such as pumps, valves, and micromixers) in order to carry out the desired operation. A system comprises of two or more devices, meaning that it will have integrated onto it multiple processing steps. The ultimate goal is to incorporate all of the molecular processing steps onto a single platform to provide sample in/answer out capabilities with no operator intervention.

1.2 Microfluidics and DNA Analysis

The capability of handling a volume of liquid as small as a few nanoliters and even a few picoliters, the common sample size in most microfluidic systems, can be utilized to permit DNA extraction following cell lysis and thermal reactions without creating sample dilution, minimize reagent usage, provide process automation, allow in-the-field

analyses, and minimize possible contamination. Microfluidic systems also offer rapid, accurate, and cost-effective analyses. Performing sequencing or genotyping using microfluidic platforms can lead to significant increases in throughput. For example, DNA sequencing read lengths of 600 – 800 bases can be achieved in 25 min using microcapillary electrophoresis (μCE) with a separation channel length of 20 cm (Sanger sequencing),[15] whereas the same separation would require 1 – 2 h in a capillary array electrophoresis (CAE) system.[16, 17] In the sections that follow, we will give a brief introduction to the various microdevices that have been fabricated to handle steps in the processing of nucleic acids, such as cell lysis, extraction and/or purification of the nucleic acids, their amplification, determination sequence variations, and readout.

1.2.1 Cell Lysis

Cell lysis is the first step in most DNA analyses and involves disassembly of the cell membranes and release of the genomic material and other cellular contents. A variety of lysis methods, including chemical lysis,[18, 19] thermal lysis,[20] and lysis by mechanical forces,[21, 22] or electrical pulse,[23-26] have been successfully demonstrated in microfluidic devices.

Transitioning chemical lysis methods commonly used in macro-scale workups to microfluidic devices is straightforward. Chemical lysis methods involve mixing the target cells with lytic agents, such as sodium dodecyl sulfate or guanidium hydrochloride and hydroxide that can solubilize the lipid membranes. One issue associated with the use of chemical lysis is that lytic agents can interfere with downstream processing, such as PCR, and therefore must be removed from the sample before subsequent reactions, increasing the microfluidic design complexity. Carol and co-workers[18] reported a polydimethylsiloxane (PDMS) microfluidic device for on-chip cell lysis based on local

hydroxide electro-generation. In this device, hydroxide ions porated the cell membrane, leading to cell lysis. During lysis, hydrogen ions, which were simultaneously generated on-chip, reacted with excess hydroxide ions creating a neutral pH lysate and eliminating the need for a final washing step.

Thermal lysis, which involves disrupting the cell membranes by heating cells to near boiling temperatures, is another method that can be incorporated into a microfluidic device as long as the microfluidic material can withstand the temperature required to lyse the cells. The advantage of thermal lysis is that no interfering reagents are required that may interfere with downstream reactions.[27] The device design can be further simplified by lysing cells in the initial denaturation step of downstream PCRs.[28] But, thermal methods are not applicable for certain cell types, such as Gram-positive bacteria.

Mechanical forces, such as sonication, can be integrated to the microdevice to disrupt cells via gaseous cavitation. In this process, air pockets form from dissolved gases in the aqueous media and collapse rapidly, creating high pressure and high temperature environments sufficient to break cell membranes. This method is suitable for hard-to-lyse cells or spores, but can generate considerable amounts of heat and free radicals.[29] Belgrader *et al.*[21] reported a minisonicator combined with a spore lysis cartridge. *Bacillus* spores were sonicated in the presence of glass beads and were successfully lysed to release DNA for PCR amplification in ~30 s.

Electrical pulse methods represent another method for cell lysis and are based upon electroporation of the membrane. In the electroporation process, the application of high electric field pulses causes the formation of small pores in cell membranes.[30] However, the use of high electric fields can lead to heating and gas generation. To overcome this

limitation, a microfluidic electroporation device for the lysis of human carcinoma cells was demonstrated by Lu *et al*.[23] In their design, a straight microchannel was constructed in glass, where the side-walls consisted of gold saw-tooth-shaped electrodes supported by the polymer, SU-8. Using pressure-driven flow, cells were directed through the channel and electroporated by the saw-tooth electrodes (see **Figure 1.2**). The magnitude of the electric field was in the range of a few kilovolts per centimeter, while the AC voltage was >10 V peak-to-peak, minimizing heat generation and bubble formation.

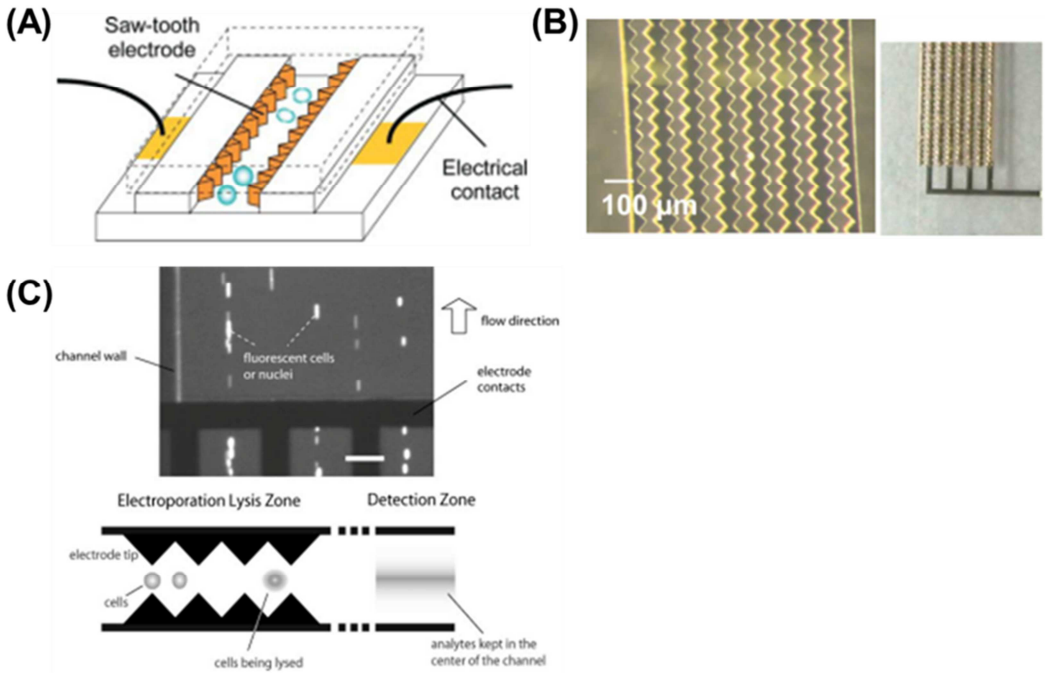

Figure 1.2 (A) Microelectroporation device for cell lysis. (B) Devices at various steps of the fabrication process: after metallization and electrode-mold formation (left) and after electroplating (right). (C) Dielectrophoresis (DEP) effect observed in the flow channels (top). Saw-tooth microelectrodes acting as a DEP device for focusing intracellular materials after electroporation (bottom). Reproduced from [23] with permission.

1.2.2 Nucleic Acid Extraction, Purification and Pre-concentration

Following cell lysis, DNA extraction, purification, and pre-concentration are usually achieved by micro-solid phase extraction (micro-SPE) devices. This step is essential in

order to purify and isolate the genomic materials from other cellular components, contaminants, and chemicals introduced in the cell lysis step that might potentially interfere with downstream enzymatic reactions. In addition, the nucleic acids may be enriched in this phase of the processing strategy to pre-concentrate the targets to a level that is amenable for further downstream processing.

A variety of well-established macro-scale SPE methods for nucleic acid extraction have been successfully transferred to micro-scale devices.[10, 31-57] Although the physical principles of these methods may be different (e.g. chaotropic interactions, electrostatic interactions, affinity interactions, etc.), micro-SPE protocols typically consist of three steps: (1) selective adsorption of nucleic acids onto a solid phase; (2) removal of contaminants by a washing step; and (3) elution of the pre-concentrated nucleic acids from the solid support using water or a low salt buffer.[31] Like their macro-scale counterparts, micro-SPE devices possess a loading level of target material that is dependent upon the available surface area within the extraction bed and, thus, are manufactured either by packing the solid phase (typically consisting of silica beads) into the device or by directly fabricating microstructures inside the device to increase the available load capacity of the device.

As noted above, micro-SPE devices can be fabricated by packing silica beads, sol-gel immobilized silica beads, photo-polymerized monoliths, or modified magnetic particles into microfabricated channels.[10, 31-43] For example, Landers and his research group[32] demonstrated the extraction of PCR-amplifiable DNA from lysed white blood cells using silica particles packed into a capillary tube; the DNA recovery was found to be ~70% in a 10 min processing time. The load of DNA into the device was found to be on the order of 10 – 30 ng/mg of DNA. To circumvent the high backpressure introduced

by flowing silica beads into a microchannel and to improve reproducibility, a silica bead/sol-gel hybrid matrix was packed into a glass microchip (see **Figure 1.3A**).[31, 33] Other matrices, such as a sol-gel monolith[35] or photo-polymerized monoliths[36] were explored by the same group in effort to overcome the aging and shrinkage problems associated with the silica bead/sol-gel hybrid matrix. Klapperich and co-workers[37-39] used a similar photo-polymerized monolith as a solid-support matrix to confine silica beads within a cyclic olefin copolymer (COC) microchip to extract a variety of samples, such as lambda (λ)-DNA, Gram-positive and Gram-negative bacterial genomic DNA, inoculated human blood and urine samples (see **Figure 1.3B**).

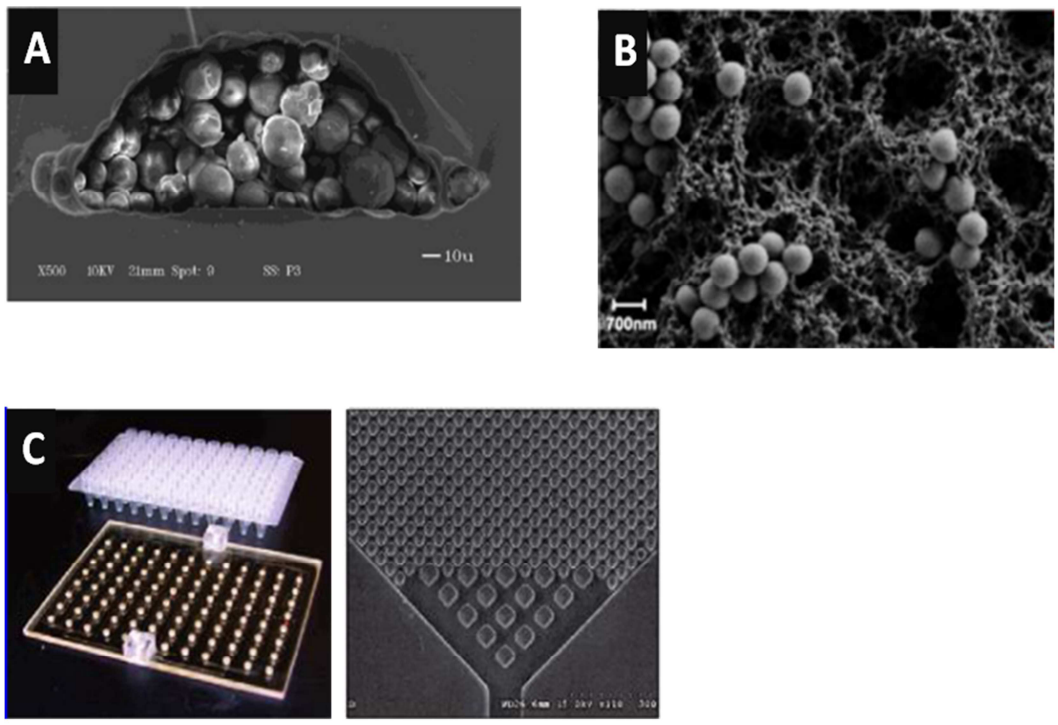

Figure 1.3 (A) SEM image of the cross-section of a glass microchip channel packed with silica bead/sol-gel hybrid at 500x magnification. Reproduced from [33] with permission. (B) SEM image of a porous polymer monolith filled with silica beads at 10,000x magnification. Reproduced from [39] with permission. (C) Photograph of a 96-well polycarbonate solid phase extraction microfluidic plate and a commercial 96-well titer plate (left). SEM image of the micro-pillars that were fabricated in the purification bed (right). Reproduced from [47] with permission.

Issues associated with SPE beds comprised of silica beads or polymerized polymer monoliths include: (1) residual chaotropic reagents, such as guanidinium or sodium iodide salts, present in the initial elution phase and interfering with downstream amplification steps; (2) packing the matrix, which requires a post-fabrication process that can be tedious and demands experienced engineers to accomplish; and (3) aging and shrinkage of the packing material, which can affect the efficiency and reproducibility of the extraction process.

Alternatively, one can produce a SPE surface directly in the device via microfabrication techniques. Micro-post or micro-pillar structures can be fabricated inside the extraction chamber to increase the available surface area, thus enhancing the load of target material as well as enhance the interaction probability between the solution borne nucleic acids and the SPE bed. Christel *et al.*[44] fabricated, using deep reactive ion etching (DRIE) and anodic bonding, a micro-SPE device in silicon that contained high aspect ratio (aspect ratio = structure height divided by structure diameter) micro-pillars with a total surface area of 3.5 mm^2. The binding capacity of DNA was found to be 40 ng/cm^2 with a 50% extraction efficiency for short (500 bp) and medium sized (48 kbp) DNAs. Cady *et al.*[45] extended this work to *Escherichia coli* cell lysates. To circumvent the tedious DRIE and bonding processes required for fabricating these high aspect ratio microstructures in silicon, Soper and co-workers[46] developed a micro-SPE device made from photo-activated polycarbonate (PPC). This micro-SPE device contained high aspect ratio (5/1) micro-pillars, hot embossed from a LIGA-fabricated nickel molding tool. The SPE bed possessed a total active surface area of 2.3×10^7 μm^2. Nucleic acids were selectively immobilized onto the PPC surface, which contained carboxylic acid groups generated using UV radiation, using an immobilization buffer

containing polyethylene glycol, NaCl, and ethanol. After cleanup using ethanol, purified and concentrated nucleic acids were eluted from the PPC surface using water or PCR buffer. The load capacity and recovery of *E. coli* genomic DNA were estimated to be 790 ng/cm^2 and 85 ±5%, respectively. This work was followed by a report on the fabrication of a high-throughput device consisting of 96 micro-SPE beds, each containing an array of 3,800 20-µm diameter micro-pillars (see **Figure 1.3C**).[47, 48] Both genomic DNA and total RNA could be extracted and purified from bacterial cells seeded into mammalian blood samples.

Another approach for the SPE of nucleic acids is the use of commercially available nano-porous aluminum oxide membranes (AOM). In a high salt concentration buffer, genomic DNA or RNA will aggregate and bind to the nano-porous membrane; both nano-filtration and electrostatic interactions contribute to the retention and purification of the target DNA or RNA. The retained DNA/RNA can be recovered using a PCR buffer. Kim *et al*.[49] investigated the extraction of genomic DNA from blood samples with a recovery of ~90% using an AOM sandwiched between PDMS microchannels. The AOM SPE device was later integrated to a micro-chamber PCR device, demonstrating successful amplification of both DNA from a bacterial sample and RNA from virus samples.[50] The advantages of this method included the ability to use high flow rates to shorten processing time and low protein absorption onto the AOM. However, the handling of the thin and brittle AOM remains a challenge.

In addition to genomic DNA or RNA purification and pre-concentration before an amplification step, some applications, for example the purification of dye terminator Sanger sequencing products, require high quality DNA free of background species such as salts, unincorporated primers, dNTPs, and dye-labeled ddNTPs prior to the

electrophoresis step. Soper and co-workers[51] demonstrated the use of a PPC micro-SPE device for the purification of Sanger sequencing products to provide high quality DNA free from background species. PPC micro-SPEs were successfully coupled to capillary gel electrophoresis[54] that also contained a continuous flow Sanger extension thermal cycler.[51, 52]

Mathies and his group[53] purified Sanger extension products using a micro-chamber containing a sparsely crosslinked polyacrylamide gel co-polymerized with complementary oligonucleotide probes appended onto the target DNA products. DNA elution was achieved by thermal denaturation of the hybrids. This micro-chamber was coupled to a Sanger extension chamber and microchip electrophoresis to form an integrated Sanger sequencing bioprocessor. With a 400-fold reduction in sequencing reagents and 10- to 100-fold reduction in DNA template required compared to bench-top approaches, 556 continuous bases were sequenced using this bioprocessor with 99% accuracy.[54]

1.3 Microfluidic Polymerase Chain Reactors (Micro-PCR)

Since the discovery of the PCR in 1986 by Mullis *et al.*,[58] PCR has become a crucial tool in basic molecular biology discovery, genome sequencing, clinical research, *in vitro* diagnostics, and evolutionary studies.[59] PCR is an enzymatic reaction that allows any nucleic acid fragment to be generated *in vitro* and in high abundance. Theoretically, the amount of product doubles during each PCR cycle, as shown by the following equation:

$$N = N_0 2^n \qquad (1)$$

where N is the number of amplified DNA molecules, N_0 is the initial copy number of DNA molecules and n is the number of amplification cycles.[60, 61] Experimentally, the

amplification efficiency (*E*) can range from 0 to 1, and therefore the true copy number produced is given by:

$$N = N_0(1 + E)^n \qquad (2)$$

In PCR, denaturation and annealing are nearly instantaneous events that occur as soon as the correct temperature is reached (*e.g.,* ~94 ℃ for denaturation; 50 – 60 ℃ for annealing) and at 72 ℃ the extension step is limited only by the kinetics of the polymerase enzyme. Implementation of the thermostable *Taq* polymerase as a substitute for the Klenow fragment of *E. coli* DNA polymerase I[62] has made it possible to automate the PCR amplification step by using various thermal cycles carried out by a block thermal cycler. Investigators have shown that *Taq* DNA polymerase has an extension rate of 60 – 100 nucleotides/s at 72 ℃. [63] For efficient amplification, a device with low heat capacity that can transfer heat quickly to the sample and quickly draw away the heat when cooling is preferable. Most conventional thermal cyclers have large thermal masses resulting in high power requirements and slow heating and cooling rates with long reaction times, typically exceeding 1.5 h in spite of the fact that kinetically, a 500 bp PCR product should be produced in as little as 5 s.

Due to the intrinsically small PCR chamber volumes and mass, exquisite heat transfer capabilities can be realized in micro-PCR devices that can significantly reduce the processing time compared to conventional bench-top thermal cyclers. Short thermal cycling times can be realized and still provide amplification efficiencies comparable to their macro-scale counterparts with designs that are sometimes not conducive to macro-scale formats. Micro-PCR devices have adopted design formats such as chamber-type PCR devices, in which the PCR cocktail and target are mixed inside a micro-chamber and the chamber is then cycled between the various temperatures

required for the amplification process. Another design approach uses the continuous-flow format, in which the PCR device consists of isothermal zones brought to equilibrium prior to the amplification process. The PCR cocktail is shuttled between these isothermal zones either electrokinetically or hydrodynamically to affect the thermal processing. Another format that has been employed for micro-scale PCR devices is a thermal convection-driven PCR device in which a temperature gradient is applied to a closed reaction chamber and the fluid is shuttled through the temperature gradient using a Rayleigh-Bénard convection cell. In the following sections, we will briefly introduce these PCR designs.

1.3.1 Chamber-type Micro-PCR Devices

In chamber-type micro-PCR devices, a static PCR cocktail containing the target is repeatedly cycled between three different temperatures: one for denaturation, a second for renaturation, and a third for polymerase extension, which is similar to that used in a conventional PCR thermal cycler. Chamber-type micro-PCR devices consist of either a single chamber or multiple chambers configured on a single wafer with the appropriate heating modalities to allow thermal cycling. The primary advantage of these types of micro-thermal cyclers is the low thermal masses that must be heated/cooled, providing faster reaction times compared to block thermal cyclers.

1.3.1.1 Single-chamber Micro-PCR Devices

In 1993, Northrup *et al.*[64] reported the first PCR microfluidic device, which consisted of a 50-µL well structure serving as the reaction chamber and was fabricated in silicon using wet chemical etching. Twenty amplification cycles were carried out, with the cycling time four times faster than a conventional bench-top PCR device. In 1994, Wilding *et al.*[65, 66] developed a silicon/glass hybrid device that held 5 – 10 µL of reaction

mixture in a chamber, whose performance was improved by surface passivation through salinization of the microchamber surface[67] and was heated using an external copper block. Single-chamber PCR devices have been widely investigated since these initial reports.[68-77] However, single-chamber micro-PCR devices possess low throughput.

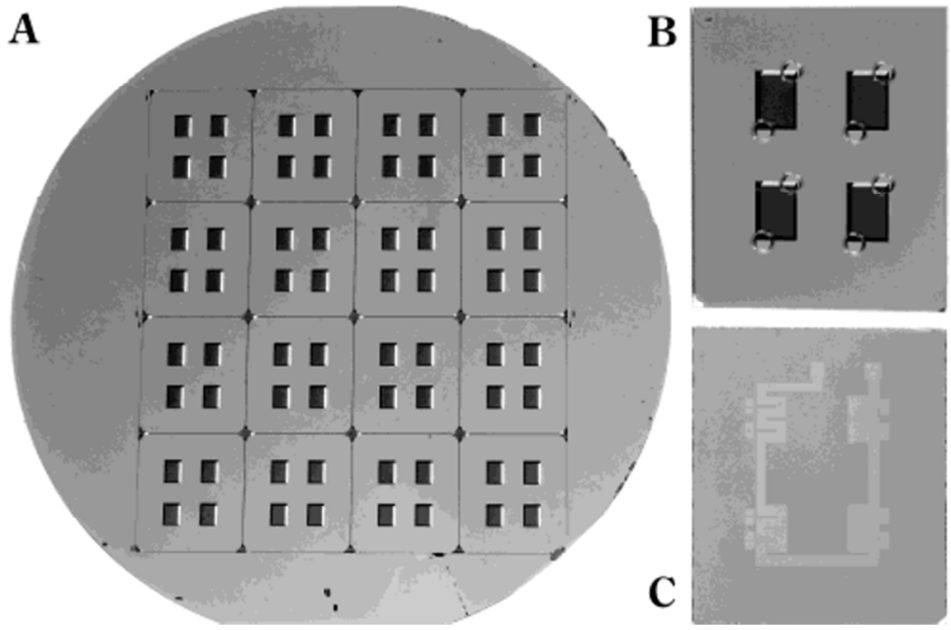

Figure 1.4 Photographs of µ-DAAD production steps. (A) Front side of a 4" silicon wafer populated with etched microreactors; 16 µ-DAAD are processed in parallel, each consisting of four microreactors. (B) Front side view of a single µ-DAAD (16 x 1 mm^2) after bonding a cover plate and dicing. DNA arrays are printed onto the bottom of the microreactor cavities, but cannot be seen in this image because of their small size. Holes of 1 mm in diameter are drilled in the cover glass for the filling of the µ-DAAD reactors with reagent. (C) Back-side view of the device with platinum heater coil and thermoresistors placed at the corresponding area of the micro-reactor. Reproduced from [81] with permission.

1.3.1.2 Multi-chamber Micro-PCR Devices

Multiple PCR chambers have been fabricated on a single microfluidic chip and explored for high throughput PCRs.[78-83] An example of a multi-chamber micro-PCR device, micro-DNA amplification and analysis device (µ-DAAD) consisted of 16 µ-DAADs in parallel with each µ-DAAD consisting of four microreactors fabricated on a 4"

silicon wafer (see **Figure 1.4**). Multi-chamber micro-PCR devices[84] have been demonstrated for DNA amplifications of five gene sequences related to *E. coli* from three different DNA templates and detected by TaqMan chemistry with a limit of detection (LOD) of 0.4 copies of target DNA.

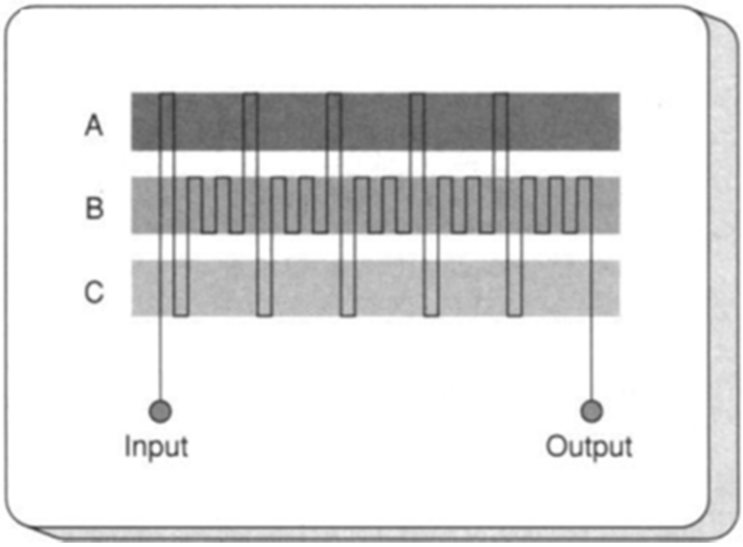

Figure 1.5 Chip for CF PCR. Three well-defined isothermal zones are poised at 95 (A), 77 (B), and 60 ℃ (C) by means of thermostated copp er blocks. The sample is hydrostatically pumped through a single channel etched into a glass wafer. The channel passing through the three temperature zones defines the thermal cycling process. Reproduced from [87] with permission.

1.3.2 Continuous Flow PCR (CF PCR) Devices

Another configuration for micro-PCR devices employs a flow-through format with a "time–space conversion" concept, in which the sample is continuously transitioned through isothermal zones for denaturation, annealing, and extension. This is in contrast to chamber-type PCR devices, in which heating and cooling occurs on a static sample with the entire device heated and cooled to the desired temperatures.[79, 83, 85, 86] The CF PCR approach allows for short reaction times because the small-volume fluid elements can be heated or cooled to the required temperature within 100 ms.[59] In 1998, Kopp *et*

al.[87] reported the first CF PCR microdevice (see **Figure 1.5**). This device consisted of 20 thermal cycles comprised of a serpentine channel design whose dimensions were 40 µm in width and 90 µm in depth, with a total length of 2.2 m, producing a pressure drop of ~14.5 psi. For DNA amplification, 10 µL of a PCR mixture was hydrostatically pumped at volumetric flow rates ranging from 5.8 to 72.9 nL/s with a flow-through time of 18.7 to 1.5 min.[87] The channel walls were silanized with dichlorodimethylsilane to reduce possible adsorption of the polymerase enzyme (*Taq* polymerase) and DNA onto the glass surface. A zwitterionic buffer and nonionic surfactant were used as the PCR buffer additives to impart a dynamic coating.[88]

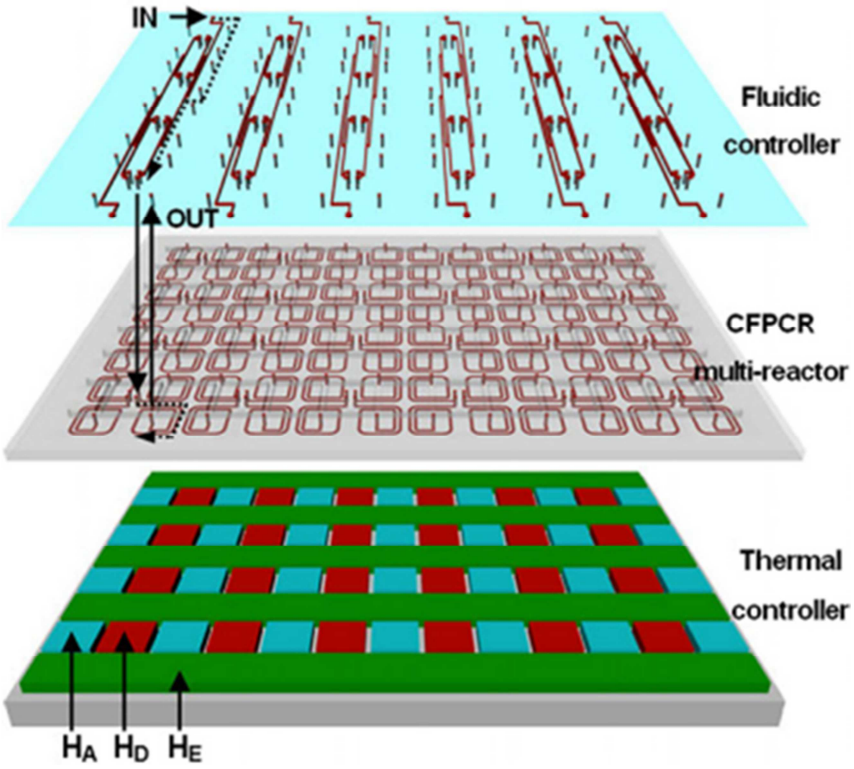

Figure 1.6 High throughput CF PCR multireactor platform consisting of three functional units: a fluidic controller for distributing reagents and analyte to the reactors, a CF PCR multireactor, and a distributed temperature controller. H_D denotes the denaturation heaters (90 – 95 ℃), H_A the annealing heaters (50 – 70 ℃), and H_E the extension heaters (70 – 77 ℃). Reproduced from [92] with per mission.

Using a 20-cycle spiral microchannel hot embossed into a polycarbonate (PC) substrate configured for performing CF PCR,[89] the PCR cycle time was reduced to the kinetic limit set by the polymerase incorporation rate; 500-bp and 997-bp fragments were amplified in a total time of 1.7 min (5.2 s/cycle) and 3.2 min (9.7 s/cycle), respectively. The amplification efficiency was further optimized through proper thermal management using numerical models and experiments to evaluate the effects of different combinations of temperature distribution in a typical CF PCR device fabricated by hot embossing PC substrates.[90] Chen *et al*.[91-93] reduced the footprint of each spiral reactor to 8 mm by 8 mm and arranged 96 reactors in titer-plate format (12 x 8) for high throughput processing (**Figure 1.6**).

The attractive features of CF PCR devices consist of: (1) very rapid heat transfer during the PCR, with run times on the order of minutes; (2) low possibility of contamination (closed architecture);[4, 10, 94] and (3) facile integration with various liquid transport processes, such as magneto-hydrodynamic (MHD) actuation.[95] Additional advantages include reduced sample consumption and reagents (lower cost) and simple integration to other DNA processing devices.[11, 96] A limitation of this approach is the fixed cycle number that can be employed by the chip, which is dictated by the device layout. To overcome this drawback, Chen *et al.*[97] demonstrated the use of a microfabricated PC chip for DNA amplification in a CF mode using electrokinetically driven synchronized pumping (**Figure 1.7**). A 500-bp fragment from λ-DNA was obtained with a total time of amplification of ~18.1 min for 27 cycles.

The arrangement of the three temperature zones on most rectangular serpentine channel CF PCR devices consists of denaturation, extension, and annealing in that order. Although this arrangement can establish a smooth temperature gradient,

amplification efficiency may degrade because the melted single-stranded DNA is likely to form double strands with the template DNA or their complementary fragments when passing through the extension zone. To circumvent this problem, a novel three temperature zones arrangement in a “circular” format consisting of denaturation, annealing, and extension has been exploited.[95, 98-100]

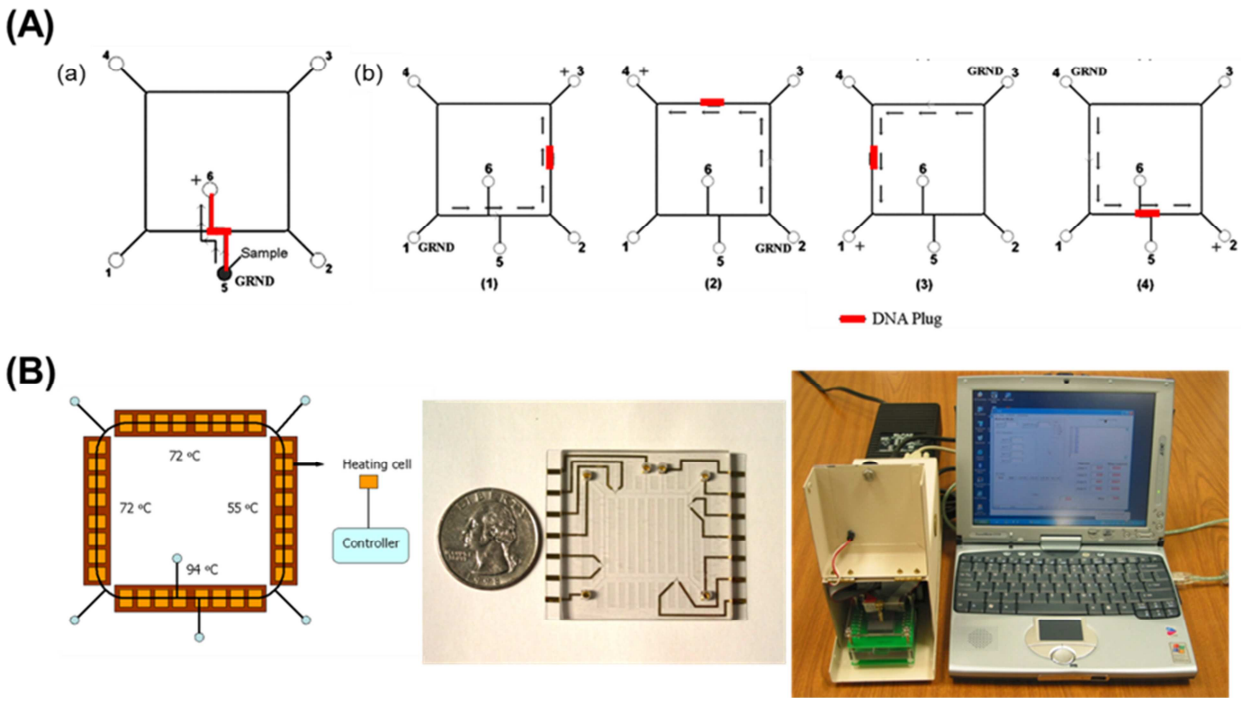

Figure 1.7 (A) Principle of electrokinetic synchronized cyclic CF PCR process. Sample injection (a): DNA was filled into reservoir 5 and a voltage was applied to the electrodes in reservoirs 5 (GRND indicates ground) and 6 (+ indicates high voltage input). Sample moved across the reactor channel to fill the crossed-T injector. Sample cycling (b): Following injection, the sample is shuttled through the various isothermal zones by moving the position of the applied electric field in a cyclic fashion as denoted in diagrams 1 – 4. (B) Schematic view and photographs of the electrokinetically synchronized CF PCR microchip. The actual microchip, fabricated via replication technology into PC, is shown in the middle photograph next to the quarter. Poised on the PC chip are electrode contacts for applying the voltage in an automated fashion to the various reservoirs. Reproduced from [97] with permission.

The PCR channel for these CF PCR devices can also consist of either capillary tubes[99, 100] or an on-chip annular channel[95, 101]. The serpentine channel formats on a monolithic chip can utilize thermal insulation with the aid of air gaps[102, 103] or by utilizing

glass chips with a low thermal conductivity.[104, 105] Recently, a novel spiral channel configuration was also used to perform CF PCR on a single PC wafer with a circular arrangement of three temperature zones, allowing for a compact footprint and a minimal number of heaters for temperature control.[106, 107] CF PCR microfluidics can also use a unidirectional PCR or oscillatory flow.[108]

1.3.3 Thermal Convection-driven PCR

Convectively driven PCR is an alternative thermal cycling process, which was first reported in 2002 by Krishnan *et al*.[109] The authors used a Rayleigh-Bénard convection cell consisting of a 35-μL cylindrical cavity to perform the PCR amplification of the β-actin gene (295-bp fragment). Rayleigh-Bénard convection is generated by buoyancy-driven instability in a confined fluid layer heated from below.[110]. The inherent structure of Rayleigh-Bénard convection-steady circulatory flow between surfaces employs two fixed temperature zones to facilitate the convection-driven sample flow. In contrast to CF PCR, the temperature cycling is achieved as the fluid continuously shuttles vertically between the two temperature zones poised for annealing/extension (top, 61 ℃) and denaturation (below, 97 ℃). Therefore, there is no need of an external force to drive the fluid through different temperature zones, simplifying its operation and allowing the implementation of the desired number of thermal cycles.

1.3.4 Microfluidic Thermal Heating Methods

The choice of a heating method for micro-PCR devices is important in achieving efficient temperature ramping rates. The diversity of materials exhibiting differences in thermal mass means that different heating methods may be required. At present, temperature cycling on microfluidic devices can be performed either with contact or

noncontact heating methods. Summarized below are various heating methods that have been employed in microfluidic devices.

1.3.4.1 Contact Heating

For contact heating, heaters are fabricated directly within the microchip or are in contact with the outside of the microchip. Contact heating utilizes an electrothermal conversion to heat the PCR solution.[111] Contact heating can be achieved through the use of thin film heating elements, which are mainly fabricated using deposition techniques; through the use of metal heating blocks, which primarily consist of inserting a heating cartridge into the metal blocks; or by utilizing Peltier elements.

1.3.4.1.1 Thin Film Heating

Heating elements can be fabricated on-chip using thin film deposition. Platinum,[78, 79, 112-116] is the most commonly used material for heating elements due to its ability to withstand high temperatures, good chemical stability, and ease of micromanufacturing. Some other metals, alloys, or inorganic compounds have also been used as thin film heaters in micro-PCR devices, such as Al,[70, 81, 82, 117] Ni,[104] W,[101] Ag/graphite inks,[85] Ag/Pd,[102, 118] Ni/Cr,[119] Cr/Al,[82] Al_2N_3,[120] and indium-tin oxide (ITO).[121-123] Microheaters fabricated by Pt thin film deposition often require a thin layer of Ti serving as an adhesion layer. The Ti layer exhibits a high diffusion rate at high temperatures, which can deteriorate the Pt heater.[124] Commercial thin film resistive heaters[85, 106, 107] have proven to be efficient and robust for achieving fast PCR cycling, in contrast to conventional PCR devices.

1.3.4.1.2 Metal Heating Blocks

Conventional PCR instruments typically utilize contact heating, which involves a metal heating block in contact with the sample container, to cycle the temperature of the

PCR solution that is held within a thin-walled polypropylene tube. In spite of their large thermal mass and slow temperature ramping rates, metallic heating blocks and Peltier-based Thermo-Electric (TE) ceramic heating blocks are widely applied in micro-PCR devices.[69, 84, 87, 125-130] To achieve fast thermal transition, two[8, 98, 125, 131] or more TE devices can be coupled to thermally cycle the PCR solution, and a total of six TE devices have been used in a portable miniaturized thermal cycling system.[84] The temperature of the peltiers could be independently controlled and programmed to be at different temperature levels necessary for effective annealing and denaturation. To ensure good thermal contact between the TE element and the cycled region of the device, supporting substances with higher thermal conductivity, such as mineral oil[8, 131] or a metallic thin wafer,[132] can be added to the interface of the TE element. Normally, the TE cell consists of an array of parallel P–N junctions and each parallel P–N junction establishes its own temperature differential for a given voltage. The P–N junction is formed by joining P-type and N-type semiconductors and when an electric current flow through the junction, either heat is absorbed or released depending on the direction of the current flow. Consequently, a radial temperature gradient on the hot surface of the TE cell is created, which causes non-homogeneity of the surface temperature of the TE cell and compromises the efficiency of the PCR.[111] To achieve a homogenous temperature distribution across the surface of the TE cell, an oxygen-free thin copper wafer is necessary to redistribute the surface temperature.[128] Other reliable contact heaters are resistive heating coils[99, 129, 133] and single-sided flexible printed circuits (FPCs).[134]

It is important to note that the thermal-cycling rate is limited by the thermal mass of the heating element itself and of the entire micro-PCR device as well. Moreover, in the

case of an external contact element, localized heating is ultimately limited in terms of lateral resolution by the thermal conductivity of the substrate material. In the case of on-chip integrated heaters, these devices still require tedious and complicated micromanufacturing processes, which restrict the flexibility to reconfigure the PCR design.[135]

1.3.4.2 Non-contact Heating

The inherent problem with contact thermal heaters is their relatively large thermal mass. More thermal mass is added to the PCR device when contacting the chamber containing the PCR solution, which hinders fast thermal cycling rates. For the integration of PCR with μCE, thermal management becomes difficult because contact resource is regarded as part of the PCR chip and not part of the electrophoresis chip itself. These restrictions have triggered interest in the development of non-contact thermal cycling in which the heating is remote from the microfluidic device and not in physical contact with the PCR chamber.[111]

1.3.4.2.1 Non-contact Heating based on IR Radiation

Non-contact heating method using IR radiation was first reported by Oda *et al*.[136] in 1998. In their work, an IR light, which used a single and inexpensive tungsten lamp as the non-contact heat source, was used for heating glass microchambers. The authors achieved temperature ramping rates of 10 ℃/s for heating and 20 ℃/s for cooling. In 2000, Hühmer and Landers[71] reported IR-mediated fused-silica capillary cycling with nanoliter volumes (160 nL), with improved heating and cooling rates of 65 and 20 ℃/s, respectively. Giordano *et al*.[74] developed a novel polyimide (PI) PCR microchip, which utilized IR-mediated thermal cycling for the amplification of a 500-bp λ-phage DNA fragment in a 1.7-μL chamber with a total reaction time of only 240 s for 15 cycles. In

2003, Ferrance *et al*.[72] presented IR-mediated PCR amplification of genomic DNA using primers defining a 380-bp fragment of the β-globin gene followed by electrophoretic analysis on a single glass chip for the analysis of Duchenne muscular dystrophy (DMD) in less than 15 min for 35 cycles.

1.3.4.2.2 Non-contact Heating based on Hot Air Cycling

Wittwer *et al*.[137, 138] developed non-contact heating for PCR based on hot air cycling. In their work, temperature cycling was performed without physical contact between the heating source and the reaction chamber by rapidly switching streams of air set to the desired temperature. Due to the low thermal mass of air, a high temperature ramping rate could be obtained, which has been further improved by several research groups.[68, 114, 115, 139-141]

1.3.4.2.3 Non-contact Heating based on Laser-mediated Heating

The tungsten lamp is a non-coherent source with large focus projection, which limits the heating efficiency when applied to microchips with a small cross-section. Laser-mediated non-contact heating utilizes a photothermal effect produced by a diode laser coherent light source to heat an absorbing target. Tanaka *et al*.[142] used a diode laser to control the temperature of a chemical reaction by heating an absorbing target of a black ink point placed on top of a glass microchip cover plate above the reaction channel. The integrated glass microchip with non-contact IR laser-mediated heating has been demonstrated for fast and localized temperature control under flowing conditions with ultrafast heating and cooling rates of 67 and 53 ℃/s, which is 30 times faster than a conventional device and 3 – 6 times faster than electrothermal miniaturized thermal cyclers.[135] This heating method may be very attractive and desirable due to its high resolution for spatially localized heating, ease of manipulation along the chip, and its

property of being a point light source. Unfortunately, this heating method has not been applied for temperature control in microfluidics.

1.3.4.2.4 Non-contact Heating based on Microwave Irradiation

Non-contact heating utilizing a focused microwave source was demonstrated by Fermér *et al*.[143] In their work, a single-mode microwave cavity was used to heat 100 µL PCR mixture in a 0.5-mL polypropylene tube for 25 cycles. Most recently, microwave-induced milliliter-scale PCR (see **Figure 1.8**) was reported[144] for real-time PCR analysis.

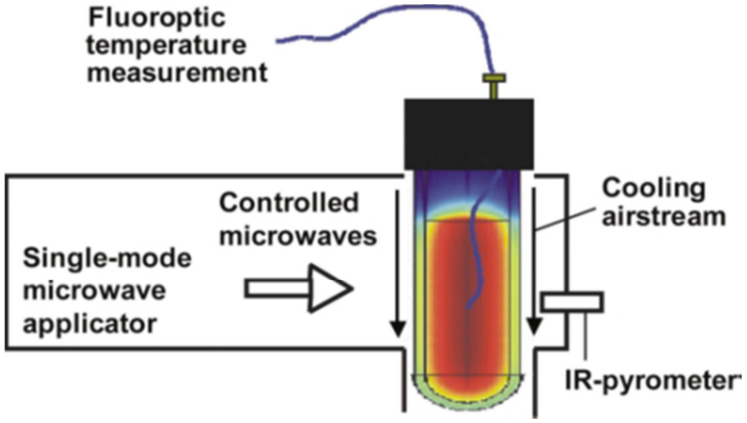

Figure 1.8 Experimental set up for microwave-heated PCR that is used to perform milliliter-scale PCR utilizing highly controlled microwave thermal cycling. Reproduced from [144] with permission.

Although the amount of amplified nucleic acid product after 33 cycles indicated incomplete amplification, which was attributed to temperature "over-shooting" at the denaturation phase and subsequent deactivation of the *Taq* polymerase,[145] microwave heating was quite promising due to the following properties:[143] (1) the efficiency of the optimized microwave conditions nearly reached 70% that of conventional PCR; (2) the irradiation energy was used to heat only the PCR solution and not a heating block or the sample containment tube; (3) the temperature ramping time was substantially shortened; (4) the required temperature was reached almost instantaneously and simultaneously,

allowing for shortening of the incubation time; and (5) modern microwave cavities can deliver a uniform field density without “hot-spots”.

1.3.4.2.5 Other Non-contact Heating Methods

Other non-contact heating methods have also been described, such as non-contact heating using a halogen lamp as a low power radiation source for rapid temperature ramping in a silicon micro-reaction chamber.[146] This method achieved a rate of 4 ℃/s for heating and 4 ℃/s for cooling. Another non-con tact heating method is based on induction heating first reported by Pal *et al*.[147] Induction heaters are much simpler to fabricate, and heating and cooling rates of 6.5 and 4.2 ℃/s can be achieved by optimizing the heater dimensions and frequency. The advantage of this method is that accurate positioning of the reaction mixture with respect to the heater is not necessary, deposition steps to pattern thin-film heaters on the chip are not required, and elaborate percentage/integrator/differentiator (PID) control is not needed.[146]

1.4 Analysis Methods of Reaction Products

Following amplification, the identification of amplification products must be performed to read the results and/or to confirm that the correct product was generated. Analysis techniques that can be used should provide short analysis times, high sensitivity and specificity, and favorable LODs. A variety of analysis methods have been successfully demonstrated for microdevice examples, including μCE and DNA microarrays. While there are a number of alternative techniques for reading successful PCRs, we will restrict our discussion to the DNA microarray technique.

1.4.1 DNA Microarrays

DNA microarrays were first developed in the early 1990s[148-150] and have become an important tool for high-throughput DNA analysis. A DNA microarray consists of a

collection of oligonucleotide probes attached to a solid support in an orderly manner, typically a two-dimensional array. The probes readily hybridize to amplified gene fragments (targets) that are complementary to a specific probe. Readout of successful hybridization events is accomplished using a fluorescent dye or other such label attached covalently to the target. The mRNA expression levels or DNA sequence variations from hundreds to thousands of genes can be interrogated simultaneously. A few recent reviews of microarray technology are recommended to interested readers.[151-155]

The basic elements required for the DNA microarray are the solid substrate, the attachment chemistry of the probe to the solid support, the approach adopted to "spot" the probes at particular locations of the 2-dimensional array, the method employed to bring the solution target to the appropriate location of the array (passive or active), and the readout modality. A brief discussion of some of these important elements will be discussed below.

1.4.2 Substrate Materials for Microarray Construction

A variety of solid substrates have been explored for microarrays, such as glass,[156, 157] polymers,[69, 98, 158-166] gold,[167] optical fibers[168] and microbeads.[169, 170] Several issues must be considered in choosing the appropriate substrate, including the level of scattering and fluorescence background generated from the substrate, its chemical stability and complexity, the amenability to modification or derivatization of the substrate, loading capacity, and the degree of non-specific interactions.[156] Glass has been widely adopted as a substrate material due to its favorable optical properties, which are highly desired for signal readout of the microarray using fluorescence. However, the microarray fabrication process involved for glass uses siloxane chemistry to tether

oligonucleotide probes to the glass. These linkages are susceptible to hydrolytic cleavage, especially at extreme pH values. Recently, polymers have been used as alternative microarray substrate materials because of their diverse properties that can be selected to suite different immobilization strategies of probes to the substrate, and the ability to microfabricate structures in a low cost, mass-production mode for single-use applications. Polymers that have been used for microarray applications include PDMS,[158, 159] PC,[69, 98, 160] PMMA,[161-164, 166] and polystyrene.[165]

The use of microbeads as substrates for the immobilization of oligonucleotide probes has also been reported. Fan and co-workers[169] described a dynamic DNA hybridization approach using paramagnetic beads as a transportable solid support. DNA targets were immobilized onto beads via streptavidin-biotin linkages for interrogation with probes that were transported via pneumatic pumping. Their experiment showed that beads containing DNA targets could be sequentially interrogated up to 12 times with no measurable change in the hybridization signal. Ali *et al.*[170] demonstrated a chip-based array composed of avidin-coated agarose microbeads for the discrimination of single-nucleotide mismatches. In their work, the biotinylated oligonucleotide probes containing microbeads were selectively arranged in micromachined cavities localized on silicon wafers, and the fluorophore-conjugated DNA target was a complement to the probe. The microcavities possessed *trans*-wafer openings allowing for both fluid flow through the bead chambers and optical analyses at numerous bead sites. Hybridization times on the order of minutes, with point mutation selectivity factors greater than 10,000 and an LOD of 10^{-13} M were achieved using this microbead array.

1.4.3 Surface Modification for the Immobilization of Probes

Various surface modification strategies have been used to attach probes to different solid supports. Oligonucleotide probes can be electrostatically attached to polylysine-derivatized or amino-silanized glass slides, representing a non-covalent approach.[171] Probes can also be covalently linked to the surface of the array by brief exposure to UV light.[172] Biotinylated DNA probes can be attached to streptavidin-coated magnetic beads,[169] or thiol-terminated oligonucleotide probes can be immobilized to gold.

Methods for the end attachment of chemically modified oligonucleotide probes to a solid substrate have been reported as well. For example, Joos *et al.*[157] developed the covalent attachment of amine-terminated oligonucleotide probes to a glass substrate. Glass slides were derivatized with aminophenyl or aminopropyl silanes, and amine-terminated oligonucleotides were attached to the silanized glass with a crosslinking reagent such as glutardialdehyde. Using this approach, up to 90% of the attached oligonucleotides were available for hybridization.

Lenigk and co-workers[160] demonstrated the use of bi-functional linkers for the immobilization of amine-terminated oligonucleotide probes. In their work, a PC surface was coated with a photosensitive polymer (SurModic's photoreactive reagents) followed by 60 s UV irradiation to generate functional groups that allowed amine-terminated oligonucleotide probes to be covalently attached onto the surface. Detection of four pathogenic bacteria surrogate strains from multiple samples was accomplished using this device.

Wang *et al*.[161] reported the covalent attachment of amine-terminated oligonucleotide probes to a chemically modified PMMA substrate. In their protocol, the PMMA surface was aminated using a *N*-lithioethylenediamine solution, where methyl-ester functional

groups were replaced by *N*-lithioethylenediamine. After aminolysis, the surface was activated with a homo-bi-functional crosslinker, glutardialdehyde, via a Schiff's base reaction and was converted to an aldehyde-terminated surface, which allowed for the covalent attachment of oligonucleotide probes. They found that the oligonucleotide coupling chemistry allowed reuse of the array >12 times without significant hybridization signal loss.

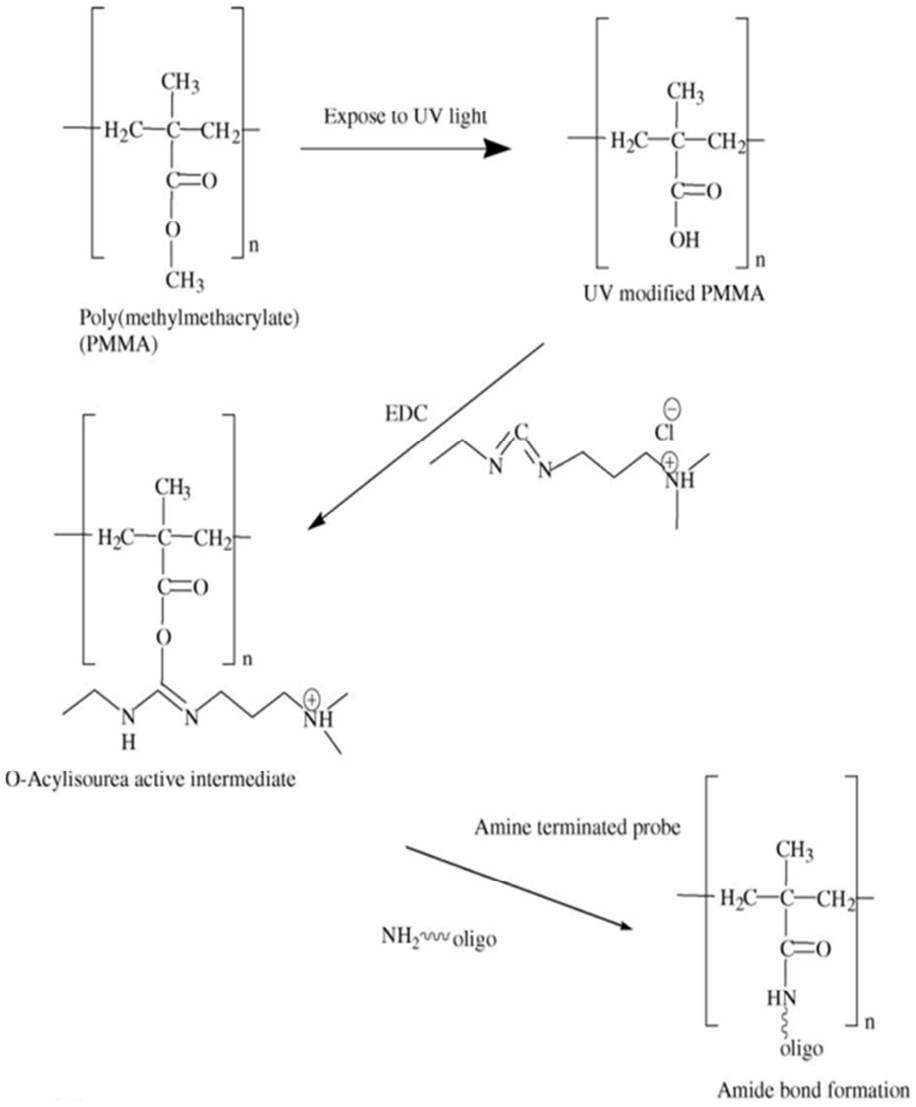

Figure 1.9 UV activation of PMMA forming surface-confined carboxylic acid groups with the subsequent attachment of 5' amine-containing oligonucleotides. Reproduced from [164] with permission.

McCarely *et al*.[173, 174] described a simplified photo-modification protocol of PMMA and PC substrates through direct and controlled UV exposure of the substrates in an oxygen-rich environment to yield surface carboxylic acid moieties. Patterns of carboxylic acid sites could be formed by exposure of the polymers in air at 254-nm with a power density of 15 mW/cm^2 for ~60 min without significant physical damage to the polymer surface. The so-formed chemical patterns allowed for further functionalization to yield arrays or other structured architectures through covalent attachment chemistry.

Soper *et al*.[164] presented the fabrication of DNA microarrays onto PMMA surfaces using a UV modification protocol as shown in **Figure 1.9**. Briefly, the PMMA surface was first activated via exposure to UV irradiation, which produced carboxylic acid functional groups onto its surface. EDC treatment was then used to facilitate the formation of the O-acylisourea reactive intermediates, which allowed for carbodiimide coupling of amine-terminated oligonucleotide probes to the surface via an amide bond. Recently, this same group enhanced the density of surface carboxylate groups by utilizing oxygen plasma treatment to create low density arrays on the surface of a free-standing, air-embedded PMMA waveguide.[163]

1.4.4 Hybridization Efficiency Improvements

Merging microarrays to microfluidics is a step toward building integrated microfluidic systems for genetic analysis. In addition, it can provide significant reductions in target/probe hybridization reaction times resulting from diffusion-limited hybridization kinetics. Compared to a conventional two-dimensional hybridization array in a 1 x 1 cm format, hybridization occurring within a microfluidic channel significantly reduces the diffusional distances between the target molecules and the probes immobilized onto the

surface. Shuttling back-and-forth, the hybridization mixture inside a microchannel can further facilitate mass transport and, thus, reduce hybridization time. Examples demonstrating improvements in hybridization efficiency using microfluidics have been reported.[158, 159, 161, 175-178]

Liu and Rauch[175] investigated DNA hybridization in a microfluidic channel fabricated from a variety of plastic materials. By oscillating the hybridization mixture in the microfluidic channel, maximum signal was observed within a hybridization time of 15 min. Wang *et al*.[161] reported a low density array constructed inside a PMMA microfluidic device and used flow-through feed of the hybridization mixture, which successfully reduced the hybridization time from ~5 h to 1 min and reported an LOD of 10 pM for the identification of low abundance point mutations (one mutant in 10,000 wild-type DNA molecules) found in a K-*ras* oncogene. Erickson *et al*.[158] developed a theoretical model for electrokinetically controlled DNA hybridization in microfluidic devices, which predicted that reducing the height of the microchannel would effectively accelerate the diffusion-limited reaction kinetics and reduce the time required for the hybridization reaction to reach steady state. Following numerical simulations, the experimental results indicated that all processes from sample dispensing to hybridization detection could be completed within 5 min inside a glass–PDMS microchannel with a height of 8 μm. Yuen and co-workers[159] fabricated a microfluidic device consisting of two interconnected reaction chambers molded in PDMS on a standard microscope slide for closed-loop fluidic circulation and mixing. Fluid samples were circulated and mixed by the rotation of a magnetic stirring bar driven by a standard magnetic stirrer. A 2 – 5 fold increase in hybridization efficiency was observed with fluid circulation. Wei *et al*.[176] described the use of discrete sample plugs in a hybrid glass/PMMA microfluidic device for droplet

hybridization (see **Figure 1.10**). In this case, plugs were shuttled back and forth inside a channel sweeping over the probes, which were thoroughly mixed by the natural re-circulating flows, significantly reducing the hybridization reaction volume to 1 µL. The total reaction time was 500 s, and the LOD was 19 amol.

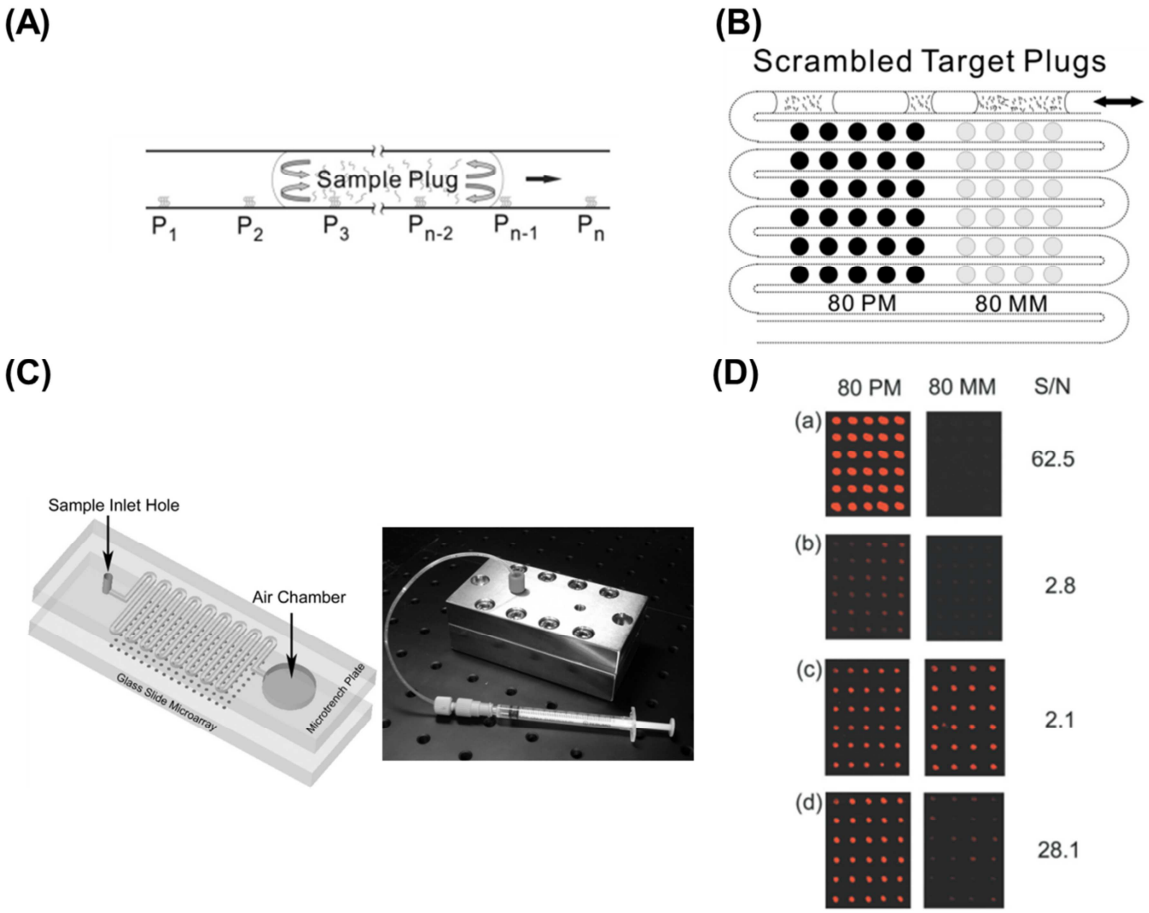

Figure 1.10 (A) Droplet shuttle hybridization in a microchannel. P_1, P_2… P_n refer to the probe spots. (B) Illustration showing that scrambled discrete plugs sweep over different probes in the channel. 80PM and 80MM denote the perfect match and mismatch probes, respectively. (C) Microtrench plate is stacked on a glass microarray slide (right) with a photograph of the assembled device (left). (D) Signal-to-noise (S/N) ratios for various hybridization formats: (a) shuttle hybridization at 500 s, sample volume 1 µL; (b) static microfluidic hybridization at 500 s, sample volume 10 µL; (c) flat glass hybridization at 500 s, sample volume 30 µL; and (d) flat glass hybridization at 18 h, sample volume 30 µL. The target concentration is 90 nM. The left column presents the fluorescence images with 80 PM probe, and the right column presents the fluorescence images with 80 MM probe. Reproduced from [176] with permission.

1.5 Integrated Microfluidic Systems with Microarray Readout

The integration of sample pretreatment with analytical processing steps for the analysis of biological samples has remained the primary goal of micro-Total Analysis Systems (μTAS) as described by Manz and coworkers[14] over two decades ago. Many of these visions are becoming a reality and some of these systems will be described here. As noted previously, genetic analysis systems are defined as a single wafer or a collection of wafers seamlessly interconnected that possess two or more processing steps for the analysis of a genetic sample. Genetic analysis encompasses a large number of different types of applications, for example, DNA forensics where unique genetic markers are used for human identification either at crime scenes or in battlefields. For *in vitro* diagnostics, mutations in certain gene fragments can be detected and used to discover the presence of a disease in a particular patient, and also provide information to the clinician on how to treat that patient. In this section, we will discuss systems that include the sample preprocessing functions followed by microarray readout of the preprocessing steps.

Unitizing the advantages of microchip-based DNA microarrays such as the highly parallel nature of the readout and the ability to screen DNA sequences with high specificity, numerous attempts have been made to incorporate front-end sample processing strategies with DNA microarrays used as the terminal readout step onto a single microfluidic platform. The front-end processing strategies that are needed prior to microarray readout are similar in nature to those required for μCE and are delineated in **Figure 1**. The operational differences, in terms of microsystems using arrays versus μCE include: (1) no need for high voltage power supplies; (2) imaging over relatively larger areas when fluorescence detection is employed (imaging optics versus point

detection of μCE); (3) on-chip heaters to control the temperature of the array depending on the level of hybridization stringency required; and (4) reduced processing times compared to μCE due to the small diffusional distances associated with microfluidics. Several examples of front-end process integration and microarrays to form functional microsystems have been reported in literature.[69, 78, 98, 116, 162, 166, 179-181]

One of the initial microsystems reported was by Anderson *et al*.[69] over a decade ago. A monolithic biochemical processing unit (BPU) was interfaced to a GeneChip commercialized by Affymetrix for performing multi-step molecular processing of genomic samples and included extracting/concentrating of nucleic acids from a serum lysate, amplification (RT-PCR and nested PCR), enzymatic reactions (fragmentation, dephosphorylation, and labeling), metering, mixing and hybridization to the GeneChip. The system was fabricated in PC using conventional computer-controlled micromachining. Temperatures were controlled by pressing thermal elements against the thin wall of the PC cartridge, with Peltier junctions used for heating and cooling. Fluidic manipulation was achieved through the use of a fluid barrier or hydrophobic membrane in conjunction with a pneumatically controlled diaphragm valve and hydrophobic vent. The system performance was evaluated using serum samples loaded with HIV virus. Analysis of the GeneChip results yielded an average accuracy of 99.7%, as determined by independent sequencing.

Liu *et al*.[98] presented a disposable, monolithic device that integrated PCR and DNA microarray. The system was also fabricated in PC using CO_2 laser machining (see **Figure 1.11A**). This system was assembled using a two-step process: (1) First, thermal fusion bonding of PC was performed at 139 ℃ and under 2 tons of pressure for 45 min with a square window for the DNA array left open. Second, following surface activation

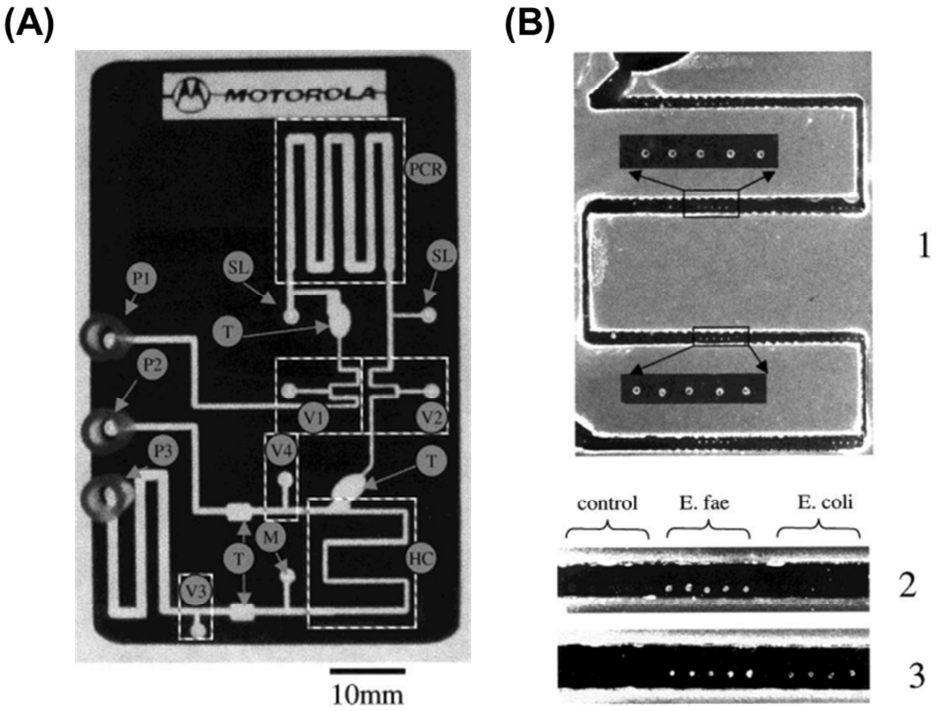

Figure 1.11 (A) Monolithic integrated polycarbonate DNA analysis system. The system contained a serpentine PCR channel (PCR), a hybridization channel (HC), a syringe coupled to a hybridization wash solution channel, a waste channel coupled to a waste syringe, Pluronic traps (T), one hydrophobic air-permeable membrane valve (M), four Pluronics valves (V1 – V4), two PCR reagent loading holes (SL), and three external syringe pumps interfaced to reservoirs–sample driving syringe pump (P1), waste-withdrawing syringe pump (P2), and wash syringe pump (P3). The dimensions of the system were 5.4 cm x 8.6 cm x 0.75 mm. (B) PCR hybridization results from the monolithic integrated system. (1) *E. coli* 221-bp hybridization after amplification. Portions of the channel are enlarged for better viewing. (2) Fluorescent image of portion of the channel after *E. faecalis* amplification and hybridization. (3) Fluorescent image of portion of the channel after multiplex (*E. faecalis* and *E. coli*) amplification and hybridization. Reproduced from [98] with permission.

and oligonucleotide probe immobilization using a Motorola proprietary attachment chemistry through the access window, the window was closed with another piece of properly sized PC using double-sided tape. The bonding was enforced by applying 2 tons of pressure for 2 min, and then the edges were sealed with epoxy. During PCR thermal cycling, the PCR device of the monolithic chip was sandwiched between two Peltier elements to allow thermal processing of the sample, with temperatures being

monitored using thermocouples. Microfluidic control was accomplished through the use of three external syringe pumps docked to the system in combination with four on-chip Pluronics polymer valves and one hydrophobic valve. Asymmetrical PCR amplification and subsequent hybridization analysis of both *E. coli* and *Enterococcus faecalis* was demonstrated. However, the use of PC as the microarray platform generated a significant amount of autofluorescence, which degraded the detection limits for fluorescence readout (see **Figure 1.11B**).

To overcome this problem, Hashimoto *et al.*[162] coupled CF PCR and continuous flow LDR (CF LDR) devices, both fabricated using a PC substrate, with a universal microarray fabricated using a PMMA substrate, which possesses better optical properties with low autofluorescence levels compared to PC (see **Figure 1.12**). The chip was generated via micro-replication (hot embossing) from metal molding tools fabricated using high-precision micromilling. The CF PCR/CF LDR chip was directly attached to thin film heaters for providing the set temperatures for the isothermal zones, with thermocouples embedded between the cover plate and the film heaters for monitoring the set temperatures required for both PCR and LDR. In this work, low density universal microarrays were produced on the bottom floor of a UV-photoactivated PMMA microchannel, with the DNA zipcode probes attached to UV-generated carboxylic acid groups. PCR amplicons were used as templates for the allele-specific CF LDR, which produced single-stranded targets that were uniformly flowed over the universal array to reduce incubation times. Using a mixed population of genomic DNA as starting materials, one mutant in 80 wild-type sequences could be successfully discriminated in a total reaction time of 50 min, including 18.7 min for PCR, 8.1 min for LDR, 5 min for hybridization, 10 min for washing, and 2.6 min for fluorescence imaging

of the low-density array. The authors also showed the ability to reduce reagent consumption by one order of magnitude compared to similar bench-top assays.

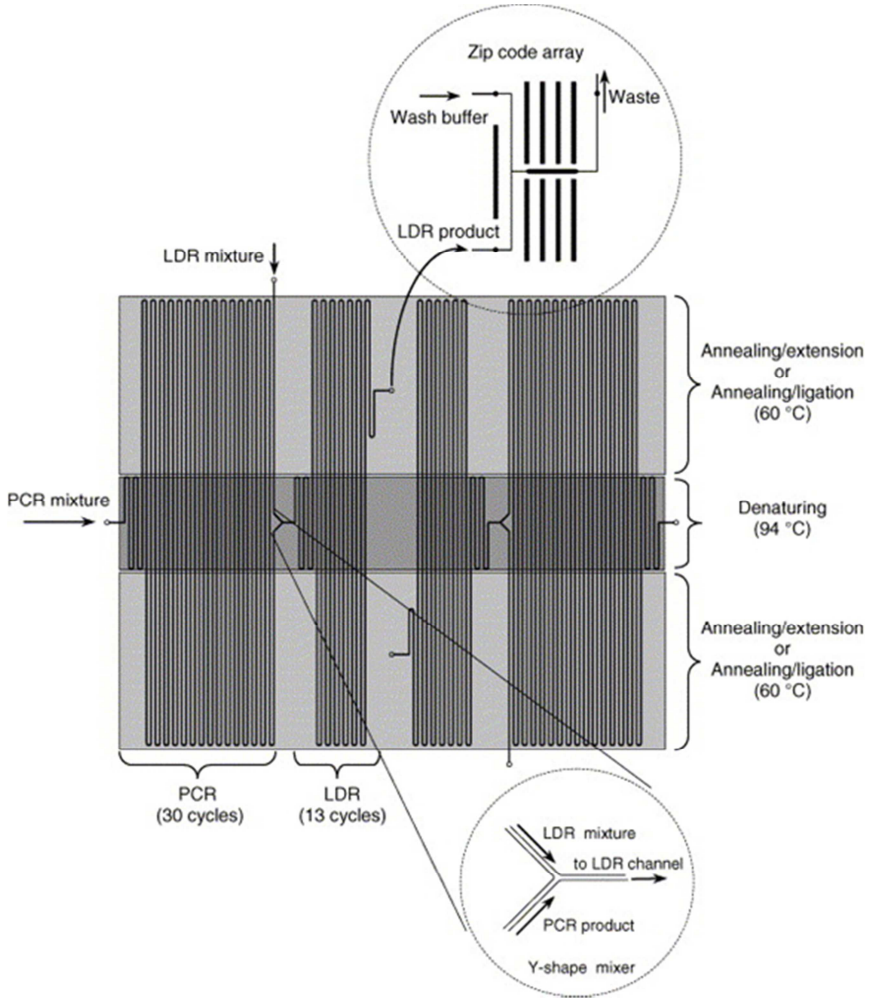

Figure 1.12 Topographical layout of a CF PCR/CF LDR/universal zipcode array biochip. The microchip possessed channels that were 50 µm in width and 100 µm in depth with a 400 µm interchannel spacing. The total length of the thermal cycling channel was 2.28 m and consisted of a 30-cycle PCR (1.57 m long) and a 13-cycle LDR (0.71 m long). The top inset represents a microscope image of the turns of the CF thermal cycling channel. The bottom inset is an enlarged schematic of the Y-shaped passive micromixer for mixing the PCR product with the LDR cocktail. Three different Kapton film heaters were attached to the appropriate positions on the CF PCR/CF LDR chip for providing the required isothermal zones. Thermocouples were inserted between the microchip cover plate and the film heaters for monitoring the temperatures. Reproduced from [162] with permission.

A self-contained biochip that integrated cell isolation and lysis with PCR amplification and electrochemical microarray-based detection was described by Liu *et al*.[181] The chip

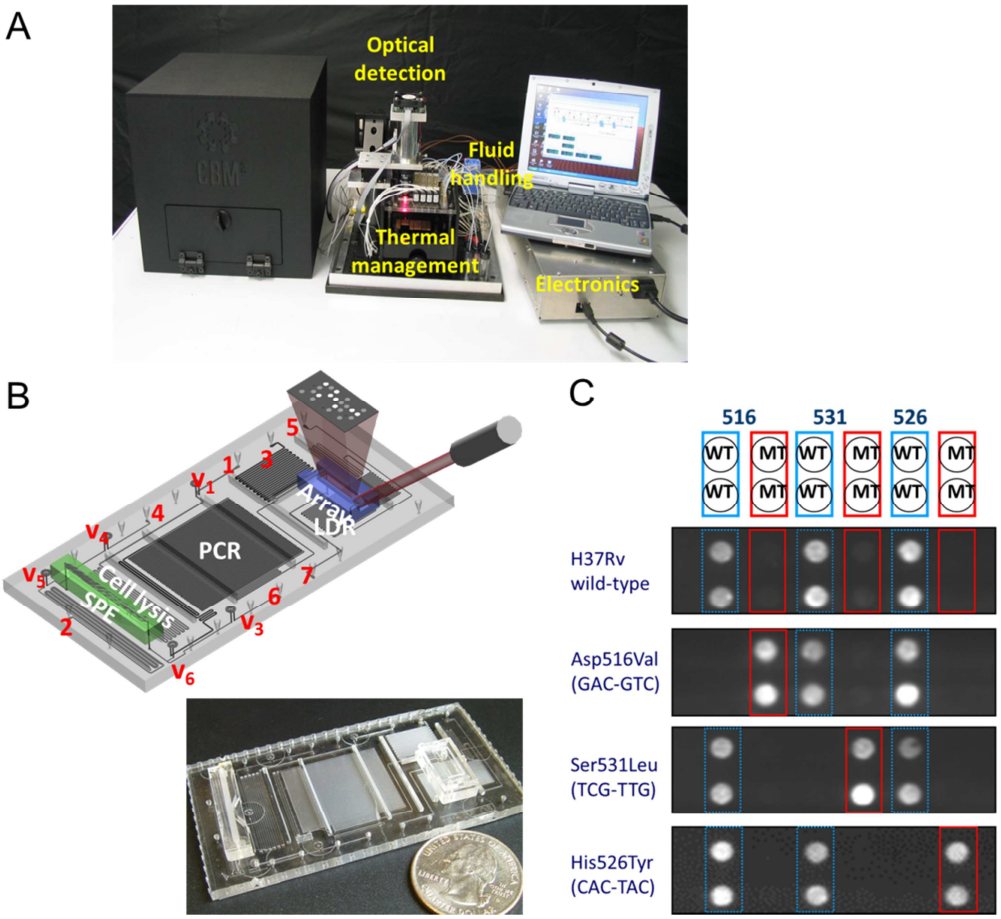

Figure 1.13 Integrated, modular microfluidic chip for TB analysis. (A) Overview of the integrated system. The system had dimensions 12” (length) x 12” (width) x 12” (height), and all fluid handling, thermal management, and optical detection were controlled by off-chip supporting peripherals and assembled into a small form factor instrument. (B) Schematic and photograph of the fluidic cartridge. The fluidic cartridge was composed of two modules and a fluidic motherboard. The fluidic motherboard was made from PC and consisted of processing steps for cell lysis, PCR, and LDR. One module was made from PC and used for SPE of genomic DNA, while the other module was made from PMMA and contained an air-embedded planar waveguide and the DNA array. Sample inlet (1), PCR mixture inlet (2), LDR mixture inlet (3), ethanol and air inlet (4), array wash inlet (5), vacuum connection (6), and waste outlet (7). V1 – V6 are on-chip membrane valves. V2 is positioned next to the SPE module on the cell lysis microchannel and is not visible in current view. (C) Molecular assay results from drug-susceptible *Mycobacterium tuberculosis* (Mtb) strains and drug-resistant Mtb strains. 516WT, 531WT, and 526WT are probes targeting drug-susceptible Mtb strains. 516MT, 531MT, and 526MT are probes targeting drug-resistant Mtb strains. Reproduced from [166] with permission.

was machined in a PC substrate using a conventional computer-controlled milling machine and included a mixing unit for cell capture using immunomagnetic beads, a cell

pre-concentration/purification/lysis/PCR unit, and a DNA microarray chamber. In this work, fluidic components (e.g. paraffin-based microvalves, cavitation microstreaming mixers, and electrochemical or thermopneumatic pumps), embedded resistive heaters, and DNA microarray sensors were coupled to the system to perform DNA analysis of biological samples. Electrical power, PCR thermal cycling, DNA electrochemical signal readout, and magnetic elements for bead arrest were controlled by an off-chip instrument. Implementation of cavitation microstreaming has been shown to achieve cell capture efficiencies on the order of 73% using immunomagnetic beads and up to a 5-fold reduction in hybridization time compared to passive incubation of the array with solution targets, as well as improved signal uniformity. Detection of pathogenic *E. coli* K12 cells seeded into rabbit blood and single-nucleotide polymorphism analysis from diluted blood samples were completed in 3.5 h and 2.7 h, respectively.

Soper *et al.*[166] designed a polymer-based modular microsystem that could accept a crude sample and automatically carry out the entire molecular processing pipeline in an enclosed fluidic cartridge (see **Figure 1.13**). The multi-step assay included bacterial cell lysis, SPE of genomic DNA from the lysate, PCR amplification, LDR, and universal DNA array readout. The fluidic cartridge was generated via micro-replication from the appropriate metal molding tools, which were used to create structures on both sides of the polymer substrate (i.e., double-sided hot embossing). The integrated fluidic cartridge was comprised of a fluidic motherboard and two modules. One module was made from PC and used for SPE, while the other module was made from PMMA and contained DNA probes patterned on a planar waveguide for evanescent excitation. These modules were interconnected to a fluidic motherboard fabricated in PC and were used for processing steps for thermal cell lysis, PCR, and LDR. Fluid handling, thermal

management, and optical detection were controlled by off-chip supporting peripherals, which could be packaged into a small footprint instrument (1 ft^3). Identification of multi-drug resistant tuberculosis (MDR-TB) resulting from *Mycobacterium tuberculosis* (Mtb) strains in clinical sputum samples were demonstrated with a detection limit of ~50 bacterial cells from sputum (processing time <40 min). In addition to MDR-TB detection, the modular fluidic cartridge could be reconfigured for use with other assay formats, such as PCR-μCE.

1.6 Concluding Remarks

There have been extensive reports on devices designed toward to perform a single-step in the analysis of a variety of nucleic acids, such as DNAs and RNAs. These devices have been fabricated using a variety of micro-manufacturing techniques in different substrate materials. Devices have been developed for the SPE of nucleic acids from clinical, environmental, or crime-scene samples employing beads, polymer monoliths, or fabricated pillars to produce the desired solid phase. In addition, a plethora of devices focused on thermal cycling (such as that required for PCR, cycle sequencing, or allele-specific LDR) have been detailed in the literature and typically use either a chamber-type approach, in which the chamber and its contents are cycled between the desired temperatures, or a continuous flow operation, in which isothermal zones are situated on the chip and the reaction fluid is transported through these isothermal zones. Devices have also been reported that perform μCE separation of DNAs using sieving matrices with various channel lengths to reach the desired resolution demanded of the separation. While these represent innovative concepts, the complete analysis of different sample types required for genetic analyses typically requires a number of processing steps (see **Figure 1.1**). Therefore, it is clear that

integration of many of the aforementioned devices to form functional and autonomously operated systems needs to be undertaken. However, process integration to form autonomous systems is not simply a matter of “hooking” together the various devices outlined previously. For example, many of the upstream processing steps and the reagents they require may be detrimental to those poised downstream. Also, some steps demand hydrodynamically driven flow, while others require electrokinetically driven flow. Another concern is unswept volumes, which can generate sample carryover artifacts or sample loss, especially when dealing with ultrasmall sample volumes. Some substrate materials do not accommodate particular processing steps, and high optical quality materials must be used for assays employing fluorescence as the detection mode. Finally, some process steps require thermal control, such as PCR, and these thermally actuated units must be isolated from those that are sensitive to temperature, such as microarrays.

Several examples of integrated microfluidic systems have been presented herein, most of which are proof-of-concept demonstrations with only a few examples that have actually dealt with clinical or “real-world” samples. Unfortunately, many of these demonstrators of integrated microfluidic systems, while attractive in terms of their ability to reduce sample processing time and reagent consumption, have only been utilized in research settings. Some of the more compelling applications for integrated microfluidic systems, such as *in vitro* diagnostics, homeland security, or forensics, will demand systems that can accommodate field analysis and/or one-time use operation. For example, in the case of *in vitro* diagnostics, it will be necessary to use the entire microfluidic system for a single patient sample, demanding that the cost of the chip be low. In addition, field analysis applications will require not only that the chip possesses a

small footprint, but also that the support peripherals must have the same characteristic. These support peripherals include pumps, valves, reagent reservoirs, electronics, and optomechanics if some type of optical readout is used. The chip and support peripherals must all be packaged into small form factor instrument and must consume minimal amounts of power to enable battery operation for extended periods of time. All this must be engineered without sacrificing assay performance in terms of reproducibility, LOD, sensitivity, and specificity.

Another interesting aspect is related to manufacturability of the system. For wide spread commercialization, the fluidic system must be produced in high volume and at low cost. Chip production not only includes the microfabrication of the channel networks, but also chip assembly, integration of various components such as electrodes, optical elements, and valves and, finally, the surface attachment of necessary biologics to effect the desired process step. Although microfluidics has shifted from the use of silicon, glass, and other similar materials that require extensive microfabrication procedures to the use of polymer substrates that can use micro-replication processes (similar to those used to produce CDs and DVDs) to produce the desired fluidic networks in a high production mode with good fidelity, the challenge still remains in chip finishing following production of the fluidic network.

The driving force behind the increasing development of integrated microfluidic systems is certainly due to their potential commercialization, but also in their diverse applications in such areas as biology, chemistry, and other disciplines that strongly demand the emergence of new analysis platforms to achieve higher performance and throughput. Because direct integration of PCR with other sample preparation protocols, including µCE, fluorescence, and microarrays has been demonstrated for a wide range

of applications (pathogen detection, DNA typing, and DNA sequencing), these success stories will demand higher functionality at lower cost and with higher throughput. Such systems offer compelling advantages such as short assay turnaround times, automated operation, improved operator protection, lower cross-contamination, reduced human error, and lower overall assay cost. Minimization of potential carryover contamination from run-to-run is a key consideration in providing accurate and reliable results and the use of disposable fluidic cartridges will effectively minimize this risk.

1.7 References

1. F. S. Collins, M. Morgan and A. Patrinos, *Science*, 2003, **300**, 286-290.

2. M. J. Aboud, M. Gassmann and B. R. McCord, *Electrophoresis*, 2010, **31**, 2672-2679.

3. A. J. Hopwood, C. Hurth, J. Yang, Z. Cai, N. Moran, J. G. Lee-Edghill, A. Nordquist, R. Lenigk, M. D. Estes, J. P. Haley, C. R. McAlister, X. Chen, C. Brooks, S. Smith, K. Elliott, P. Koumi, F. Zenhausern and G. Tully, *Analytical Chemistry*, 2010, **82**, 6991-6999.

4. K. M. Horsman, J. M. Bienvenue, K. R. Blasier and J. P. Landers, *Journal of Forensic Sciences*, 2007, **52**, 784-799.

5. P. Liu, T. S. Seo, N. Beyor, K. J. Shin, J. R. Scherer and R. A. Mathies, *Analytical Chemistry*, 2007, **79**, 1881-1889.

6. T. Chovan and A. Guttman, *Trends in Biotechnology*, 2002, **20**, 116-122.

7. E. Verpoorte, *Electrophoresis*, 2002, **23**, 677-712.

8. J. Khandurina, T. E. McKnight, S. C. Jacobson, L. C. Waters, R. S. Foote and J. M. Ramsey, *Analytical Chemistry*, 2000, **72**, 2995-3000.

9. C. G. Koh, W. Tan, M. Q. Zhao, A. J. Ricco and Z. H. Fan, *Analytical Chemistry*, 2003, **75**, 4591-4598.

10. C. J. Easley, J. M. Karlinsey, J. M. Bienvenue, L. A. Legendre, M. G. Roper, S. H. Feldman, M. A. Hughes, E. L. Hewlett, T. J. Merkel, J. P. Ferrance and J. P. Landers, *Proceedings of the National Academy of Sciences*, 2006, **103**, 19272-19277.

11. R. Pal, M. Yang, R. Lin, B. N. Johnson, N. Srivastava, S. Z. Razzacki, K. J. Chomistek, D. C. Heldsinger, R. M. Haque, V. M. Ugaz, P. K. Thwar, Z. Chen, K. Alfano, M. B. Yim, M. Krishnan, A. O. Fuller, R. G. Larson, D. T. Burke and M. A. Burns, *Lab on a Chip*, 2005, **5**, 1024-1032.

12. A. J. deMello, *Nature*, 2006, **442**, 394-402.

13. D. J. Beebe, G. A. Mensing and G. M. Walker, *Annual Review of Biomedical Engineering*, 2002, **4**, 261-286.

14. A. Manz, N. Graber and H. M. Widmer, *Sensors and Actuators B-Chemical*, 1990, **1**, 244-248.

15. C. W. Kan, C. P. Fredlake, E. A. S. Doherty and A. E. Barron, *Electrophoresis*, 2004, **25**, 3564-3588.

16. A. T. Woolley and R. A. Mathies, *Analytical Chemistry*, 1995, **67**, 3676-3680.

17. D. Schmalzing, A. Adourian, L. Koutny, L. Ziaugra, P. Matsudaira and D. Ehrlich, *Analytical Chemistry*, 1998, **70**, 2303-2310.

18. D. Di Carlo, C. Ionescu-Zanetti, Y. Zhang, P. Hung and L. P. Lee, *Lab on a Chip*, 2005, **5**, 171-178.

19. D. Irimia, R. G. Tompkins and M. Toner, *Analytical Chemistry*, 2004, **76**, 6137-6143.

20. L. C. Waters, S. C. Jacobson, N. Kroutchinina, J. Khandurina, R. S. Foote and J. M. Ramsey, *Analytical Chemistry*, 1998, **70**, 158-162.

21. P. Belgrader, D. Hansford, G. T. A. Kovacs, K. Venkateswaran, R. Mariella, F. Milanovich, S. Nasarabadi, M. Okuzumi, F. Pourahmadi and M. A. Northrup, *Analytical Chemistry*, 1999, **71**, 4232-4236.

22. M. T. Taylor, P. Belgrader, B. J. Furman, F. Pourahmadi, G. T. A. Kovacs and M. A. Northrup, *Analytical Chemistry*, 2001, **73**, 492-496.

23. H. Lu, M. A. Schmidt and K. F. Jensen, *Lab on a Chip*, 2005, **5**, 23-29.

24. S. W. Lee and Y. C. Tai, *Sensors and Actuators a-Physical*, 1999, **73**, 74-79.

25. H. Y. Wang, A. K. Bhunia and C. Lu, *Biosensors & Bioelectronics*, 2006, **22**, 582-588.

26. J. T. Nevill, R. Cooper, M. Dueck, D. N. Breslauer and L. P. Lee, *Lab on a Chip*, 2007, **7**, 1689-1695.

27. A. Abolmaaty, M. G. El-Shemy, M. F. Khallaf and R. E. Levin, *Journal of Microbiological Methods*, 1998, **34**, 133-141.

28. P. Belgrader, W. Benett, D. Hadley, J. Richards, P. Stratton, R. Mariella and F. Milanovich, *Science*, 1999, **284**, 449-450.

29. J. M. Yang, J. Bell, Y. Huang, M. Tirado, D. Thomas, A. H. Forster, R. W. Haigis, P. D. Swanson, R. B. Wallace, B. Martinsons and M. Krihak, *Biosensors & Bioelectronics*, 2002, **17**, 605-618.

30. M. B. Fox, D. C. Esveld, A. Valero, R. Luttge, H. C. Mastwijk, P. V. Bartels, A. van den Berg and R. M. Boom, *Analytical and Bioanalytical Chemistry*, 2006, **385**, 474-485.

31. K. A. Wolfe, M. C. Breadmore, J. P. Ferrance, M. E. Power, J. F. Conroy, P. M. Norris and J. P. Landers, *Electrophoresis*, 2002, **23**, 727-733.

32. H. J. Tian, A. F. R. Huhmer and J. P. Landers, *Analytical Biochemistry*, 2000, **283**, 175-191.

33. M. C. Breadmore, K. A. Wolfe, I. G. Arcibal, W. K. Leung, D. Dickson, B. C. Giordano, M. E. Power, J. P. Ferrance, S. H. Feldman, P. M. Norris and J. P. Landers, *Analytical Chemistry*, 2003, **75**, 1880-1886.

34. L. A. Legendre, J. M. Bienvenue, M. G. Roper, J. P. Ferrance and J. P. Landers, *Analytical Chemistry*, 2006, **78**, 1444-1451.

35. Q. R. Wu, J. M. Bienvenue, B. J. Hassan, Y. C. Kwok, B. C. Giordano, P. M. Norris, J. P. Landers and J. P. Ferrance, *Analytical Chemistry*, 2006, **78**, 5704-5710.

36. J. Wen, C. Guillo, J. P. Ferrance and J. P. Landers, *Analytical Chemistry*, 2007, **79**, 6135-6142.

37. A. Bhattacharyya and C. M. Klapperich, *Analytical Chemistry*, 2006, **78**, 788-792.

38. M. Mahalanabis, H. Al-Muayad, M. D. Kulinski, D. Altman and C. M. Klapperich, *Lab on a Chip*, 2009, **9**, 2811-2817.

39. M. D. Kulinski, M. Mahalanabis, S. Gillers, J. Y. Zhang, S. Singh and C. M. Klapperich, *Biomedical Microdevices*, 2009, **11**, 671-678.

40. A. F. Sauer-Budge, P. Mirer, A. Chatterjee, C. M. Klapperich, D. Chargin and A. Sharon, *Lab on a Chip*, 2009, **9**, 2803-2810.

41. Y. C. Chung, M. S. Jan, Y. C. Lin, J. H. Lin, W. C. Cheng and C. Y. Fan, *Lab on a Chip*, 2004, **4**, 141-147.

42. J. Wen, C. Guillo, J. P. Ferrance and J. P. Landers, *Analytical Chemistry*, 2006, **78**, 1673-1681.

43. L. A. Legendre, C. J. Morris, J. M. Bienvenue, A. Barron, R. McClure and J. P. Landers, *Journal of the Association for Laboratory Automation*, 2008, **13**, 351-360.

44. L. A. Christel, K. Petersen, W. McMillan and M. A. Northrup, *Journal of Biomechanical Engineering-Transactions of the Asme*, 1999, **121**, 22-27.

45. N. C. Cady, S. Stelick and C. A. Batt, *Biosensors & Bioelectronics*, 2003, **19**, 59-66.

46. M. A. Witek, S. D. Llopis, A. Wheatley, R. L. McCarley and S. A. Soper, *Nucleic Acids Research*, 2006, **34**, 9.

47. M. A. Witek, M. L. Hupert, D. S. W. Park, K. Fears, M. C. Murphy and S. A. Soper, *Analytical Chemistry*, 2008, **80**, 3483-3491.

48. D. S. W. Park, M. L. Hupert, M. A. Witek, B. H. You, P. Datta, J. Guy, J. B. Lee, S. A. Soper, D. E. Nikitopoulos and M. C. Murphy, *Biomedical Microdevices*, 2008, **10**, 21-33.

49. J. Kim and B. K. Gale, *Lab on a Chip*, 2008, **8**, 1516-1523.

50. J. Kim, M. Mauk, D. F. Chen, X. B. Qiu, B. Gale and H. H. Bau, *Analyst*, 2010, **135**, 2408-2414.

51. Y. C. Xu, B. Vaidya, A. B. Patel, S. M. Ford, R. L. McCarley and S. A. Soper, *Analytical Chemistry*, 2003, **75**, 2975-2984.

52. H. Wang, J. F. Chen, L. Zhu, H. Shadpour, M. L. Hupert and S. A. Soper, *Analytical Chemistry*, 2006, **78**, 6223-6231.

53. B. M. Paegel, S. H. I. Yeung and R. A. Mathies, *Analytical Chemistry*, 2002, **74**, 5092-5098.

54. R. G. Blazej, P. Kumaresan and R. A. Mathies, *Proceedings of the National Academy of Sciences of the United States of America*, 2006, **103**, 7240-7245.

55. R. D. Oleschuk, L. L. Shultz-Lockyear, Y. B. Ning and D. J. Harrison, *Analytical Chemistry*, 2000, **72**, 585-590.

56. T. Nakagawa, T. Tanaka, D. Niwa, T. Osaka, H. Takeyama and T. Matsunaga, *Journal of Biotechnology*, 2005, **116**, 105-111.

57. W. D. Cao, C. J. Easley, J. P. Ferrance and J. P. Landers, *Analytical Chemistry*, 2006, **78**, 7222-7228.

58. R. K. Saiki, T. L. Bugawan, G. T. Horn, K. B. Mullis and H. A. Erlich, *Nature*, 1986, **324**, 163-166.

59. A. J. DeMello, *Nature*, 2003, **422**, 28-29.

60. R. Higuchi, C. Fockler, G. Dollinger and R. Watson, *Bio-Technology*, 1993, **11**, 1026-1030.

61. R. J. Wiesner, *Nucleic Acids Research*, 1992, **20**, 5863-5864.

62. N. J. Schönbrunner, E. H. Fiss, O. Budker, S. Stoffel, C. L. Sigua, D. H. Gelfand and T. W. Myers, *Biochemistry*, 2006, **45**, 12786-12795.

63. M. A. Innis, K. B. Myambo, D. H. Gelfand and M. A. D. Brow, *Proceedings of the National Academy of Sciences of the United States of America*, 1988, **85**, 9436-9440.

64. M. A. Northrup, M. T. Ching, R. M. White and R. T. Watson, 1993, Proceedings of the 7th International Conference on Solid State and Transducer'93, 97-10 June 1993, Yokohamma, Japan, pp 1924.

65. P. Wilding, J. Pfahler, H. H. Bau, J. N. Zemel and L. J. Kricka, *Clin. Chem.*, 1994, **40**, 43-47.

66. P. Wilding, M. A. Shoffner and L. J. Kricka, *Clin. Chem.*, 1994, **40**, 1815-1818.

67. P. Wilding, M. A. Shoffner, J. Cheng, G. Hvichia and L. J. Kricka, *Clin. Chem.*, 1995, **41**, 1367-1367.

68. S. A. Soper, S. M. Ford, Y. C. Xu, S. Z. Qi, S. McWhorter, S. Lassiter, D. Patterson and R. C. Bruch, *Journal of Chromatography A*, 1999, **853**, 107-120.

69. R. C. Anderson, X. Su, G. J. Bogdan and J. Fenton, *Nucleic Acids Research*, 2000, **28**.

70. M. A. Burns, C. H. Mastrangelo, T. S. Sammarco, F. P. Man, J. R. Webster, B. N. Johnson, B. Foerster, D. Jones, Y. Fields, A. R. Kaiser and D. T. Burke, *Proceedings of the National Academy of Sciences of the United States of America*, 1996, **93**, 5556-5561.

71. A. F. R. Huhmer and J. P. Landers, *Analytical Chemistry*, 2000, **72**, 5507-5512.

72. J. P. Ferrance, Q. R. Wu, B. Giordano, C. Hernandez, Y. Kwok, K. Snow, S. Thibodeau and J. P. Landers, *Analytica Chimica Acta*, 2003, **500**, 223-236.

73. B. C. Giordano, J. Ferrance, S. Swedberg, A. F. R. Huhmer and J. P. Landers, *Analytical Biochemistry*, 2001, **291**, 124-132.

74. B. C. Giordano, E. R. Copeland and J. P. Landers, *Electrophoresis*, 2001, **22**, 334-340.

75. P. Wilding, L. J. Kricka, J. Cheng, G. Hvichia, M. A. Shoffner and P. Fortina, *Analytical Biochemistry*, 1998, **257**, 95-100.

76. Z. Zhao, Z. Cui, D. F. Cui and S. H. Xia, *Sensors and Actuators a-Physical*, 2003, **108**, 162-167.

77. A. T. Woolley, D. Hadley, P. Landre, A. J. deMello, R. A. Mathies and M. A. Northrup, *Analytical Chemistry*, 1996, **68**, 4081-4086.

78. D. Trau, T. M. H. Lee, A. I. K. Lao, R. Lenigk, I. M. Hsing, N. Y. Ip, M. C. Carles and N. J. Sucher, *Analytical Chemistry*, 2002, **74**, 3168-3173.

79. E. T. Lagally, C. A. Emrich and R. A. Mathies, *Lab on a Chip*, 2001, **1**, 102-107.

80. J. Liu, C. Hansen and S. R. Quake, *Analytical Chemistry*, 2003, **75**, 4718-4723.

81. Q. B. Zou, Y. B. Miao, Y. Chen, U. Sridhar, C. S. Chong, T. C. Chai, Y. Tie, C. H. L. Teh, T. M. Lim and C. Heng, *Sensors and Actuators a-Physical*, 2002, **102**, 114-121.

82. Q. B. Zou, U. Sridhar, Y. Chen and J. Singh, *IEEE Sensors Journal*, 2003, **3**, 774-780.

83. W. C. Dunn, S. C. Jacobson, L. C. Waters, N. Kroutchinina, J. Khandurina, R. S. Foote, M. J. Justice, L. J. Stubbs and J. M. Ramsey, *Analytical Biochemistry*, 2000, **27**, 157.

84. Y. Matsubara, K. Kerman, M. Kobayashi, S. Yamamura, Y. Morita and E. Tamiya, *Biosensors and Bioelectronics*, 2005, **20**, 1482-1490.

85. C. G. Koh, W. Tan, M. Q. Zhao, A. J. Ricco and Z. H. Fan, *Analytical Chemistry*, 2003, **75**, 6379-6379.

86. C. J. Easley, J. M. Karlinsey and J. P. Landers, *Lab on a Chip*, 2006, **6**, 601-610.

87. M. U. Kopp, A. J. de Mello and A. Manz, *Science*, 1998, **280**, 1046-1048.

88. N. Chiem and D. J. Harrison, *Analytical Chemistry*, 1997, **69**, 373-378.

89. M. Hashimoto, P. C. Chen, M. W. Mitchell, D. E. Nikitopoulos, S. A. Soper and M. C. Murphy, *Lab on a Chip*, 2004, **4**, 638-645.

90. P. C. Chen, D. E. Nikitopoulos, S. A. Soper and M. C. Murphy, *Biomedical Microdevices*, 2008, **10**, 141-152.

91. P. C. Chen, D. S. Park, B. H. You, N. Kim, T. Park, S. A. Soper, D. E. Nikitopoulos and M. C. Murphy, *Sensors and Actuators B-Chemical*, 2010, **149**, 291-300.

92. D. S. W. Park, P. C. Chen, B. H. You, N. Kim, T. Park, T. Y. Lee, P. Datta, Y. Desta, S. A. Soper, D. E. Nikitopoulos and M. C. Murphy, *Journal of Micromechanics and Microengineering*, 2010, **20**.

93. D. S. Park, H. Wang, P.-C. Chen, T. Park, N. Kim, B. H. You, D. E. Nikitopoulos, S. A. Soper and M. C. Murphy, 2010, Proceedings of the 14th International Conference on Miniaturized Systems for Chemistry and Life Sciences, 13-17 October 2010, Groningen, Netherlands, p1126.

94. S. H. I. Yeung, P. Liu, N. Del Bueno, S. A. Greenspoon and R. A. Mathies, *Analytical Chemistry*, 2009, **81**, 210-217.

95. J. West, B. Karamata, B. Lillis, J. P. Gleeson, J. Alderman, J. K. Collins, W. Lane, A. Mathewson and H. Berney, *Lab on a Chip*, 2002, **2**, 224-230.

96. M. G. Roper, C. J. Easley and J. P. Landers, *Analytical Chemistry*, 2005, **77**, 3887-3893.

97. J. F. Chen, M. Wabuyele, H. W. Chen, D. Patterson, M. Hupert, H. Shadpour, D. Nikitopoulos and S. A. Soper, *Analytical Chemistry*, 2005, **77**, 658-666.

98. Y. Liu, C. B. Rauch, R. L. Stevens, R. Lenigk, J. Yang, D. B. Rhine and P. Grodzinski, *Analytical Chemistry*, 2002, **74**, 3063-3070.

99. M. Curcio and J. Roeraade, *Analytical Chemistry*, 2002, **75**, 1-7.

100. N. Park, S. Kim and J. H. Hahn, *Analytical Chemistry*, 2003, **75**, 6029-6033.

101. J. Liu, M. Enzelberger and S. Quake, *Electrophoresis*, 2002, **23**, 1531-1536.

102. D. J. Sadler, R. Changrani, P. Roberts, C. F. Chou and F. Zenhausern, *Ieee Transactions on Components and Packaging Technologies*, 2003, **26**, 309-316.

103. A. W. Chow, *AIChE Journal*, 2002, **48**, 1590-1595.

104. W. Zheng and S. Chen, Continuous-flow submicroliter-scale PCR chip for DNA amplification, 2001.

105. I. Schneegass and J. M. Kohler, *J Biotechnol*, 2001, **82**, 101-121.

106. M. L. Hupert, M. A. Witek, Y. Wang, M. W. Mitchell, X. Liu, Y. Bejat, D. E. Nikitopoulos, J. Goettert, M. C. Murphy and S. A. Soper, Polymer-based microfluidic devices for biomedical applications, 2003.

107. M. W. Mitchell, X. Liu, Y. Bejat, D. E. Nikitopoulos, S. A. Soper and M. C. Murphy, Modeling and validation of a molded polycarbonate continuous-flow polymerase chain reaction devic, 2003.

108. Z. Chen, S. Qian, W. R. Abrams, D. Malamud and H. H. Bau, *Analytical Chemistry*, 2004, **76**, 3707-3715.

109. M. Krishnan, V. M. Ugaz and M. A. Burns, *Science*, 2002, **298**, 793.

110. S. Chandrasekhar, *Hydrodynamic and Hydromagnetic Stability*, Clarendon Press, 1961.

111. C. S. Zhang, J. L. Xu, W. L. Ma and W. L. Zheng, *Biotechnology Advances*, 2006, **24**, 243-284.

112. M. Q. Bu, T. Melvin, G. Ensell, J. S. Wilkinson and A. G. R. Evans, *Journal of Micromechanics and Microengineering*, 2003, **13**, S125-S130.

113. E. T. Lagally, J. R. Scherer, R. G. Blazej, N. M. Toriello, B. A. Diep, M. Ramchandani, G. F. Sensabaugh, L. W. Riley and R. A. Mathies, *Analytical Chemistry*, 2004, **76**, 3162-3170.

114. D. S. Lee, S. H. Park, H. S. Yang, K. H. Chung, T. H. Yoon, S. J. Kim, K. Kim and Y. T. Kim, *Lab on a Chip*, 2004, **4**, 401-407.

115. D. S. Lee, M. H. Wu, U. Ramesh, C. W. Lin, T. M. Lee and P. H. Chen, *Sensors and Actuators B-Chemical*, 2004, **100**, 401-410.

116. T. M. H. Lee, M. C. Carles and I. M. Hsing, *Lab on a Chip*, 2003, **3**, 100-105.

117. I. Rodriguez, M. Lesaicherre, Y. Tie, Q. B. Zou, C. Yu, J. Singh, L. T. Meng, S. Uppili, S. F. Y. Li, P. Gopalakrishnakone and Z. E. Selvanayagam, *Electrophoresis*, 2003, **24**, 172-178.

118. C. F. Chou, R. Changrani, P. Roberts, D. Sadler, J. Burdon, F. Zenhausern, S. Lin, A. Mulholland, N. Swami and R. Terbrueggen, *Microelectronic Engineering*, 2002, **61-2**, 921-925.

119. S. Poser, T. Schulz, U. Dillner, V. Baier, J. M. Kohler, D. Schimkat, G. Mayer and A. Siebert, *Sensors and Actuators a-Physical*, 1997, **62**, 672-675.

120. P. Belgrader, S. Young, B. Yuan, M. Primeau, L. A. Christel, F. Pourahmadi and M. A. Northrup, *Analytical Chemistry*, 2001, **73**, 286-289.

121. K. Sun, A. Yamaguchi, Y. Ishida, S. Matsuo and H. Misawa, *Sensors and Actuators B-Chemical*, 2002, **84**, 283-289.

122. T. Fukuba, T. Yamamoto, T. Naganuma and T. Fujii, *Chemical Engineering Journal*, 2004, **101**, 151-156.

123. N. A. Friedman and D. R. Meldrum, *Analytical Chemistry*, 1998, **70**, 2997-3002.

124. H. Yang, C. A. Choi, K. H. Chung, C. H. Jun and Y. T. Kim, *Analytical Chemistry*, 2004, **76**, 1537-1543.

125. C. J. Bruckner-Lea, T. Tsukuda, B. Dockendorff, J. C. Follansbee, M. T. Kingsley, C. Ocampo, J. R. Stults and D. P. Chandler, *Analytica Chimica Acta*, 2002, **469**, 129-140.

126. N. C. Cady, S. Stelick, M. V. Kunnavakkam and C. A. Batt, *Sensors and Actuators B: Chemical*, 2005, **107**, 332-341.

127. A. M. Chaudhari, T. M. Woudenberg, M. Albin and K. E. Goodson, *Journal of Microelectromechanical Systems*, 1998, **7**, 345-355.

128. I. Erill, S. Campoy, J. Rus, L. Fonseca, A. Ivorra, Z. Navarro, J. A. Plaza, J. Aguilo and J. Barbe, *Journal of Micromechanics and Microengineering*, 2004, **14**, 1558-1568.

129. P. Grodzinski, R. H. Liu, B. Chen, J. Blackwell, Y. Liu, D. Rhine, T. Smekal, D. Ganser, C. Romero, H. Yu, T. Chan and N. Kroutchinina, *Biomedical Microdevices*, 2001, **3**, 275-283.

130. P. J. Obeid, T. K. Christopoulos, H. J. Crabtree and C. J. Backhouse, *Analytical Chemistry*, 2003, **75**, 288-295.

131. X. Zhou, D. Liu, R. Zhong, Z. Dai, D. Wu, H. Wang, Y. Du, Z. Xia, L. Zhang, X. Mei and B. Lin, *Electrophoresis*, 2004, **25**, 3032-3039.

132. A. Gulliksen, L. Solli, F. Karlsen, H. Rogne, E. Hovig, T. Nordstrøm and R. Sirevåg, *Analytical Chemistry*, 2003, **76**, 9-14.

133. P. Sethu and C. H. Mastrangelo, *Sensors and Actuators B: Chemical*, 2004, **98**, 337-346.

134. K. Shen, X. Chen, M. Guo and J. Cheng, *Sensors and Actuators B: Chemical*, 2005, **105**, 251-258.

135. M. N. Slyadnev, Y. Tanaka, M. Tokeshi and T. Kitamori, *Analytical Chemistry*, 2001, **73**, 4037-4044.

136. R. P. Oda, M. A. Strausbauch, A. F. R. Huhmer, N. Borson, S. R. Jurrens, J. Craighead, P. J. Wettstein, B. Eckloff, B. Kline and J. P. Landers, *Analytical Chemistry*, 1998, **70**, 4361-4368.

137. C. T. Wittwer, G. C. Fillmore and D. R. Hillyard, *Nucleic Acids Research*, 1989, **17**, 4353-4357.

138. C. T. Wittwer, G. C. Fillmore and D. J. Garling, *Analytical Biochemistry*, 1990, **186**, 328-331.

139. S. A. Soper, S. M. Ford, Y. Xu, S. Qi, S. McWhorter, S. Lassiter, D. Patterson and R. C. Bruch, Nanoliter-scale sample preparation methods directly coupled to PMMA-based microchips and gel-filled capillaries for the analysis of oligonucleotides, 1999.

140. H. Swerdlow, B. J. Jones and C. T. Wittwer, *Analytical Chemistry*, 1997, **69**, 848-855.

141. Q. Wang and H. Gong, An integrated software solution for real-time PCR analysis based on microfluidic biochip, 2003.

142. Y. Tanaka, M. N. Slyadnev, A. Hibara, M. Tokeshi and T. Kitamori, *Journal of Chromatography A*, 2000, **894**, 45-51.

143. C. Fermér, P. Nilsson and M. Larhed, *European Journal of Pharmaceutical Sciences*, 2003, **18**, 129-132.

144. K. Orrling, P. Nilsson, M. Gullberg and M. Larhed, *Chemical Communications*, 2004, 790-791.

145. J. Dietrich, P. Schmitt, M. Zieger, B. Preve, J.-L. Rolland, H. Chaabihi and Y. Gueguen, *FEMS Microbiology Letters*, 2002, **217**, 89-94.

146. C. Ke, H. Berney, A. Mathewson and M. M. Sheehan, *Sensors and Actuators B-Chemical*, 2004, **102**, 308-314.

147. D. Pal and V. Venkataraman, *Sensors and Actuators A: Physical*, 2002, **102**, 151-156.

148. S. P. A. Fodor, J. L. Read, M. C. Pirrung, L. Stryer, A. T. Lu and D. Solas, *Science*, 1991, **251**, 767-773.

149. S. P. A. Fodor, R. P. Rava, X. H. C. Huang, A. C. Pease, C. P. Holmes and C. L. Adams, *Nature*, 1993, **364**, 555-556.

150. M. Schena, D. Shalon, R. W. Davis and P. O. Brown, *Science*, 1995, **270**, 467-470.

151. G. A. Churchill, *Nature Genetics*, 2002, **32**, 490-495.

152. M. J. Heller, *Annual Review of Biomedical Engineering*, 2002, **4**, 129-153.

153. S. Venkatasubbarao, *Trends in Biotechnology*, 2004, **22**, 630-637.

154. A. C. Syvanen, *Nature Genetics*, 2005, **37**, S5-S10.

155. J. D. Hoheisel, *Nature Reviews Genetics*, 2006, **7**, 200-210.

156. Z. Guo, R. A. Guilfoyle, A. J. Thiel, R. F. Wang and L. M. Smith, *Nucleic Acids Research*, 1994, **22**, 5456-5465.

157. B. Joos, H. Kuster and R. Cone, *Analytical Biochemistry*, 1997, **247**, 96-101.

158. D. Erickson, X. Z. Liu, U. Krull and D. Q. Li, *Analytical Chemistry*, 2004, **76**, 7269-7277.

159. P. K. Yuen, G. S. Li, Y. J. Bao and U. R. Muller, *Lab on a Chip*, 2003, **3**, 46-50.

160. R. Lenigk, R. H. Liu, M. Athavale, Z. J. Chen, D. Ganser, J. N. Yang, C. Rauch, Y. J. Liu, B. Chan, H. N. Yu, M. Ray, R. Marrero and P. Grodzinski, *Analytical Biochemistry*, 2002, **311**, 40-49.

161. Y. Wang, B. Vaidya, H. D. Farquar, W. Stryjewski, R. P. Hammer, R. L. McCarley, S. A. Soper, Y. W. Cheng and F. Barany, *Analytical Chemistry*, 2003, **75**, 1130-1140.

162. M. Hashimoto, F. Barany and S. A. Soper, *Biosensors & Bioelectronics*, 2006, **21**, 1915-1923.

163. F. Xu, P. Datta, H. Wang, S. Gurung, M. Hashimoto, S. Wei, J. Goettert, R. L. McCarley and S. A. Soper, *Analytical Chemistry*, 2007, **79**, 9007-9013.

164. C. Situma, Y. Wang, M. Hupert, F. Barany, R. L. McCarley and S. A. Soper, *Analytical Biochemistry*, 2005, **340**, 123-135.

165. S. R. Rasmussen, M. R. Larsen and S. E. Rasmussen, *Analytical Biochemistry*, 1991, **198**, 138-142.

166. M. L. Hupert, H. Wang, H.-W. Chen, P.-C. Chen, W. Stryjewski, D. Patterson, M. A. Witek, P. Datta, J. Goettert, M. C. Murphy and S. A. Soper, 2008, Proceedings of the 12th International Conference on Miniaturized Systems for Chemistry and Life Sciences, 12-16 October 2008, San Diego, California, USA, pp 1946.

167. A. Csaki, R. Moller, W. Straube, J. M. Kohler and W. Fritzsche, *Nucleic Acids Research*, 2001, **29**.

168. S. Ahn and D. R. Walt, *Analytical Chemistry*, 2005, **77**, 5041-5047.

169. Z. H. Fan, S. Mangru, R. Granzow, P. Heaney, W. Ho, Q. P. Dong and R. Kumar, *Analytical Chemistry*, 1999, **71**, 4851-4859.

170. M. F. Ali, R. Kirby, A. P. Goodey, M. D. Rodriguez, A. D. Ellington, D. P. Neikirk and J. T. McDevitt, *Analytical Chemistry*, 2003, **75**, 4732-4739.

171. M. Schena, D. Shalon, R. Heller, A. Chai, P. O. Brown and R. W. Davis, *Proceedings of the National Academy of Sciences of the United States of America*, 1996, **93**, 10614-10619.

172. V. G. Cheung, M. Morley, F. Aguilar, A. Massimi, R. Kucherlapati and G. Childs, *Nature Genetics*, 1999, **21**, 15-19.

173. R. L. McCarley, B. Vaidya, S. Y. Wei, A. F. Smith, A. B. Patel, J. Feng, M. C. Murphy and S. A. Soper, *J. Am. Chem. Soc.*, 2005, **127**, 842-843.

174. S. Y. Wei, B. Vaidya, A. B. Patel, S. A. Soper and R. L. McCarley, *Journal of Physical Chemistry B*, 2005, **109**, 16988-16996.

175. Y. J. Liu and C. B. Rauch, *Analytical Biochemistry*, 2003, **317**, 76-84.

176. C. W. Wei, J. Y. Cheng, C. T. Huang, M. H. Yen and T. H. Young, *Nucleic Acids Research*, 2005, **33**.

177. G. G. Yaralioglu, I. O. Wygant, T. C. Marentis and B. T. Khuri-Yakub, *Analytical Chemistry*, 2004, **76**, 3694-3698.

178. J. Vanderhoeven, K. Pappaert, B. Dutta, P. Vanhummelen, G. V. Baron and G. Desmet, *Electrophoresis*, 2004, **25**, 3677-3686.

179. S. W. Yeung, T. M. H. Lee, H. Cai and I. M. Hsing, *Nucleic Acids Research*, 2006, **34**.

180. S. S. W. Yeung, T. M. H. Lee and I. M. Hsing, *Analytical Chemistry*, 2008, **80**, 363-368.

181. R. H. Liu, J. N. Yang, R. Lenigk, J. Bonanno and P. Grodzinski, *Analytical Chemistry*, 2004, **76**, 1824-1831.

CHAPTER 2 IDENTIFICATION OF METHICILLIN-RESISTANT *STAPHYLOCOCCUS AUREUS* USING AN INTEGRATED AND MODULAR MICROFLUIDIC SYSTEM

2.1 Introduction

Molecular testing is of significant importance in diagnostics and prognostics of numerous diseases and in recognizing variation that can influence response to therapy.[1-3] These tests can be accomplished using a number of task-specific instruments and typically consists of the following set of processing steps: (1) cell lysis and target extraction/purification from other cellular components (e.g. cell debris and proteins) that may interfere with downstream processing; (2) amplification of trace amounts of nucleic acids to produce sufficient copy numbers to aid in detection; and (3) analysis of unique sequence variations within certain genes to provide the proper clinical information. To complete an entire assay, a well-equipped laboratory and significant technical expertise are commonly required with operator intervention required at several stages of the processing pipeline. In addition, the total time required for sample processing can be several hours to several days. These operational characteristics have hampered the implementation of molecular testing into resource limited settings, which has resulted in the limited usage of these valuable techniques.[4]

Derived from the concept of micro-total analysis systems or lab-on-a-chip platforms first proposed by Manz *et al.*[5] in the early 1990s, the emergence of integrated microfluidic systems, which incorporate several molecular processing steps into a single microfluidic platform with sample-in-answer-out capabilities, are particularly attractive for automated, fast and cost-effective genotyping. These systems can incorporate many of the sample processing steps into a single system and negate the need for extensive operator expertise and minimize the amount of equipment required to carry out the

analysis. In addition, when configured with the support peripherals, the instrument can be designed to operate directly at the point-of-care, even in resource limited environments.[6]

Several demonstrations of integrated microfluidic systems for DNA analyses have been described.[7-10] Many of these reports utilized microfluidic structures fabricated in glass, silicon or glass polymer hybrids and thus, required direct photolithographic processing steps to manufacture the desired structures incorporated into the fluidic network. This production format leads to rather complicated fabrication processes and as such, generates challenges for meeting the demanding of low-cost systems that can be produced in a high production mode for realizing one-time use chips, a requirement in many clinical applications.

Thermoplastic materials have been explored as alternatives to glass or silicon for the production of microfluidic platforms.[11] The development of suitable polymer manufacturing techniques, such as hot embossing and injection molding, can generate high quantities of chips at low costs. Several groups have reported polymeric microfluidic systems for carrying out nucleic acid analysis. For example, a disposable monolithic microsystem, which integrated PCR and DNA microarrays, was described by Liu *et al*.[12] The chip was fabricated in PC using CO_2 laser milling with an asymmetrical PCR amplification step employed. The system was demonstrated for the analysis of both *E. coli* and *Enterococcus faecalis*. Liu and coworkers fabricated a self-contained biochip with integrated cell isolation and lysis units, PCR amplification and electrochemical microarray detection for sample-to-answer DNA analyses.[13] The system was machined into a PC substrate and was capable of detecting *E. coli* in 3.5 h. Klapperich's group developed a low-cost chip system for the analysis of bacterial DNA

using a substrate consisting of cyclic olefin copolymer, COC, with the fluidic structures directly milled into the COC chip.[14] The system contained functional devices for cell lysis, DNA isolation and purification, PCR and end-point fluorescence detection. Wang and coworkers[15] reported a magnetic bead-based system fabricated using a polydimethylsiloxane substrate, which combined DNA extraction and isothermal amplification of the targets followed by optical analysis utilizing a spectrophotometer. The system was used to perform a loop-mediated isothermal amplification and to detect *Staphylococcus aureus* with a limit-of-detection (LOD) of ~10 fg/µL of target DNA.

While the above examples of polymer-based systems are attractive in demonstrating the utility of using thermoplastics for generating low-cost integrated systems for DNA processing, however, extensive post-processing steps were required after fabrication of the desired fluidic microstructures, which can significantly add to the cost of chip production. Examples of post-fabrication processing steps included the lithographic patterning of electrodes onto the fluidic chip,[12] need of priming the chip with a buffer,[14] integration of wax-based valves,[12] or the addition of magnetic beads.[13, 15] Another challenge is the use of PC as the microarray, which can generate a significant amount of autofluorescence[16] degrading the detection limits for fluorescence readout. Also, PC can also produce large levels of non-specific adsorption.[17]

S. aureus is identified as a human normal commensal and can cause a variety of diseases ranging from minor skin infection to fatal pneumonia or septicemia.[18, 19] Shortly after the introduction of methicillin in the 1960s, MRSA strains have become a major cause of hospital-acquired infection. In recent years, CA-MRSA infections are on the rise and can result in illnesses more severe than HA-MRSA.[20-22] It is estimated that MRSA-related infections associated with death are approximately 19,000 annually in the

U.S alone. Apart from their high mortality rate, MRSA is estimated to cause $3-4 billion of additional health care costs per year.[23] In 2005, the U.S. press described MRSA as a "superbug" that killed more people than did AIDS.[24] In addition, MRSA has been identified as one of the two most out-of-control antimicrobial-resistant pathogens in U.S. hospitals.[25] Therefore, the rapid and reliable detection of MRSA strains is crucial not only for infection control but also for patient treatment at early stages.

MRSA detection typically uses culturing techniques, which requires 2-3 days to identify an MRSA culture. Methicillin resistance in *S. aureus* is mediated by the *mecA* gene, which encodes a penicillin binding protein 2a called PBP2a with a low affinity of binding to beta-lactam antibiotics.[26-28] Nucleic Acid Amplification Tests (NAATs) that can identify MRSA by interrogating the drug resistant-related signature gene (*mecA*) presents a promising opportunity for rapid drug resistance screening. Reported literatures related to NAATs-based detection of MRSA have predominately used the amplification of the *mecA* gene in conjunction with a *S. aureus*-specific gene, such as *nuc*, *coa*, *femB*, *Sa442*.[29-32] However, these tests are unable to distinguish MRSA from nonsterile clinical specimens (e.g. nasal swabs) due to the coexistence of *S. aureus* and coagulase-negative *Staphylococci* (CNS) (e.g. *S. epidermidis*); up to 80% of strains carry the *mecA* gene,[21, 33] which can lead to false-positive results.

To address the aforementioned issues, we constructed an integrated modular-based microfluidic system for the rapid and efficient identification of MRSA with high specificity. The microfluidic system could carry out all of the molecular processing steps in a single disposable fluidic cartridge. The unique aspect of this fluidic cartridge was that it used a modular approach with task-specific modules interconnected to a fluidic motherboard with the material of the modules and motherboard selected to optimize the processing

step performance. In addition, to minimize the amount of finishing steps associated with the fluidic cartridge, many of the functional elements were produced during the polymer molding step used to create the fluidic network. The fluidic cartridge was capable of performing a multi-step assay including continuous flow PCR amplification of specific gene fragments, continuous flow LDR to generate fluorescent ligation products containing zip-code complement sequences that directed the ligation products to a specific location of a two-dimensional array, and a universal DNA array, which consisted of DNA zip-code probes patterned onto a planar polymer waveguide for evanescent excitation.

The cartridge was comprised of one functional module poised on a fluidic motherboard stacked in a 3-dimensional configuration. On the basis of material properties selected to optimize the module operation and meeting manufacturing requirements, the motherboard was made from PC and used for two thermal cycling processes, PCR and LDR, due to its relatively high glass transition temperature to allow it to withstand the sustained high operating temperatures required for the thermal reactions. The module was made from PMMA and contained an air-embedded planar waveguide and the DNA microarray because PMMA has significantly lower amounts of autofluorescence compared to PC[16] as well as minimal non-specific adsorption artifacts.[17]

The fluidic cartridge was generated via micro-replication from the appropriate metal molding tools, which were used to create structures on both sides of the polymer substrate (*i.e.*, double-sided hot embossing). Fluid handling (e.g. pumps, valves, etc.), thermal management (e.g. heaters, temperature sensors, etc.) and optical readout hardware were located off-chip and packaged into a small footprint instrument. Only the

fluidic cartridge was in contact with the sample, which eliminated any potential carryover contamination.

To demonstrate the utility of the modular system, MRSA analysis was carried out using a multiplexed PCR/LDR assay coupled to a universal zip-code array with four representative strains, methicillin-susceptible *S. aureus* (MSSA), MRSA, methicillin-susceptible *S. epidermidis* (MS-CNS) and methicillin-resistance *S. epidermidis* (MR-CNS). The multiplexed PCR described in this work used five sets of specific primers to target SG16S, *spa*, *femA*, PVL and *mecA* genes followed by a multiplexed LDR that was used to minimize false-positive results. The integrated system was further demonstrated to be capable of detecting a mixture of MSSA and MR-CNS strains, which are common commensal organisms found in clinical samples, for the presence of *S. aureus* bacteria and determining their drug susceptibility status.

2.2 Experimental

2.2.1 Reagents

PC and PMMA sheets used as the fluidic substrates were purchased from Good Fellow (Berwyn, PA). Chemicals used for the PMMA surface modification and hybridization assays included 1-ethyl-3-(3-dimethylaminopropyl) carbodiimide hydrochloride (EDC), *N*-hydroxysuccinimide (NHS) and 20x SSC buffer (3 M sodium chloride, 0.3 M sodium citrate, pH 7.0), which were purchased from Sigma-Aldrich (St. Louis, MO). A 10% sodium dodecyl sulfate (SDS) stock solution, which was used for post-hybridization washing, was received from Ambion (Austin, TX). Disodium hydrogen phosphate (Na_2HPO_4), sodium phosphate (Na_3PO_4), and 2-propanol were obtained from Sigma-Aldrich (St. Louis, MO). Oligonucleotide primers and probes were obtained from Integrated DNA Technologies (Coralville, IA). Their sequences and melting

temperatures (T_m) are listed in **Table 2.1**. All solutions were prepared in nuclease free water purchased from Invitrogen Corporation (Carlsbad, CA).

2.2.2 Fabrication of the Fluidic Cartridge

The modular fluidic cartridge consisted of one module and a motherboard (see **Figure 2.1A**); the motherboard made from PC was used for two thermal reactions, PCR and LDR, while the module fabricated in PMMA contained DNA probes spotted on an air-embedded waveguide that used evanescent excitation for fluorescence readout. The PMMA module was interconnected to the PC motherboard using short pieces of Tefzel™ tubing (OD = 1/16", ID = 250 µm, Upchurch) inserted between conically-shaped holes placed on the backsides of both the motherboard and module to provide a leak-free interconnection.

The PC motherboard was replicated using double-sided hot embossing from two brass molding tools mounted opposite to each other on a JENOPTIK HEX02 hot embossing machine (Jena, Germany). Brass mold masters were used to create microstructures on the PC substrate and contained microchannels for PCR and LDR on the frontside of the substrate and thermal isolation grooves[34] and conical interconnectors on the backside. The mold masters were fabricated using high-precision micromilling.[35] The layout of the PC motherboard is depicted in **Figure 2.1A**. The dual-depth serpentine channel, which consisted of 32 cycles for PCR and 15 cycles for LDR was 80 µm in width and 80/240 µm in depth and was designed to prolong the residence time in the extension/ligation zone by increasing the channel cross-section causing a net decrease in the linear flow rate in these zones. The fluid access channels (DNA sample and LDR mixture) were 200 µm in width and 240 µm in depth. The PC

motherboard was assembled by thermal fusion bonding the substrate and a PC cover plate (250 µm thick) placed in a convection oven at 150 ℃ for 20 min.

The PMMA module was assembled from two hot-embossed PMMA parts; one consisted of a 100 µm deep microchannel for the universal microarray on the frontside and a 1.2 mm x 10 mm air-embedded planar waveguide with an integrated prism on the backside (see **Figure 2.1B**). Located on the backside were also positioned conical ports for fluidic connections to the PC motherboard. The air-embedded waveguide was double-sided hot embossed into the PMMA substrate via micro-replication from two brass molding tools. Twenty-four (4 x 6) waveguide modules could be replicated on one PMMA wafer.

PMMA surface modification for amine modified oligonucleotide zip-code probe attachment was carried out using a previously published protocol,[36-38] which is schematically illustrated in **Scheme 2.1**. Briefly, surface carboxylic acids were generated by placing PMMA substrates in the vacuum chamber of a Technics Series 8000 micro-reactive ion etcher (Surplus Process Equipment Corp., Santa Clara, CA) for 1 min using a 200 mTorr oxygen pressure and a 50 W radio frequency. Then, the PMMA substrates were incubated in a coupling buffer containing 50 mg/mL EDC and 5 mg/mL NHS in MES (2-(N-morpholino)ethanesulfonic acid) buffer (pH 6.0) for 10 min to form succinimidyl ester intermediates, which can react with amine-terminated oligonucleotide probes (3'-end) to form a stable amide bond. The 3'-amino-modified oligonucleotide zip-code probes (see **Table 2.1** for sequences) were dissolved in 200 mM Na_2HPO_4/Na_3PO_4 buffer (pH 9.0) to a final concentration of 50 µM and were dispensed on the activated PMMA surface using a Perkin-Elmer Piezorray® non-contact

(A)

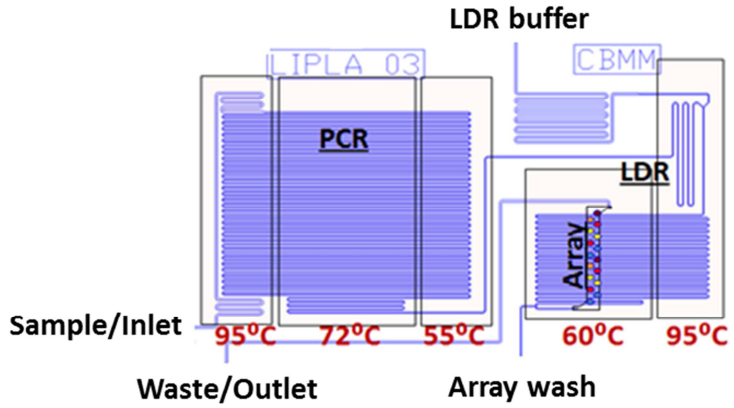

(B)

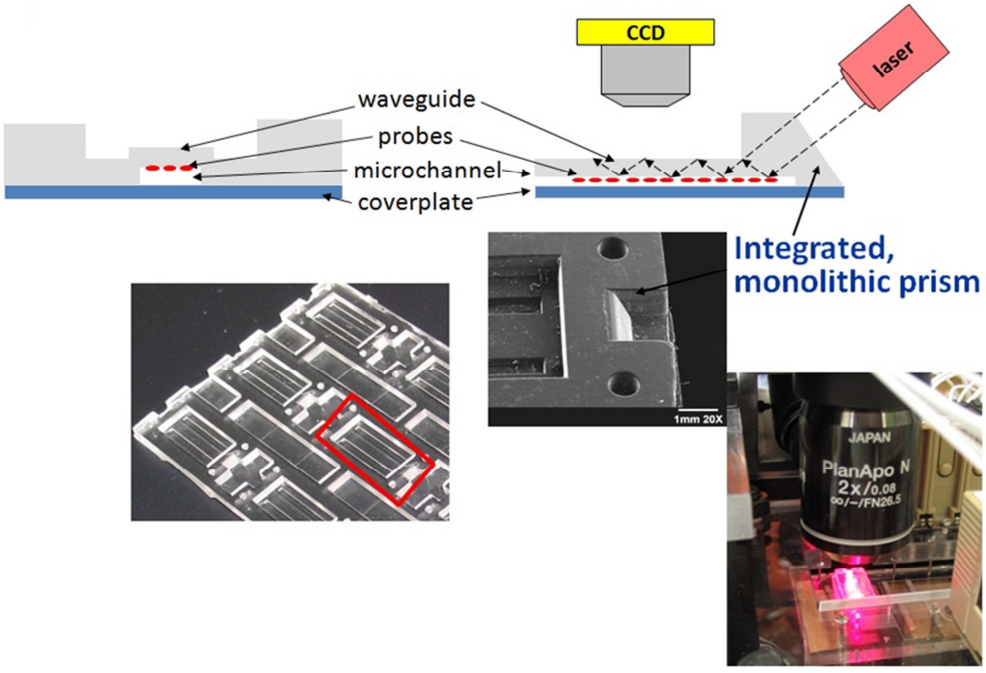

Figure 2.1 Integrated microfluidic system for MRSA Identification. (A) Schematic of the fluidic cartridge. The fluidic cartridge was composed of one module and a fluidic motherboard. The motherboard was made from PC and consisted of processing steps for PCR and LDR, while the module was made from PMMA and contained an air-embedded planar waveguide in which a DNA microarray was spotted onto. (B) Layout of the PMMA module (right picture) consisting of the air-embedded waveguide, a coupling prism and the DNA universal array. The waveguide and coupling prism (see center picture) were located on the backside of the module and the frontside contained the fluidic channel, which had as its floor the waveguide. DNAs could be spotted (see picture on the top) onto the waveguide using a conventional spotter prior to thermal fusion bonding the cover plate to this module's substrate. Optical setup (left picture) was composed of a laser diode and a CCD imaging sensor. Excitation of the array probes was achieved through the evanescent field produced by a waveguide underneath microfluidic channel with spotted probes. Fluorescence signal of the array was collected in a single exposure and imaged onto a CCD through two 2x objectives.

microarraying instrument (Downers Grove, IL). Dispensing volumes per spot were 330 ±30 pL and the size of spots were ~150 µm in diameter. After incubation in a humidified chamber at room temperature for 4 h, the spotted PMMA substrates were washed with 0.1% SDS to remove non-specifically adsorbed oligonucleotides and stored at 4℃ until used for the measurements. Following spotting of the DNA probes onto the waveguide, the waveguide and the interconnection wafer were assembled together using a thermal annealing method at 107 ℃ for 20 min.

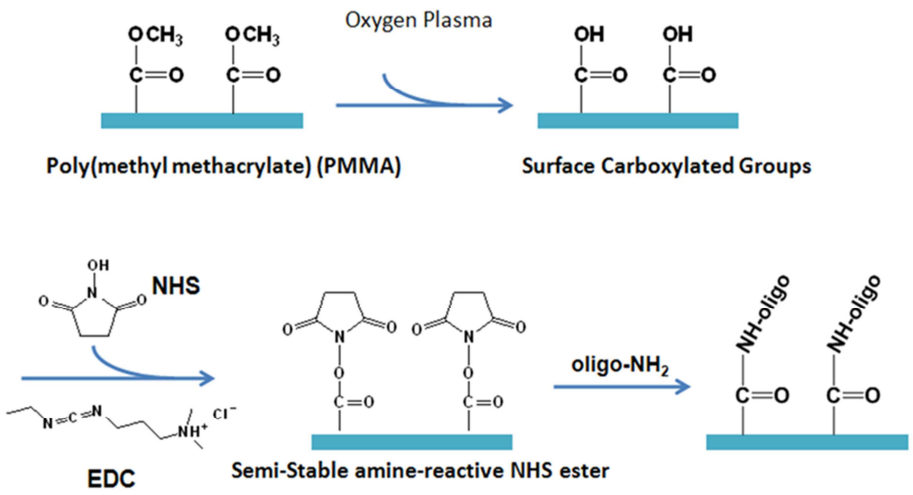

Scheme 2.1 The procedure of PMMA surface modification and oligonucleotide probe immobilization. The plasma-modification process for DNA microarray fabrication involved three steps; (1) oxygen plasma exposure of the polymer surface; (2) EDC/NHS treatment to facilitate the formation of the succinimidyl ester intermediate; and (3) carbodiimide coupling of amine-terminated oligonucleotide probes to the activated PMMA surface (via an amide bond).

2.2.3 Contact Angle Measurements

Water contact angle measurements were used to probe the effect of oxygen plasma exposure on the PMMA surface. Substrates (2.54 cm x 1.27 cm x 0.25 cm) were cut from a commercial PMMA sheet. After oxygen plasma treatment, contact angle values of the PMMA surfaces were measured using a VCA 2000 contact angle system

equipped with a CCD camera (VCA, Billerica, MA) based on the sessile drop method. Approximately 2 µL of deionized water was placed on the PMMA surface using a syringe and the contact angle of the water droplet was measured immediately using the software provided by the manufacturer. The measurements were repeated at least three times at separate positions on each sample surface. The data points represent the mean of three measurements with the error bars showing ±1 standard deviation.

2.2.4 X-ray Photoelectron Spectroscopy

PMMA sheets (1 cm x 1 cm x 0.25 cm) treated under the chamber pressure range of 50 – 300 mTorr were analyzed with an Axis 165 X-ray photoelectron spectrometer (Kratos Analytical) using a monochromatized X-ray source (Al Kα 1486.6 eV) with a power of 150 W. The binding energy scale was calibrated to $Au4f_{7/2b}$ = 84.0 eV. The base pressure was 2 x 10^{-10} Torr and the operating pressure was 2 x 10^{-9} Torr. The photoelectron takeoff angle was 90° (with respect to the sample surface). Survey and high-resolution spectra were obtained using pass energies of 160 and 20 eV, respectively. The neutralizer was turned on during the analysis to compensate for any possible charge effects on the insulating polymer surfaces. Core level binding energies for C1s and O1s were determined by referencing the methyl carbons to 285.0 eV and carbonyl oxygens to 532.2 eV.[39] Curve fitting of the high-resolution spectra of the pristine and oxygen plasma-modified PMMA was performed using asymmetric 70% Gaussian and 30% Lorentzian component profiles after subtraction of the baseline using a linear background.

Table 2.1 Sequences of oligonucleotides used in the PCR/LDR/universal zip-code hybridization assay for MRSA

PCR product size (bp)	Oligos	Sequence (5'→3')	T_m (℃) [e]
148	mecA-forward	TGGTATGTGGAAGTTAGATTGG	51.2
	mecA-reverse	ATATGCTGTTCCTGTATTGGC	52.8
	mecA-com	[a]pATTCCTGGAATAATGACGCTA–Cy5[b]	51.2
	cZip1-mecA	[c]**GCTGAGGTCGATGCTGAGGTCGCA**ATGTATGCTTTGGTCTTTCTGC	69.2
	Zip-code 1	TGCGACCTCAGCATCGACCTCAGC–sp-NH_2[d]	64.9
98	spa-forward	CATTACTTATATCTGGTGGCG	50.6
	spa-reverse	GTTAGGCATATTTAAGACTTG	46.5
	spa-com	[a]pTTGCGCAGCATTTGCAG–Cy5[b]	54.9
	cZip21-spa	[c]**GGTCAGGTTACCGCTGCGATCGCA**TTTTGTTGAGCTTCATCGTG	69.0
	Zip-code 21	TGCGATCGCAGCGGTAACCTGACC–sp-NH_2[d]	65.3
161	SG16S-forward	TGGAGCATGTGGTTTAATTCGA	54.7
	SG16S-reverse	TGCGGGACTTAACCCAACA	56.8
	SG16S-com	[a]pTTGGTAAGGTTCTTCGCG–Cy5[b]	52.5
	cZip25-SG16S	[c]**GGTCTACCTACCCGCACGATGGTC**GAGTTGTCAAAGGATGTCAAGAT	68.8
	Zip-code 25	GACCATCGTGCGGGTAGGTAGACC–sp-NH_2[d]	62.7
172	femA-foward	CAACTCGATGCAAATCAGCAA	54.1
	femA-reverse	GAACCGCATAGCTCCCTGC	58.6
	femA-com	[a]pATAATTAATCCGTTTGAAGTAGTTT–Cy5[b]	49.0
	cZip15-femA	[c]**CGCATACCAGGTCGCATACCGGTC**CCATCTCTGCTGGCTTCTTT	71.0

Table 2.1 Continued

	Zip-code 15	GACCGGTATGCGACCTGGTATGCG–sp-NH_2[d]	63.5
176	PVL-forward	ACACACTATGGCAATAGTTATTT	50.2
	PVL-reverse	AAAGCAATGCAATTGATGTA	48.4
	PVL-com	[a]pGAGTTTTCCAGTTCACTTCATATT–Cy5[b]	51.3
	cZip5-PVL	[c]**GCTGTACCCGATCGCAAGGTGGTC**TTATGTCCTTTCACTTTAATTTCAT	66.5
	Zip-code 5	GACCACCTTGCGATCGGGTACAGC–sp-NH_2[d]	63.7

[a] p: phosphorylated.
[b] Cy5: λ_{ex} = 649 nm, λ_{em} = 670 nm.
[c] The bold sequences are complementary to the sequences of zip-code probes.
[d] sp-NH_2: $(CH_2CH_2O)_6PO_4$-NH_2.
[e] Conditions: oligo concentration, 1 µM; Na^+ concentration, 50 mM.

2.2.5 PCR and LDR

DNA samples including MSSA (ATCC 25923D-5), MRSA (ATCC BAA-1556D-5), MS-CNS (ATCC 12228D-5) and MR-CNS (ATCC 35984D-5) were all purchased from American Type Culture Collection (Manassas, VA). The sequences of oligonucleotide primer pairs used for the PCR and LDR are listed in **Table 2.1**.[40-42] The targets included SG16S, *spa*, *femA*, PVL and *mecA* genes. The PCR mixture consisted of 10 mM Tris-HCl (pH 8.3), 50 mM KCl, 1.5 mM $MgCl_2$, 200 µM dNTPs, 0.5 µg/µL ultra-pure bovine serum albumin (BSA), 0.5 µM of each primer, and 0.1 U/µL *Taq* DNA polymerase (New England Biolabs, Beverly, MA). The LDR mixture contained 20 mM Tris-HCl (pH 7.6), 25 mM KCl, 5 mM $MgCl_2$, 10 mM DTT, 1 mM NAD^+ (a cofactor for ligase enzyme), 0.1% Triton X-100, 0.5 µg/µL ultra-pure BSA, 50 nM of each discriminating primer, 100 nM of each Cy5-labeled common primer, and 2 U/µL *Taq* DNA ligase (New England Biolabs, Beverly, MA). Off-chip PCR and LDR were performed using a commercial thermal cycler (Techne, Burlington, NJ) with the same assay conditions as a control. PCR amplicons were subjected to electrophoresis on a 3% ethidium bromide-prestained agarose gel at 5 V/cm for 30 min. The gel image was captured using Gel Logic 200 Visualizer (Carestream Molecular imaging, New Haven, CT). LDR products were separated using a Beckman CEQ8000 capillary genetic analysis system (Beckman Coulter, Fullerton, CA). Data acquisition was performed using the Beckman software.

2.2.6 Operational Protocol of the Fluidic Cartridge

Prior to analysis, the fluidic cartridge was loaded with the PCR mixture containing the DNA sample and the LDR reaction mixture into individual storage reservoirs (see **Figure 2.1A**). It was then aligned using a fluidic distribution board-to-motherboard stainless steel interconnects and pressed against Cu heating blocks surface covered

with thermal conductive tap to provide good thermal contact. This ensured both tight fluidic connections and proper heat transfer. In the next step, the PCR mixture was pumped out of the storage reservoir through the PCR thermal reactor. After 15 min, the LDR mixture was introduced through the fluidic cartridge at the appropriate volumetric flow rate and was mixed with the PCR products. Mixing was achieved using a passive Y-shaped micromixer, which consisted of 80 μm wide and 80 μm deep inlet and outlet channels, with the mixing ratio of PCR amplicons to the LDR mixture set at 1 to 1. The reaction mixture was then processed through the LDR thermal reactor and further through the array module and finally to waste. The array was flushed with a wash buffer (2x SSC, 0.1% SDS) and DNA hybridization events were imaged using a compact optical reader, which consisted of a laser diode (HL6320G, 10 mW, Hitachi) and a CCD image sensor (S7030-0907; 512 x 58 pixels; 24 x 24 μm/pixel; Hamamatsu), with a 12 mm x 3 mm field-of-view using an integration time of 20 s. The reader was composed of two 2x microscope objectives (PLAPON 2x, Olympus), a 3RD660LP long pass filter and 3RD660-680 band pass filter (Omega Optics, Brattleboro, VT).

Excitation of the array was achieved through the evanescent field produced by the waveguide serving as the floor to the microfluidic channel housing the universal array. The laser light was coupled into the waveguide via a 64° prism. Both the waveguide and coupling prism were incorporated into the array microchip and fabricated using the same embossing step that was used for making the fluidic network.

In this work, we used continuous flow thermal cycling for several reasons including its ability to provide ultrafast cycling times ultimately limited by the kinetic rate of dNTP incorporation by the polymerase and the lack of valves required to contain the PCR mixture during thermal cycling as is required for batch-type thermal cyclers.[34, 43, 44] The

temperatures for the continuous flow PCR (CF PCR) were set at 95 ℃ for denaturation, 55 ℃ for annealing and 72 ℃ for extension. As for the continuous flow LDR (CF LDR), the temperatures were set at 95 ℃ for denaturation and 60 ℃ for ligation. Commercial polyimide (KAPTON®) heaters were used to deliver heat to the PCR and LDR thermal reactors. Heaters were attached to 2 mm thick Cu blocks to achieve uniform heat flux and distribution. Temperatures were controlled by type K thermocouples (CHAL-005, Omega Engineering, USA) placed in microgrooves milled into the Cu blocks. An integral part of the heat management of the fluidic chip were thermal isolation grooves formed on the backside of the PC motherboard during the embossing process, which allowed for efficient thermal isolation between adjacent reaction zones.[34]

2.3 Results and Discussion

MRSA is a leading cause of infections in U.S. hospitals and healthcare facilities. In recent years, community-acquired MRSA (CA-MRSA) infections have caused additional concern.[45-48] It has been reported that MRSA strains carrying the Panton-Valentine leukocidin (PVL) virulence gene have been associated with an increase in severe skin infections and a new syndrome of community-associated necrotizing pneumonia in children.[42, 49] The PVL virulent determinant has been considered an important and stable marker for CA-MRSA. Consequently, in addition to methicillin resistance screening, the present work described an approach for the simple and rapid discrimination between HA-MRSA and CA-MRSA in addition the differentiation between MSSA and MRSA.

The assay employed in this work consisted of a multiplexed PCR followed by a multiplexed LDR with readout via a low-density universal array configured on a waveguide. The optimization of CF PCR, CF LDR and surface functionalization

chemistries were investigated followed by the evaluation of the integrated system for analyzing MRSA samples.

2.3.1 Optimization of Multiplexed CF PCR and CF LDR

We have demonstrated ultra-fast PCR that could amplify 500 bp fragments from a λDNA template in 1.7 min.[43] Using a continuous flow (CF) format, the thermal load in the device was reduced to the sample itself and the amplification was pushed to the enzymatic incorporation rate limit. Compared to single-plex PCR from the λDNA template, optimizing the multiplexed PCR from real genomic DNA samples in CF PCR devices presents two challenges: (1) different hybridization efficiencies among multiple PCR primer sets can introduce biased exponential amplification and alter the initial relative abundance of the target sequence. In some extreme cases, some target fragments are not amplified due to the competition for *Taq* polymerase and dNTPs. The speed of PCR is limited by the balance of hybridization among multiple primers instead of the enzymatic incorporation rate. (2) Compared to the λDNA template, the 2.8 Mbp *S. aureus* genome further complicates PCR reaction by imposing a larger amount of background DNA burden.[50] We therefore investigated the effects of different combinations of multiple PCR primers on hybridization efficiencies in terms of the product yields.

We carefully evaluated primer pairs from the literature[40-42] and chose five sets of primers, which targeted five markers, including: the SG16S gene, which is specific to the *Staphylococcus* genus; the *spa* gene, which is specific to *S. aureus*; the *femA* gene, which is specific to *S. epidermidis*; the PVL gene, which is associated to community acquired MSSA/MRSA and the *mecA* gene, which is a determinant of methicillin resistance. Five sets of PCR primers against these targets were combined in the same

reaction mixture and they can interfere with each other during PCR amplification. Before optimizing the five-plex PCR, single-plex PCRs were performed using four representative strains including MSSA, MRSA, MS-CNS and MR-CNS. Each individual PCR yielded fragments of the expected sizes, 98, 148, 161, 172 and 176 bp for the *spa*, *mecA*, SG16S, *femA* and PVL genes, respectively (data not shown). The annealing temperature tested for the 5-plex PCR ranged from 50 – 60 ℃ and was individually evaluated using a gradient thermal cycler. An optimal annealing temperature of 55 ℃ was selected for the five targets.

We next investigated the effects of flow rate on the PCR product yield. **Figure 2.2** shows the PCR products generated from the CF PCR device at volumetric flow rates of 0.25, 0.5 and 1 µL/min (0.65, 1.30 and 2.60 mm/s). The fluorescence intensities from the PCR product gel bands obtained from the CF PCR were analyzed using ImageQuant software and were normalized with respect to those from a bench-top PCR thermal cycler and the results are shown in **Figure 2.2B**. The results indicate the product yield of the CF PCR became larger as the flow rate was reduced. For the *mecA* gene, the product yield of the CF PCR at a volumetric flow rate of 0.25 µL/min was 44% of the reference PCR, higher than 10% at a volumetric flow rate of 1 µL/min. The lower product yield at 1 µL/min, which roughly provided 4 s for denaturation, 4 s for annealing and 16.2 s for extension, matched our previous experiments[43] and the lower yield was most likely due to insufficient residence time in the extension zone because this is the rate limiting step with this set by the rate of dNTP incorporation by the polymerase. Although the CF PCR produced the lower product yield at 1 µL/min, the cycling rate of 29.6 s/cycle was much shorter as compared to 118 s/cycle required at 0.25 µL/min. The lower overall yield of the CF PCR compared to the commercial thermal cycler even at

the optimal linear velocity may come from the fact that the higher surface-to-volume ratio of the microchannel as compared to a 200-µL PCR tube that provided more probability for the *Taq* polymerase to adsorb on the microchannel walls.

As demonstrated in **Figure 2.2**, the faster the flow rate of sample through the CF PCR device, the less amount of product that was generated due to reduced residence time in the extension zone. However, faster flow rates can reduce the total analysis time. Therefore, it was necessary to balance processing speed with the limit-of-detection required. A volumetric flow rate of 0.5 µL/min was chosen because it provided adequate PCR and LDR product yields for analysis. CF PCR were performed at a volumetric flow rate of 0.5 µL/min provided a cycling rate of 59.2 s/cycle (8 s for denaturation, 8 s for annealing, 32.4 s for extension and 10.8 s), completing the 32 cycles for PCR in 31.6 min.

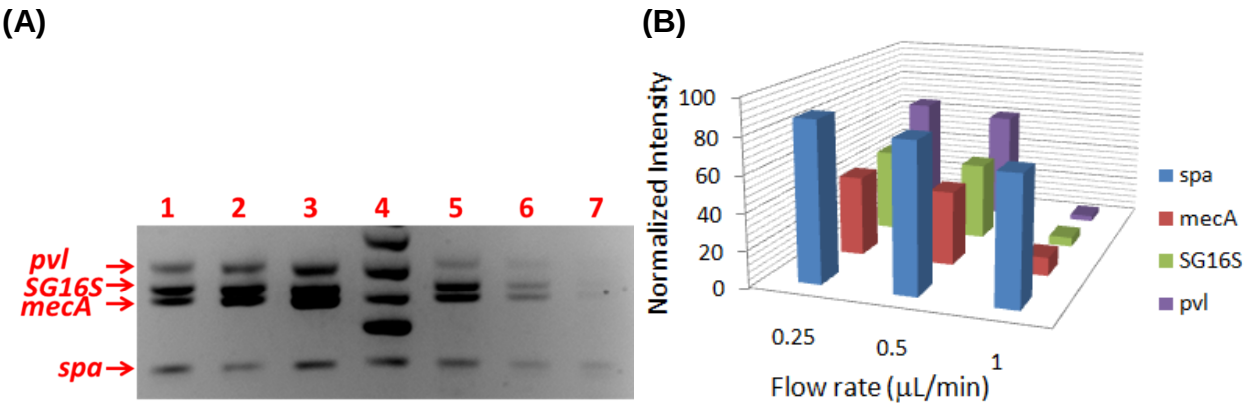

Figure 2.2 Effects of flow rate on the CF PCR product yield using the representative MRSA strain. (A) Agarose gel electrophoresis of CF PCR products. Lane 4: DNA size marker. Lanes 5 – 7: CF PCR products at various volumetric flow rates of 0.25, 0.5 and 1 µL/min (0.66, 1.33 and 2.65 mm/s), respectively. Lanes 1 – 3: bench-top PCR using the same conditions as CF PCR. (B) Intensities from CF PCR product gel bands normalized to that from the bench-top PCR products. CF PCR yielded amplicons of the expected size, *i.e.*, 98, 148, 161 and 176 bp for the *spa*, *mecA*, SG16S and PVL genes, respectively.

The multiplexed LDR is fairly straightforward due to two factors: (1) the large amount of templates, *i.e.* PCR products, are readily available and (2) LDR is a linear amplification process, which is less effected by the hybridization efficiency difference among multiple LDR primers compared to exponential PCR amplification. A detailed investigation of effects of flow rates on the LDR product yields was reported.[51] Our previous studies have shown that the amount of time required for ligation in a microfluidic device can have an impact on the LDR product yield. A significant amount of LDR product could be generated at the ligation time of ~5 s. However, as with PCR, the shorter ligation time (~5) showed reduced LDR product yield. In this work, the CF LDR was operated at a volumetric flow rate of 1 µL/min, which provided a cycling rate of 30 s/cycle (3 s for denaturation and 27 s for ligation), producing a processing time of 7.5 min for 15 cycles.

2.3.2 Characterization of Oxygen Plasma-modified PMMA Surfaces

In our protocol, PMMA sheets were subjected to an oxygen plasma treatment for the generation of surface carboxylic groups that allowed covalent attachment of amine-terminated oligonucleotide zip-code probes to these surface groups through carbodiimide coupling. The modification process is believed to be the creation of free radicals on the polymer surface and then subsequent coupling of these free radicals with active species from the oxygen plasma environment.[52] Oxygen plasma treatment of the PMMA sheets resulted in the sample surfaces becoming hydrophilic, which can be monitored using sessile water contact angle measurements.[53] Changes in the water-contact angles of the oxygen plasma treated PMMA surfaces under varied chamber pressures are summarized in **Table 2.2**. As can be seen from this data, there was a rapid decrease in the contact angle of the samples treated in the pressure range from

50 to 200 mTorr. This decrease in the contact angle could be attributed to the incorporation of polar functional groups, which caused the plasma-irritated PMMA surfaces to become more hydrophilic.[52, 54] When the chamber pressure was further increased from 200 to 300 mTorr, the contact angle actually increased from 53.7° to 65.3°. This was most likely due to the decreased activated oxygen species associated with high rates of recombination and collisional quenching at high pressure.[55] The concentration of species is proportional to the pressure. The higher the pressure the shorter the mean free path an active species can travel before having a collision quenching its activity. From the results, we can conclude as the chamber pressures increased, the PMMA surfaces became richer in oxygen-containing functional groups, leading to hydrophilic surfaces. In contrast, the plasma-irritated surfaces obtained at high pressure containing only a small amount of activated oxygen species was less hydrophilic, resulting in a larger contact angle than anticipated.

Table 2.2 Chemical compositions of the PMMA substrates before and after oxygen plasma treatment

Pressure (mTorr)	C 1s (Atomic conc., %)	O 1s (Atomic conc., %)	O/C	Water contact angle (°)
0	74.03	25.97	0.35	74.9±0.6
50	65.71	34.29	0.52	57.8±0.9
100	66.06	33.94	0.51	57.9±1.0
200	63.39	36.61	0.58	53.7±0.6
300	63.15	36.85	0.58	65.3±0.7

Pressure (mTorr)	C–C (%)	C–O (%)	C=O (%)	O=C–O (%)
0	71.83	14.06	0	14.12
50	57.91	21.97	2.31	17.81
100	59.29	16.59	6.61	17.51
200	49.58	18.71	12.96	18.75
300	50.85	17.54	14.71	16.90

In order to better understand the effects of plasma treatment on the PMMA surfaces, the chemical structure of the plasma-modified PMMA surfaces treated in different chamber pressures was analyzed by X-ray photoelectron spectroscopy (XPS). The C1s spectra were resolved into three or four characteristic peaks, which were identified according to the reported chemical shifts.[39] The peaks at binding energies (BEs) of 285.0, 286.7, 287.9 and 289.0 eV corresponded to the functional groups, C–C, C–O, C=O and O=C–O, respectively. The ratios of the peak area under various chamber pressures are given in **Table 2.2**. It can be seen that the C=O formed for all of the modified surfaces. In addition, the C=O functional group rapidly increased from 2.31% at a pressure of 50 mTorr to 12.96% at a pressure of 200 mTorr and then slowly increased to 14.71% at 300 mTorr. The C–O increased from 14.06% (pristine PMMA) to 21.97% at a pressure of 50 mTorr and then deceased to 17.54% at 300 mTorr. For pristine PMMA with 14.12% of the O=C–O, its composition increased to 18.75 % in the pressure of 200 mTorr, but then decreased to 16.90% at 300 mTorr. Thus, in the pressure range from 50 to 200 mTorr the formation of hydroxyl or peroxyl (C–O), carbonyl (C=O) and carboxylic (O=C–O) groups could contribute to the decrease in the water contact angles. In the case of 300 mTorr, the increase of C=O group and the decrease of C–O and O=C–O groups could account for the increase in the contact angle because the C=O group is less hydrophilic compared to C–O and O=C–O groups. Prediction of the predominant effect resulting in increased contact angle is difficult due to the experimental uncertainties and overlap of native PMMA peaks with oxidized species in the core-level spectra. Our XPS results are clear evident that the main effect of modification is primarily determined by the concentration of oxygen in the reaction chamber. The moderate oxygen concentration in the chamber pressure of 200 mTorr

increased both the amount of carboxylic groups and the degree of hydrophilicity of the PMMA surface.

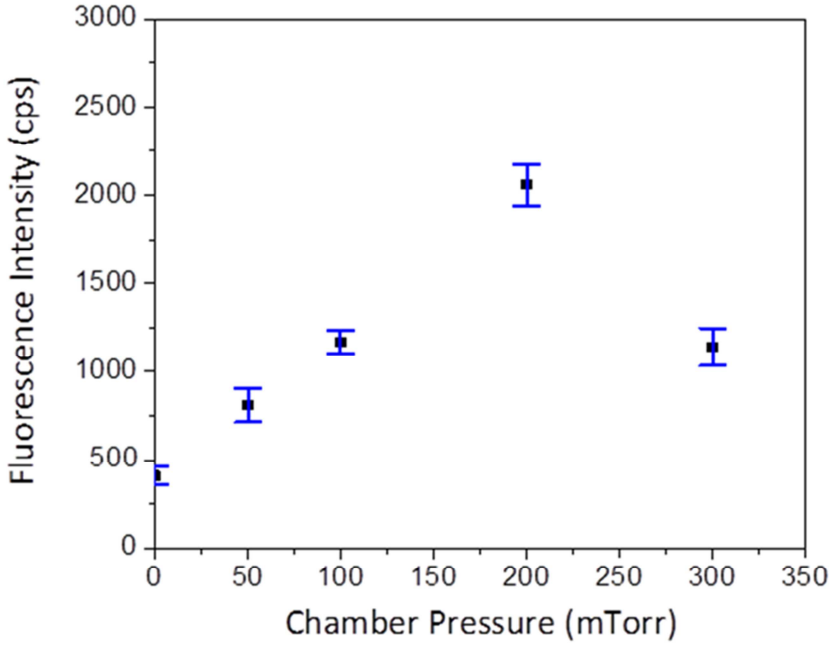

Figure 2.3 Effects of the chamber pressure on the probe density covalently tethered to PMMA surfaces. PMMA slides were oxygen plasma-irritated under various pressures ranging from 50 to 300 mTorr. The slides were activated with EDC/NHS, spotted with fluorescent dye double labeled oligonucleotide probes in 200 mM phosphate solution and allowed to incubate for 1 h. The data points represent the mean of three measurements with the error bars showing ±1 standard deviation unit.

The optimal chamber pressure of 200 mTorr was further confirmed by the immobilization of fluorescent dye (Cy5) labeled oligonucleotide probes to the plasma treated surface. **Figure 2.3** shows the fluorescence intensities of arrays as a function of the chamber pressure. The fluorescence intensity markedly increased when the pressure was increased from 50 to 200 mTorr. However, when the pressure was further increased to 300 mTorr, the fluorescence intensity decreased. We hypothesize that this decrease was attributed to the decrease in the amount of carboxylic groups on the

modified PMMA surfaces, which is supported by the XPS results. The optimum chamber pressure of 200 mTorr was hence chosen in this study.

2.3.3 Detection of MRSA Using the Modular Microfluidic Cartridge

Following PCR amplification of the appropriate gene fragments, which contained the identification loci, the amplicons were mixed with five sets of LDR primers, common primers and discriminating primers. The discriminating primers contained a zip-code complement sequence (cZip) at their 5'-end and a target-specific sequence at their 3'-end. The common primers were phosphorylated at their 5'-end and possessed a fluorescent dye at their 3'-end. A perfect match between the locus containing the unique signature sequences on the target and the sequences at the 3'-end of the discriminating primer would initiate a successful ligation event via the ligase enzyme between the common primer and the discriminating primer, which was encoded by the specific cZip and complementary sequence of the universal array. When the ligated dye-labeled LDR products and unligated discriminating primers were pumped into the microchannel containing the universal array and were captured by the appropriate zip-code probes, the uncaptured products were removed by flushing the array with a wash buffer. The fluorescence signal detected at a specific zip-code address indicated the presence of the corresponding gene in the sample. The advantages of the PCR/LDR/universal array assay employed in this work for detecting sequence variations within the DNA include: (1) PCR associated with LDR give two rounds of target amplification, which provides better signal-to-noise in the readout phases of the assay. (2) The ligation products are fluorescence dye labeled single stranded targets that can be directly used for array hybridization. A heat denaturation followed by a snap-cool step is necessary if double stranded PCR products are used directly for hybridization. However, that process is

very difficult to be integrated in microfluidic devices. (3) LDR and universal arrays can be configured to detect a variety of targets by simply appending the correct cZips to the discriminating primers used in the LDR step, which allows for a highly multiplexed assay in a single reaction.

Figure 2.4 shows the results of CF LDR products hybridized to zip-code probes 1, 5, 15, 21 and 25 using the PMMA waveguide module. Zip-code probe 25, which targeted the SG16S gene common to the *Staphylococcus* genus, was chosen as the positive control and thus, fluorescence was observed from all assays. Zip-code probes 1, 5, 15 and 21 were designed to target *mecA*, PVL, *femA*, and *spa* genes, respectively. Each strain was probed with all zip-code probes in a single hybridization step. As shown in **Figure 2.4A** and **2.4B**, the PVL-positive MSSA strain gave fluorescence signals when SG16S, *spa* and PVL genes were present and the PVL-positive MRSA strain gave fluorescence signals for the presence of SG16S, *spa*, PVL and *mecA* genes. The MR-CNS strain was detected with zip-code probes targeting SG16S, *femA*, and *mecA* genes, and the MS-CNS strain was detected with probes directed for SG16S and *femA* genes (**Figure 2.4C** and **2.4D**). Our results revealed that all strains were correctly identified. The PVL-positive strains were successfully identified with the zip-code probes for the PVL gene, and the methicillin-resistant strains were positively identified with the zip-code probes for *mecA*. The specificity of each zip-code to probe the appropriate target was evident from this data. For example, ligation products generated from MSSA or MS-CNS strains did not hybridize to *mecA* zip-code probes. LDR products generated from MS-CNS or MR-CNS strains did not hybridize to the zip-codes probes for the *spa* gene and ligation products generated from MSSA or MRSA strains did not hybridize to *femA* zip-code probes. The results showed that we could differentiate CA-MRSA from

HA-MRSA based on the presence/absence of the PVL gene, *S. aureus* from other *Staphylococcal* species based on the presence/absence of the *femA* gene as well as MRSA from MSSA based on the presence/absence of the *mecA* gene using this modular system and assay.

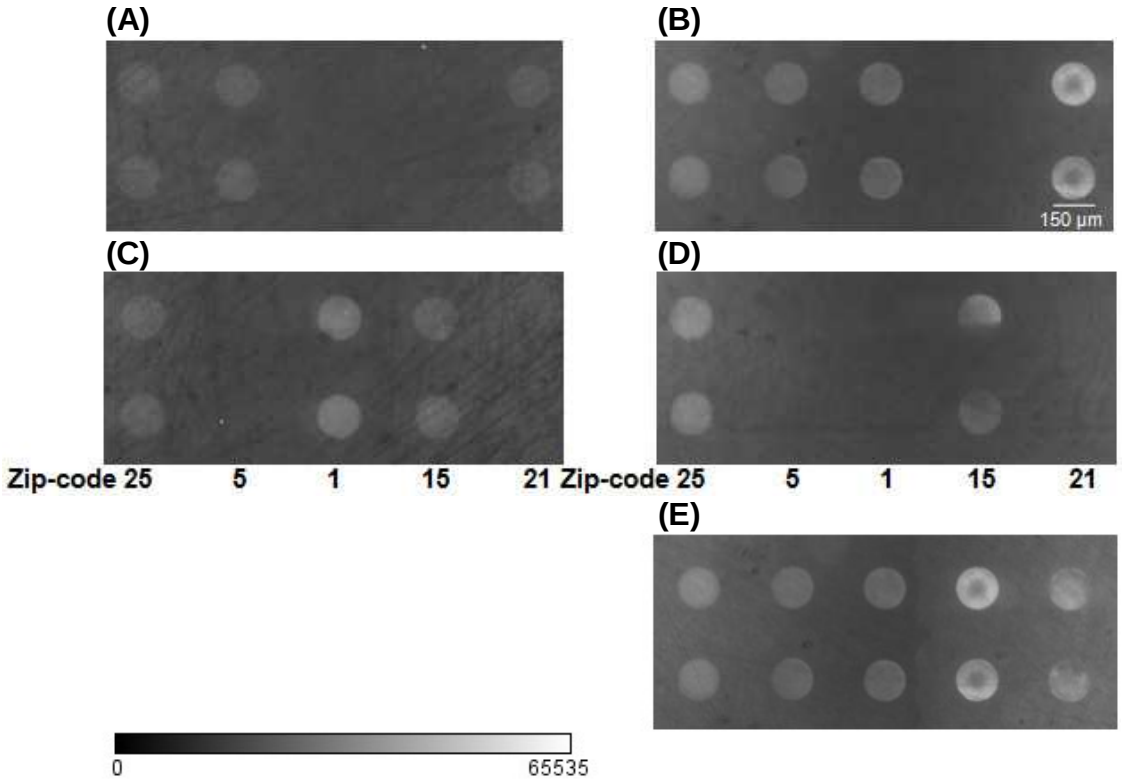

Figure 2.4 Detection of (A) MSSA, (B) MRSA, (C) MR-CNS, (D) MS-CNS and (E) a mixture of MSSA and MR-CNS strains using the integrated microfluidic system. The sample solution was flowed through the system using a volumetric flow rate of 0.5 µL/min for PCR and 1 µL/min for LDR. LDR products were subjected to hybridization to surface-tethered zip-code probes, and the arrays were imaged using the evanescent-field excitation fluorescence reader with a 20 s integration time. Zip-code probe 25 served as the positive control and was complementary to the SG16S gene. Zip-code 1, 5, 15 and 21 probed for *mecA*, PVL, *femA* and *spa* genes, respectively. The spot size of the universal array was ~150 µm in diameter.

CF LDR products generated from successful ligations using five sets of LDR primers in the presence of MSSA, MRSA, MS-CNS or MR-CNS strains were confirmed using capillary electrophoresis (**Figure 2.5**). Each individual LDR yielded ligation products of the expected sizes, *i.e.*, 61, 65, 67, 69 and 73 nt for the *spa*, SG16S, *mecA*, *femA* and

PVL genes, respectively. **Figure 2.5A** shows CF LDR products generated from the PVL-positive MSSA strain and three product peaks, SG16S, PVL and *spa*, confirming methicillin-susceptible *S. aureus*. **Figure 2.5B** shows ligation products generated from the PVL-positive MRSA strain. The additional presence of the *mecA* product peak indicated the existence of methicillin resistance in *S. aureus*. **Figure 2.5C** shows ligation products generated from the MR-CNS strain. The presence of three product peaks, SG16S, *mecA*, and *femA* demonstrated this sample was *S. epidermidis* possessing methicillin resistance. Furthermore, **Figure 2.5D** shows LDR products generated from the MS-CNS strain and two product peaks, SG16S and *femA*, revealing the presence of

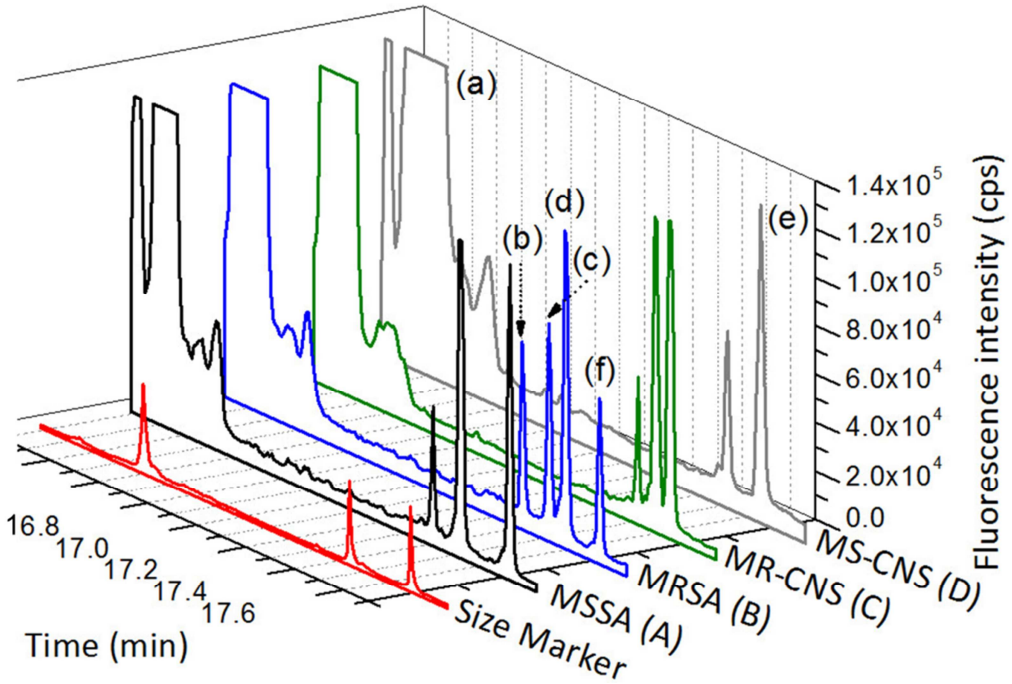

Figure 2.5 LDR products generated from (A) MSSA, (B) MRSA, (C) MR-CNS and (D) MS-CNS strains and analyzed by CEQ 8000 capillary genetic analysis system (field strength 200 V/cm). LDR was performed at capillary temperature of 60 ℃, denaturation temperature of 90 ℃ (3 min), injection at 2.0 kV (30 s) and separation at 6.0 kV (30 min). Peak (a) represents the unligated primers and peak (b) – (f) represent the LDR products generated from the *spa*, SG16S, *mecA*, PVL and *femA* genes. Size markers labeled in red are 60 nt and 70 nt. LDR yielded ligation products of the expected sizes, *i.e.*, 61, 65, 67, 69 and 73 nt for the *spa*, SG16S, *mecA*, *femA* and PVL genes, respectively.

methicillin-susceptible *S. epidermidis*. All of the electropherogram results were consistent with the array hybridization results from the integrated system.

2.3.4 Identification of MRSA from Mixed Strains

As reported by recent studies,[56] the *mecA* gene present in *S. aureus* is highly homologous to that carried by *S. epidermidis* and potentially other CNS species. CNS is a frequent human commensal found in clinical samples from non-sterile sites, so false-positive results from MSSA and MR-CNS coexisting in the sample cannot be precluded, which adds difficulty in differentiating methicillin-resistant strains of *S. aureus* from those of *S. epidermidis*. We applied our integrated system with PCR/LDR/universal array assay to test a sample containing mixed strains of MSSA and MR-CNS. **Figure 2.4E** shows a fluorescence image of the universal array following CF PCR and CF LDR in the presence of a mixture of MSSA and MR-CNS strains. The result indicated that each zip-code probe linked to SG16S, *spa*, PVL, *femA* and *mecA* gave positive fluorescence signals. The results confirmed that this modular system and assay enabled us to successfully discriminate between MRSA and MR-CNS strains.

The minimal number of bacterial cells that could be detected using our integrated system was evaluated by conducting PCR/LDR/universal zip-code hybridization assays with varied concentrations of MRSA as the input. We examined signals generated from five zip-code probes for the presence of SG16S, *spa*, PVL, *femA* and *mecA* genes. **Figure 2.6** shows a linear fit to the fluorescence intensity as a function of different initial MRSA concentrations. The result showed that as the concentration of MRSA increased, the intensities of the fluorescence signals generated from successful hybridization events increased as well. The lowest concentration that produced a positive signal with a signal-to-background threshold of 2.5 from the *mecA* gene was 30 fg/μL of MRSA.

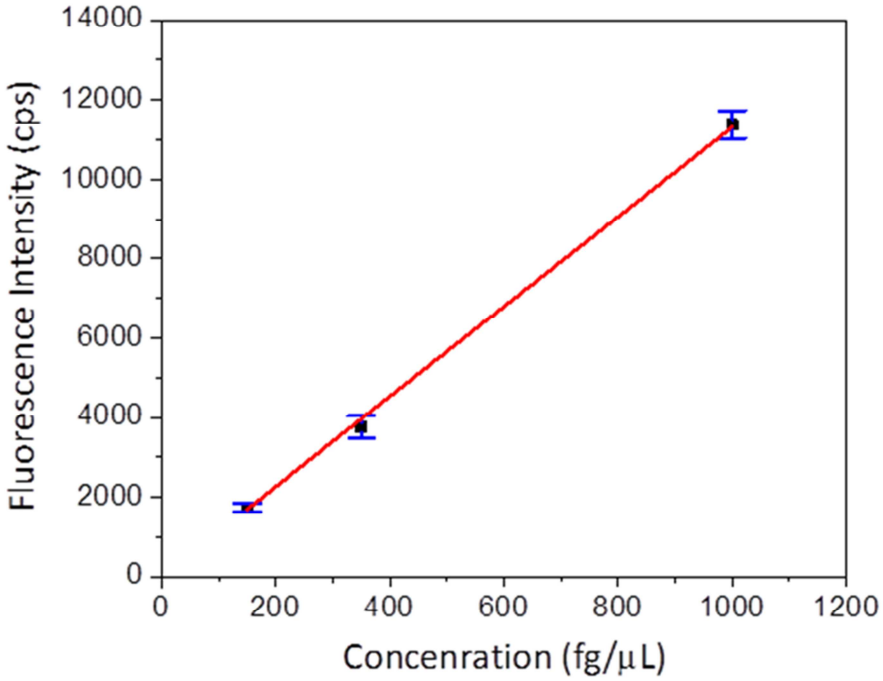

Figure 2.6 Standard curves of fluorescence signals from the MRSA strain with different concentrations as an input. Fluorescence intensities from the *mecA* gene were plotted against the corresponding MRSA concentration. The error bars represent one standard deviation, which was determined from two measurements. The linear regression analysis yielded: $y = 11.288x + 18.33$ ($r^2 = 0.998$)

2.4 Conclusions

We have fabricated an integrated polymer-based microfluidic system directed towards a rapid and specific MRSA identification that can provide information on the drug susceptibility status as well. The integrated system was realized by implementing a CF PCR/CF LDR/universal array assay into a disposable and modular fluidic cartridge made from two polymeric materials, PC and PMMA, selected to optimize material characteristics to meet processing step(s) poised on the material. For example, sequential CF PCR/CF LDR and universal array readout were distributed on a module and a fluidic motherboard, *i.e.*, PMMA module and PC motherboard, due to high glass transition temperature for PC and lower fluorescence background and minimal non-

specific DNA adsorption for PMMA. The PMMA module and the PC motherboard were assembled into a 3-dimensional architecture using a simple interconnect to form the fluidic cartridge. All of the required structures were made via hot embossing for producing the fluidic network and the waveguide for fluorescence readout. This could be done in a single embossing step, using double-sided embossing. The main advantages of the system included fast and specific detection as well as cost-effective fabrication. The use of micro-replication, of the polymeric cartridge and off-chip active components enabled the fluidic system to be manufactured at low cost, appropriate for one-time use applications, a particularly attractive format for clinical applications where disposable-type devices are a necessity to eliminate carryover contamination.

We demonstrated the utility of the integrated system by detecting specifically MRSA using four representative strains, MSSA, MRSA, MS-CNS, and MR-CNS, in the total processing time of less than 40 min. The system was further demonstrated to be capable of detecting mixed strains containing MSSA and MR-CNS, which provided critical information for clinical screening that could preclude false-positive results. In addition to methicillin resistance screening, the present study described a multiplexed assay for the detection of the PVL gene, which can provide the early identification of CA-MRSA strains and for the detection of the *femA* gene, which can serve to distinguish *S. aureus* from other *Staphylococcal* species.

2.5 References

1. P. D. Wagner, P. Maruvada and S. Srivastava, *Expert Review of Molecular Diagnostics*, 2004, **4**, 503-511.
2. J. E. Finan and R. Y. Zhao, *Pharmacogenomics*, 2007, **8**, 85-99.
3. K. L. Muldrew, *Current Opinion in Pediatrics*, 2009, **21**, 102-111.

4. P. Yager, T. Edwards, E. Fu, K. Helton, K. Nelson, M. R. Tam and B. H. Weigl, *Nature*, 2006, **442**, 412-418.

5. A. Manz, N. Graber and H. M. Widmer, *Sens. Actuator B-Chem.*, 1990, **1**, 244-248.

6. S. A. Soper, K. Brown, A. Ellington, B. Frazier, G. Garcia-Manero, V. Gau, S. I. Gutman, D. F. Hayes, B. Korte, J. L. Landers, D. Larson, F. Ligler, A. Majumdar, M. Mascini, D. Nolte, Z. Rosenzweig, J. Wang and D. Wilson, *Biosens. Bioelectron.*, 2006, **21**, 1932-1942.

7. M. A. Burns, B. N. Johnson, S. N. Brahmasandra, K. Handique, J. R. Webster, M. Krishnan, T. S. Sammarco, P. M. Man, D. Jones, D. Heldsinger, C. H. Mastrangelo and D. T. Burke, *Science*, 1998, **282**, 484-487.

8. R. G. Blazej, P. Kumaresan and R. A. Mathies, *Proc. Natl. Acad. Sci. U. S. A.*, 2006, **103**, 7240-7245.

9. E. T. Lagally, J. R. Scherer, R. G. Blazej, N. M. Toriello, B. A. Diep, M. Ramchandani, G. F. Sensabaugh, L. W. Riley and R. A. Mathies, *Analytical Chemistry*, 2004, **76**, 3162-3170.

10. C. J. Easley, J. M. Karlinsey, J. M. Bienvenue, L. A. Legendre, M. G. Roper, S. H. Feldman, M. A. Hughes, E. L. Hewlett, T. J. Merkel, J. P. Ferrance and J. P. Landers, *Proc. Natl. Acad. Sci. U. S. A.*, 2006, **103**, 19272-19277.

11. A. de Mello, *Lab Chip*, 2002, **2**, 31N-36N.

12. Y. J. Liu, C. B. Rauch, R. L. Stevens, R. Lenigk, J. N. Yang, D. B. Rhine and P. Grodzinski, *Analytical Chemistry*, 2002, **74**, 3063-3070.

13. R. H. Liu, J. N. Yang, R. Lenigk, J. Bonanno and P. Grodzinski, *Analytical Chemistry*, 2004, **76**, 1824-1831.

14. A. F. Sauer-Budge, P. Mirer, A. Chatterjee, C. M. Klapperich, D. Chargin and A. Sharon, *Lab Chip*, 2009, **9**, 2803-2810.

15. C. H. Wang, K. Y. Lien, J. J. Wu and G. B. Lee, *Lab Chip*, 2011, **11**, 1521-1531.

16. M. B. Wabuyele, S. M. Ford, W. Stryjewski, J. Barrow and S. A. Soper, *Electrophoresis*, 2001, **22**, 3939-3948.

17. Y. C. Xu, B. Vaidya, A. B. Patel, S. M. Ford, R. L. McCarley and S. A. Soper, *Analytical Chemistry*, 2003, **75**, 2975-2984.

18. F. D. Lowy, *New England Journal of Medicine*, 1998, **339**, 520-532.

19. M. C. Enright, *Current Opinion in Pharmacology*, 2003, **3**, 474-479.

20. H. F. Chambers, *Emerg. Infect. Dis*, 2001, **7**, 178-182.

21. D. J. Diekema, M. A. Pfaller, F. J. Schmitz, J. Smayevsky, J. Bell, R. N. Jones, M. Beach and S. P. Grp, *Clinical Infectious Diseases*, 2001, **32**, S114-S132.

22. K. Hiramatsu, K. Okuma, X. X. Ma, M. Yamamoto, S. Hori and M. Kapi, *Current Opinion in Infectious Diseases*, 2002, **15**, 407-413.

23. M. A. Fischbach and C. T. Walsh, *Science*, 2009, **325**, 1089-1093.

24. C. Dalla Valle, M. R. Pasca, D. De Vitis, F. C. Marzani, V. Emmi and P. Marone, *Bmc Infectious Diseases*, 2009, **9**.

25. C. A. Muto, J. A. Jernigan, B. E. Ostrowsky, H. M. Richet, W. R. Jarvis, J. M. Boyce and B. M. Farr, *Infection Control and Hospital Epidemiology*, 2003, **24**, 362-386.

26. D. F. J. Brown and P. E. Reynolds, *Febs Letters*, 1980, **122**, 275-278.

27. H. F. Chambers, M. Sachdeva and S. Kennedy, *Journal of Infectious Diseases*, 1990, **162**, 705-710.

28. H. F. Chambers, *Clinical Microbiology Reviews*, 1997, **10**, 781-&.

29. A. M. Costa, I. Kay and S. Palladino, *Diagnostic Microbiology and Infectious Disease*, 2005, **51**, 13-17.

30. A. M. Kearns, P. R. Seiders, J. Wheeler, R. Freeman and M. Steward, *Journal of Hospital Infection*, 1999, **43**, 33-37.

31. D. Jonas, M. Speck, F. D. Daschner and H. Grundmann, *Journal of Clinical Microbiology*, 2002, **40**, 1821-1823.

32. U. Reischl, H. J. Linde, M. Metz, B. Leppmeier and N. Lehn, *Journal of Clinical Microbiology*, 2000, **38**, 2429-2433.

33. M. A. De Sousa, I. S. Sanches, M. L. Ferro and H. de Lencastre, *Microbial Drug Resistance-Mechanisms Epidemiology and Disease*, 2000, **6**, 133-141.

34. P. C. Chen, D. E. Nikitopoulos, S. A. Soper and M. C. Murphy, *Biomed. Microdevices*, 2008, **10**, 141-152.

35. M. L. Hupert, W. J. Guy, S. D. Llopis, H. Shadpour, S. Rani, D. E. Nikitopoulos and S. A. Soper, *Microfluid. Nanofluid.*, 2007, **3**, 1-11.

36. C. Situma, Y. Wang, M. Hupert, F. Barany, R. L. McCarley and S. A. Soper, *Anal. Biochem.*, 2005, **340**, 123-135.

37. S. A. Soper, M. Hashimoto, C. Situma, M. C. Murphy, R. L. McCarley, Y. W. Cheng and F. Barany, *Methods*, 2005, **37**, 103-113.

38. F. Xu, P. Datta, H. Wang, S. Gurung, M. Hashimoto, S. Wei, J. Goettert, R. L. McCarley and S. A. Soper, *Analytical Chemistry*, 2007, **79**, 9007-9013.

39. G. Beamson and D. Briggs, eds., *High-Resolution XPS of Organic Polymers: the Scienta ESCA300 Database*, John Wiley & Sons: New York, 1992.

40. D. Sinsimer, S. Leekha, S. A. E. Marras, L. Koreen, B. Willey, S. Naidich, K. A. Musser and B. N. Kreiswirth, *Journal of Clinical Microbiology*, 2005, **43**, 4585-4591.

41. P. Francois, D. Pittet, M. Bento, B. Pepey, P. Vaudaux, D. Lew and J. Schrenzel, *Journal of Clinical Microbiology*, 2003, **41**, 254-260.

42. R. R. McDonald, N. A. Antonishyn, T. Hansen, L. A. Snook, E. Nagle, M. R. Mulvey, P. N. Levett and G. B. Horsman, *Journal of Clinical Microbiology*, 2005, **43**, 6147-6149.

43. M. Hashimoto, P. C. Chen, M. W. Mitchell, D. E. Nikitopoulos, S. A. Soper and M. C. Murphy, *Lab Chip*, 2004, **4**, 638-645.

44. J. F. Chen, M. Wabuyele, H. W. Chen, D. Patterson, M. Hupert, H. Shadpour, D. Nikitopoulos and S. A. Soper, *Analytical Chemistry*, 2005, **77**, 658-666.

45. Y. Gillet, B. Issartel, P. Vanhems, J. C. Fournet, G. Lina, M. Bes, F. Vandenesch, Y. Piemont, N. Brousse, D. Floret and J. Etienne, *Lancet*, 2002, **359**, 753-759.

46. J. L. Klein, Z. Petrovic, D. Treacher and J. Edgeworth, *Intensive Care Medicine*, 2003, **29**, 1399-1399.

47. J. S. Francis, M. C. Doherty, U. Lopatin, C. P. Johnston, G. Sinha, T. Ross, M. Cai, N. N. Hansel, T. Perl, J. R. Ticehurst, K. Carroll, D. L. Thomas, E. Nuermberger and J. G. Bartlett, *Clinical Infectious Diseases*, 2005, **40**, 100-107.

48. B. E. Gonzalez, G. Martinez-Aguilar, K. G. Hulten, W. A. Hammerman, J. Coss-Bu, A. Avalos-Mishaan, E. O. Mason and S. L. Kaplan, *Pediatrics*, 2005, **115**, 642-648.

49. F. Vandenesch, T. Naimi, M. C. Enright, G. Lina, G. R. Nimmo, H. Heffernan, N. Liassine, M. Bes, T. Greenland, M. E. Reverdy and J. Etienne, *Emerg. Infect. Dis*, 2003, **9**, 978-984.

50. M. L. Altshuler, Caister Academic Press, Norfolk, 2006.

51. M. Hashimoto, F. Barany and S. A. Soper, *Biosens. Bioelectron.*, 2006, **21**, 1915-1923.

52. D. M. Coates and S. L. Kaplan, *Mrs Bulletin*, 1996, **21**, 43-45.

53. C. W. Extrand, *Langmuir*, 2004, **20**, 4017-4021.

54. F. D. Egitto and L. J. Matienzo, *Ibm Journal of Research and Development*, 1994, **38**, 423-439.

55. T. Ombrello, S. H. Won, Y. G. Ju and S. Williams, *Combustion and Flame*, 2010, **157**, 1916-1928.

56. D. J. Diekema, K. J. Dodgson, B. Sigurdardottir and M. A. Pfaller, *Journal of Clinical Microbiology*, 2004, **42**, 2879-2883.

CHAPTER 3 MODULAR MICROFLUIDIC SYSTEM FABRICATED IN THERMOPLASTICS FOR THE STRAIN-SPECIFIC DETECTION OF BACTERIAL PATHOGENS

3.1 Introduction

Bacterial detection and identification plays a significant role in the surveillance of food safety, environmental quality, public health and potential patient infections. For example, food-borne diseases caused by eating contaminated food or beverages account for an estimated 76 million illnesses, 325,000 hospitalizations and 5,000 deaths annually in the United States alone.[1-3] In addition, the Center for Disease Control has estimated that medical expenses and productivity losses resulting from these diseases total nearly $5 – $6b.[4, 5] Recently, an outbreak of Shiga toxin 2 (*stx2*)-positive, intimin (*eae*)-negative Shiga toxin-producing *E. coli* (STEC) O104:H4 in Germany resulted in the death of 15 people and thousands were taken ill in a time period of only one month.[6, 7] Therefore, the rapid, specific and accurate detection of pathogens is crucial for the prevention of pathogen-related disease outbreaks and facilitating disease management as well as containment of suspected contaminated food and/or water supplies.

Conventionally, culturing and immunological techniques have been utilized for bacterial detection.[8, 9] These methods, while simple and inexpensive, take extended periods of time to secure results and lack the specificity (*i.e.*, strain identification) when compared to molecular methods that utilize DNA to effectively identify the bacterial species and/or strain.[10-14]

Although molecular methods represent a significant improvement over the traditional culturing methods, sophisticated laboratory settings and extensively trained personnel are required to ensure accurate, reliable and reproducible results, which prohibit the widespread implementation of these valuable techniques into a variety of settings, in

particular 3rd world countries. The challenge with DNA analyses is that the processing pipeline involves many individual steps, such as cell lysis, DNA extraction and purification, PCR amplification of selected gene fragments, the specific identification of sequence variations and the readout of the results, preferably in a multiplexed fashion.

Recent advances in microfluidic-based technologies have realized the development of molecular analysis systems that incorporate many of the aforementioned processing steps for nucleic acid analyses onto a monolithic platform, which can provide full process automation eliminating the need for extensive operator expertise, provide fast and timely results and reduced assay cost. These types of technologies can provide point-of-use operation directly in the field and because they can minimize operation involvement in sample processing, can increase the access of molecular analyses to a broader user community.

Several demonstrations of microfluidic systems for DNA analyses have been described. For example, Burns *et al.*[15] fabricated a nanoliter DNA analyzer on a monolithic silicon wafer possessing not only the fluidic elements, but optical elements as well and applied their system for genetic analysis. Lagally and coworkers reported a portable microsystem fabricated in a glass wafer to perform pathogen detection and genotyping directly from whole *E. coli* and *S. aureus* cells.[16] The system contained a single 200-nL PCR amplification chamber directly connected to a µCE device. Mathies and coworkers integrated several fundamental biochemical processing steps including DNA amplification, purification, and electrophoretic separation, onto a multilayer glass-polydimethylsiloxane (PDMS) wafer and utilized it for Sanger sequencing.[17] Using a similar approach, Landers' group demonstrated a sample-in-answer-out chip capable of

accepting a crude biological sample as an input.[18] The commonality associated with these systems is that they employed either Si or glass as the substrate material.

The challenge with glass-based systems is that extensive lithography steps must be employed to fabricate each chip. This production format can produce challenges for creating low-cost systems that can be produced in a high production mode appropriate for one-time use applications. To circumvent the need for employing glass as a substrate for the fluidic network, thermoplastic materials can be utilized, which have chip fabrication techniques that are conducive to high rates of production and can produce low-cost platforms; several of these manufacturing techniques include hot embossing and injection molding.[19-21]

Building on this premise, several groups have reported polymer-based systems that can analyze genetic material. For example, a monolithic system, which integrated PCR and DNA microarrays, was described by Liu *et al*.[22] The chip was fabricated in PC using CO_2 laser micromilling with an asymmetrical PCR amplification step employed. The system was demonstrated for the analysis of both *E. coli* and *Enterococcus faecalis*. Liu and coworkers fabricated a polymer-based biochip with integrated cell isolation and lysis units; PCR amplification and electrochemical microarray detection for sample-to-answer DNA analysis was demonstrated.[23] The system was machined into a PC substrate and was capable of detecting *E. coli* in 3.5 h. Koh *et al*.[24] demonstrated a microsystem fabricated in a poly(cyclic olefin copolymer), COC, substrate, which contained a PCR device directly interfaced to µCE to sort fluorescently-labeled PCR products generated from different strains of *E. coli.* The system was used to identify *E. coli* O157:H7 organisms with a limit-of-detection (LOD) of ~6 copies of target DNA. In another report, researchers developed a low-cost biochip system for the analysis of

bacterial DNA using a substrate consisting of COC with the fluidic structures directly milled into the COC chip.[25] The system contained functional devices for cell lysis, DNA isolation and purification, PCR and end-point fluorescence detection.

While the above examples of polymer microfluidic systems are attractive in demonstrating the utility of thermoplastics for generating low-cost integrated systems for DNA processing, they do have some limitations including the extensive amount of post-processing required after fabrication of the desired fluidic structures, which can significantly add to the cost of the chip. Examples of post-fabrication processing steps include the lithographic patterning of electrodes onto the fluidic chip,[22] generation of porous polymer monoliths containing silica for DNA extraction,[25] integration of wax or gel-based valves,[23, 24] or the addition of magnetic beads.[23]

Finally, the fluidic chips were made from a single material by positioning all of the functional devices onto a monolithic platform. The challenge with this approach is that certain materials may or may not be optimal for the intended processing step. For example, some polymeric material are appropriate for fluorescence detection and some are not due to the level of autofluorescence they generate.[26] Also, some polymeric materials show non-specific adsorption artifacts that can produce problems when performing electrophoresis or getting good contrast for microarray measurements.[27, 28]

In this work, we focused on addressing the aforementioned issues by constructing an integrated polymer-based, modular microfluidic system for the rapid and efficient identification of pathogens. The system was based on a modular design approach, in which certain steps of the molecular processing pipeline were situated on modules made from a material selected to suite the particular application need. In addition, the fluidic chip was made via hot embossing to generate a number of functional elements,

such as a SPE bed[29, 30] and an air-embedded waveguide,[31] minimizing the number of post-processing steps required to create the system.

The assay employed in this work for detecting reporter sequences within the DNA isolated from bacterial cells consisted of a primary PCR followed by allele-specific ligation (ligase detection reaction, LDR) with readout via a low-density universal array.[32, 33] The primary advantages of using this assay format is that it gives two rounds of target amplification (PCR and LDR) to provide better signal-to-noise in the measurement, can be easily multiplexed at the LDR phase of the assay minimizing false-positive results associated with multiplexed PCR, can detect single base sequence variations with high specificity even when the target is a minority in a mixed population and finally, can be configured to search for sequence variations in any region of the genome by simply changing primer sequences.

The system reported herein was composed of a fluidic cartridge and a control instrument. All of the molecular processing, from sample reception to readout, was performed on a programmable and modular fluidic cartridge. The sequence of sample processing steps performed included cell lysis, SPE of genomic DNA (gDNA) from the whole cell lysate, PCR, LDR and universal DNA microarray readout. The fluidic cartridge was composed of a functional module stacked in a 3-dimensional configuration onto a fluidic motherboard. Based on material properties to optimize each molecular processing step and satisfy manufacturing requirements, the motherboard was made from PC and consisted of processing steps for cell lysis, SPE, PCR and LDR due to its ability to select DNAs from cell lysates and its high glass transition temperature (Tg), while the array module was made from PMMA, which contained an air-embedded planar waveguide and the DNA array. PMMA was selected for this

module because of its low autofluorescence levels and its propensity to demonstrate minimal amounts of non-specific adsorption of DNAs compared to PC. The integrated fluidic cartridge was generated via double-sided hot embossing from metal molding tools fabricated via high precision micromilling. Fluidic handling (e.g. pumps, valves, etc.), thermal management (e.g. heaters, temperature sensors, etc.) and optical readout hardware were situated off-chip and packaged into a small form factor instrument. Only the fluidic cartridge was in contact with the sample, which eliminated any potential carryover contamination and due to the ease of manufacture, could be discarded following a single measurement. To evaluate the performance of our system, a duplexed PCR, multiplexed LDR followed by universal zip-code array readout were used to detect *E*. *coli* O157:H7 and *Salmonella* using two genes, *uidA* and *sipB/C*. The integrated system was further evaluated by detecting *E. coli* O157:H7 in waste-water samples.

3.2 Materials and Methods

3.2.1 Materials and Regents

PC and PMMA sheets were purchased from Good Fellow (Berwyn, PA). Chemicals used for the PMMA surface modification and hybridization assays included 1-ethyl-3-(3-dimethylaminopropyl) carbodiimide hydrochloride (EDC), *N*-hydroxysuccinimide (NHS), and 20x SSC buffer (3 M sodium chloride, 0.3 M sodium citrate, pH 7.0), which were purchased from Sigma-Aldrich (St. Louis, MO). A 10% sodium dodecyl sulfate (SDS) stock solution, which was used for post-hybridization washing, was received from Ambion (Austin, TX). Polyethylene glycol (PEG, *M*w=8000), sodium chloride (NaCl), ethanol, disodium hydrogen phosphate (Na_2HPO_4), sodium phosphate (Na_3PO_4), and 2-propanol were obtained from Sigma-Aldrich (St. Louis, MO). Oligonucleotide primers

and probes were obtained from Integrated DNA Technologies (Coralville, IA). Their sequences and melting temperatures (T_m) are listed in **Table 3.1**. *E. coli* K12 was obtained from American Type Culture Collection (Manassas, VA). Both *E. coli* O157:H7 and *Salmonella* cells were purchased from Kirkegaard & Perry Laboratories (Gaithersburg, MD). All solutions were prepared in nuclease free water purchased from Invitrogen Corporation (Carlsbad, CA).

3.2.2 Microfluidic Cartridge Fabrication

The modular fluidic cartridge was composed of one module and a motherboard (see **Figure 3.1A**); the motherboard was made from PC and consisted of devices for cell lysis (Sample Load chamber, see **Figure 3.1A**), SPE, PCR and LDR, while the module attached to the motherboard was fabricated in PMMA and was used for the universal array and contained a waveguide. The PMMA module was interconnected to the PC motherboard using short pieces of Tefzel^{TM} tubing (OD = 1/16", ID = 250 µm, Upchurch) inserted between conically-shaped holes placed on the backsides of both the motherboard and module to provide leak-free interconnections (see **Figure 3.1B**).

The PC motherboard contained a network of microchannels for cell lysis, SPE, PCR and LDR on the frontside of the substrate and thermal isolation grooves[34] and fluidic interconnects on the backside all of which were replicated in one-step using double-sided hot embossing from two brass molding tools mounted opposite to each other on a JENOPTIK HEX02 hot embossing machine (Jena, Germany). The brass mold masters were fabricated by high-precision micromilling as described elsewhere.[35] After hot embossing, the SPE bed contained 50 µm diameter micropillars spaced by 100 µm (center-to-center). The SPE bed on the PC motherboard as well as the corresponding area on the PC cover plate were exposed to 254 nm UV radiation (15 mW/cm^2) through

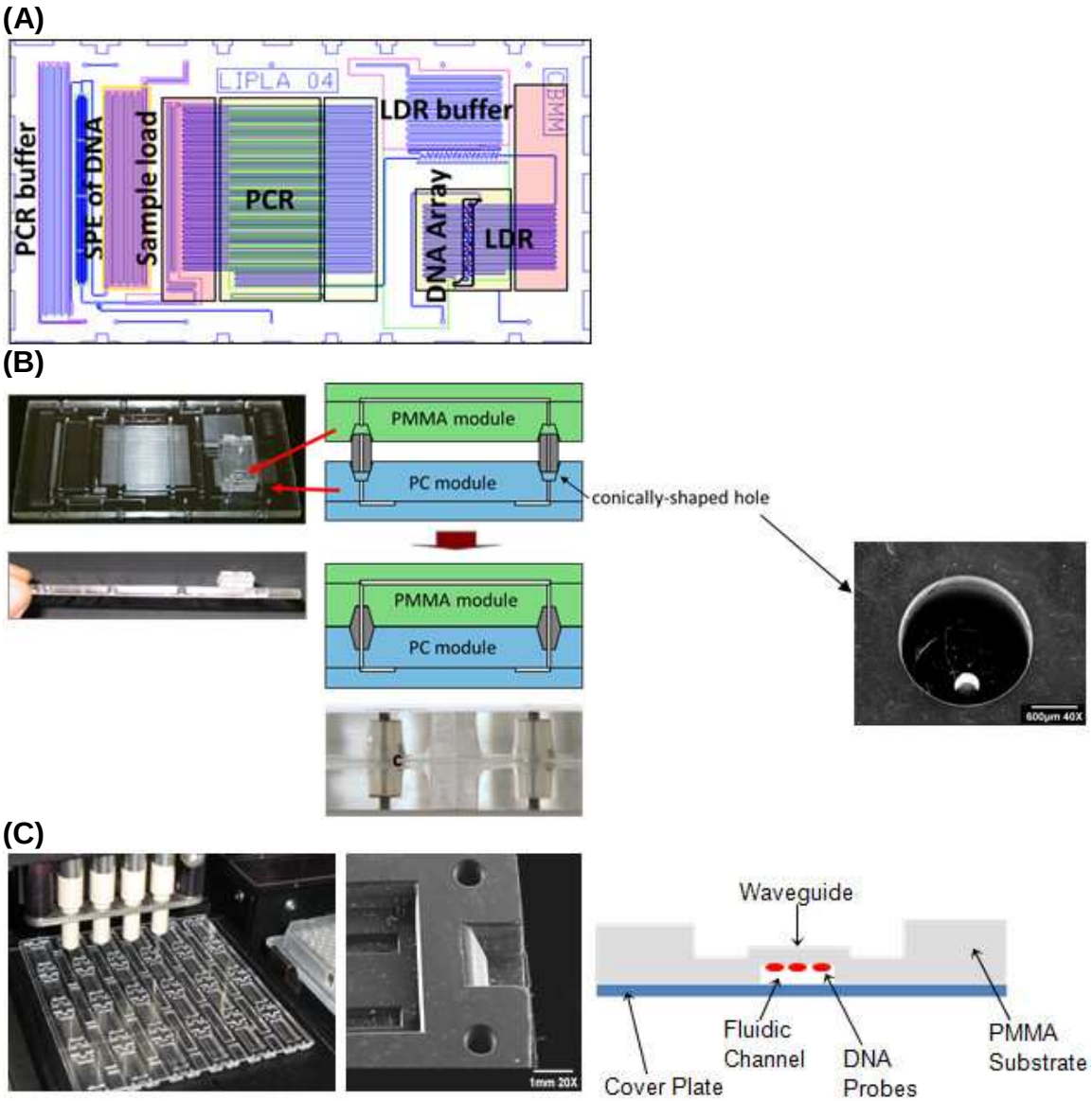

Figure 3.1 Schematic showing the layout of the modular fluidic cartridge. (A) The fluidic cartridge was composed of a module interconnected to a motherboard. The motherboard was made from PC and consisted of processing steps for cell lysis (sample load compartment), SPE of gDNA, PCR and LDR, while the module was made from PMMA and contained an air-embedded planar waveguide in which a universal DNA microarray was positioned. The PC motherboard was interconnected to the PMMA module through short pieces of tubing and conically-shaped holes laser-drilled into the PC. (B) Schematic and optical micrograph of the motherboard-to-module fluidic interconnection. c: Connecting tube inside a conically-shaped hole in which channels were filled with a black dye that used for visualization. The micrograph to the right shows the laser drilled hole. (C) Layout of the PMMA module (right picture) consisting of the air-embedded waveguide, a coupling prism and the universal array. The waveguide and coupling prism (see center picture) were located on the backside of the module and the frontside contained the fluidic channel, which had as its floor the waveguide. DNAs could be spotted (see picture on the left) onto the waveguide using a non-contact spotter prior to thermal fusion bonding the cover plate to this module's substrate.

a mask for 20 min to photo-oxidize the PC surface to allow for the solid-phase extraction of DNA from a whole cell lysate.[29] The PC motherboard was assembled to a PC cover plate (250 µm thick) using thermal fusion bonding at 150 ℃ for 20 min.

The PMMA module (**Figure 3.1C**) consisted of a microchannel network for the DNA microarray on the frontside and the backside was comprised of a planar air-embedded waveguide with integrated coupling prism. The PMMA module was replicated by double-sided hot embossing from two brass molding tools. Twenty-four (4 x 6) waveguide modules could be fabricated on one PMMA wafer in a single replication step. The PMMA module was assembled following spotting of the DNA probes onto the waveguide by thermal fusion bonding the substrate and PMMA cover plate at 107 ℃ for 20 min.

3.2.3 Surface Modification of PMMA and Array Preparation

The hot embossed PMMA microchannels were activated using a previously published method.[31, 36, 37] Briefly, the PMMA substrates were placed in a vacuum chamber for 1 min at 200 mtorr of oxygen pressure and 50 W of radio frequency using a Technics Series 8000 micro-reactive ion etcher (Surplus Process Equipment Corp., Santa Clara, CA). After plasma irradiation, the substrates were soaked in 50 mg/mL EDC dissolved in a coupling buffer (pH 6.0) containing 5 mg/mL NHS for 10 min to form a succinimidyl ester intermediate. The PMMA substrates were then rinsed with 18 MΩ nanopure water to remove excess EDC/NHS solution and dried with air. The freshly prepared PMMA substrate was then mounted onto a vacuum holder of a Perkin-Elmer Piezorray® noncontact microarraying instrument (Downers Grove, IL) through a custom made adapter. With the aid of a camera, 50 µM of 3'-amino-modified oligonucleotide

probes (see **Table 3.1** for sequences), separately dissolved in 0.2 M Na_2HPO_4/Na_3PO_4 buffer (pH 9.0), were spotted onto the bottom (waveguide backside) of the microfluidic channel (**Figure 3.1C**). Dispensing volumes per spot were 330 ±30 pL and the size of the spots were ~150 µm in diameter. Following spotting, the PMMA substrates were incubated in a humidified chamber at room temperature for 4 h, washed with 0.1% SDS to remove any non-specifically bound oligonucleotides and finally dried with air. The PMMA module substrate was thermally fusion bonded to a PMMA cover plate to enclose the fluidic network.

3.2.4 PCR and LDR Conditions

Two sets of PCR primers (see **Table 3.1** for sequences) were used to amplify a 168-bp *uidA* gene from *E. coli* and a 250-bp *sipB/C* gene fragment from *Salmonella*.[38, 39] The PCR mixture consisted of 10 mM Tris-HCl (pH 8.3), 50 mM KCl, 1.5 mM $MgCl_2$, 200 µM dNTPs, 0.5 µg/µL ultra-pure bovine serum albumin (BSA), 0.5 µM of the *uidA* primer pairs, 0.8 µM of *sipB/C* primer pairs and 0.1 U/µL *Taq* DNA polymerase (New England Biolabs, Beverly, MA). The LDR mixture contained 20 mM Tris-HCl (pH 7.6), 25 mM KCl, 5 mM $MgCl_2$, 10 mM DTT, 1 mM NAD^+ (a cofactor for ligase enzyme), 0.1% Triton X-100, 0.5 µg/µL ultra-pure BSA, 50 nM of each discriminating primer, 100 nM of each Cy5-labeled common primer and 2 U/µL*Taq* DNA ligase (New England Biolabs, Beverly, MA).

We used CF thermal cycling for several reasons including its ability to provide ultrafast cycling times ultimately limited by the kinetic rate of dNTP incorporation by the polymerase and the lack of valves required to contain the PCR mixture during thermal cycling as required for batch-type thermal cyclers.[34, 40, 41] The temperatures for the CF

PCR were set at 95 ℃ for denaturation, 60 ℃ for a nnealing and 72 ℃ for extension. As for the LDR, the temperatures were set at 95 ℃ for denaturation and 65 ℃ for ligation.

CF PCR was performed at a volumetric flow rate of 1 μL/min, which provided a cycling rate of 44.6 s/cycle (8.8 s for denaturation, 8.8 s for annealing, 18 s for extension and 9 s for flowing the sample through a shallow channel connecting the extension to the denaturation zone), completing the 32 cycles for PCR in 24 min. The CF LDR was operated at a volumetric flow rate of 2 μL/min producing a processing time of 4 min for 13 thermal cycles.

Table 3.1 Sequences of oligonucleotides used in the PCR/LDR/universal zip-code hybridization assay for *E. coli* and *Salmonella*

PCR product size (bp)	Oligos	Sequence (5'→3')	T_m (℃) [e]
168	O157-uidA-forward	TTACGTCCTGTAGAAACCCCAACC	58.6
	O157-uidA-reverse	ATCGGCGAACTGATCGTTAAAACT	56.8
	uidA-com	[a]pCAGCGTTGGTGGGAAAGCGCG-Cy5[b]	59.2
	cZip1-uidA-Wt	[c]**GCTGAGGTCGATGCTGAGGTCGCA**GATCGC GAAAACTGTGGAATTGAT	70.0
	cZip5-uidA-Mt	[c]**GCTGTACCCGATCGCAAGGTGGTC**GATCGCG AAAACTGTGGAATTGAG	70.1
250	Sal-sipB/C-forward	ACAGCAAAATGCGGATGCTT	56.1
	Sal-sipB/C-reverse	GCGCGCTCAGTGTAGGACTC	60.4
	Sal-sipB/C-com	[a]pCGCTAAAGATATTCTGAATAGTATTGG-Cy5[b]	51.8
	cZip11-Sal-sipB/C	[c]**CGCAAGGTAGGTGCTGTACCCGCA**GACAGCT TCGCAATCCGTTAG	70.9
	Zip-code 1	TGCGACCTCAGCATCGACCTCAGC-sp-NH_2[d]	64.9
	Zip-code 3	CAGCACCTGACCATCGATCGCAGC-sp-NH_2[d]	64.1
	Zip-code 5	GACCACCTTGCGATCGGGTACAGC-sp-NH_2[d]	63.7
	Zip-code 11	TGCGGGTACAGCACCTACCTTGCG-sp-NH_2[d]	65.2

[a] p: phosphorylated.
[b] Cy5: λ_{ex} = 649 nm, λ_{em} = 670 nm.
[c] The bold sequences are complementary to the sequences of zip-code probes.
[d] sp-NH_2: $(CH_2CH_2O)_6PO_4$-NH_2.
[e] Conditions: oligo concentration, 1 μM; Na^+ concentration, 50 mM.

3.2.5 Peripheral Packaging and Instrument Operation

The physical dimensions of this instrument were 12” (length) x 12” (width) x 12” (height) and included an Instrument Control Unit (ICU), actuators, pumps, solenoid valves, heating stage and solution reservoirs. Included in this footprint was also a compact optical reader used to secure fluorescence signatures from the universal zip-code array.

Operation of all peripherals (pumps, valves, heaters, laser and CCD camera) was achieved by the ICU. The ICU had an on-board microprocessor that communicated with all electronic subunits (digital-to-analog and analog-to-digital converters, CCD and stepper motor drivers, temperature monitors, etc.) and controlled their operation. It also communicated with the personal computer via a USB interface and could be programmed by the user through control software. The software allowed for control of all peripherals and was used for data collection and analysis. The software could operate in two distinct modes: (1) service mode that allowed for individual control of all of the hardware components; and (2) fully automatic mode, where all processing steps were performed according to predefined sequences without any user intervention.

Two stepper-motor driven piston micro-pumps (LPVX0502600BC, Lee Company, USA) with a step resolution of 50 nL were used as positive displacement pumps. A DC motor driven mini-pump (W309-011, Hargraves Technology Corp., USA) was used for operations requiring vacuum. All inputs to the fluidic cartridge were controlled by commercial solenoid microvalves. Pumps and valves were interfaced to the fluidic cartridge through a fluid distribution board (FDB). The FDB was fabricated in PMMA through direct milling and seats for mounting the solenoid valves (6604A0-140466,

Christian Bürkert GmbH & Co. KG, Germany). The connections between the FDB and fluidic cartridge consisted of standardized screw-type ferrule-based fluidic connectors and stainless steel tubing interconnects (see **Figures 3.2A and 3.2B**).

The optical reader included an excitation laser (HL6320G, 10 mW, Hitachi), collection optics, and CCD sensor. The reader (see **Figure 3.2C**) was composed of two 2x microscope objectives (PLAPON 2x, Olympus), a 3RD660LP long pass filter and 3RD660-680 band pass filter (Omega Optics, Brattleboro, VT). The image was captured

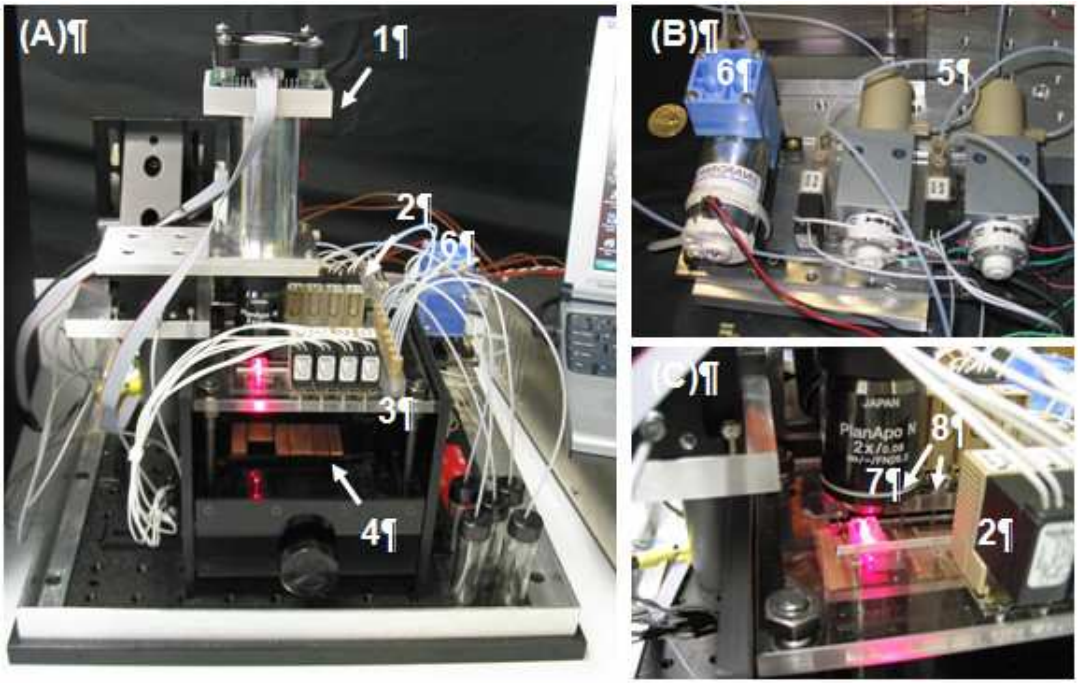

Figure 3.2 Photograph of the control instrument and support peripherals. (A) Fluidic cartridge peripherals: 1 – collection optics, 2 – solenoid valves, 3 – FDB and 4 – Cu heating blocks. (B) Close-up view of the fluidic elements: 5 – stepper-motor driven micro-pumps and 6 – mini vacuum pump. (C) Close-up picture of the FDB and optical reader: 7 – imaging objective and 8 – FDB-to-chip interconnects. The instrument included an ICU, actuators, pumps, solenoid valves, heating stage, solution reservoirs and optical reader. Once the fluidic cartridge was loaded, it was then aligned with respect to the FDB using stainless steel interconnects and pressed against them by raising them against the heating stage, which consisted for Cu blocks. This ensured both tight fluidic connections and proper heat transfer. Operation of all fluidic and electronic peripherals was achieved by the ICU.

on a rectangular CCD sensor (S7030-0907; 512 x 58 pixels; 24 x 24 µm/pixel; Hamamatsu). Excitation of the array was achieved through an evanescent field produced by the waveguide serving as the floor of the microfluidic channel housing the universal array. The laser light was coupled to the waveguide via an on-board 64° prism. Both the waveguide and coupling prism were incorporated into the array microchip and fabricated using the same embossing step for making the fluidic network (see **Figure 3.1C**).

Commercial polyimide (KAPTON®) heaters (Minco, USA) were used to deliver heat to the PCR and LDR thermal reactors. Heaters were attached to 2 mm thick Cu blocks to achieve uniform heat flux and distribution. Temperatures were controlled by type K thermocouples (CHAL-005, Omega Engineering, USA) placed in grooves milled into the Cu blocks. Integral to the heat management of the fluidic cartridge were thermal isolation grooves formed on the backside of the cartridge during the embossing step, which allowed for efficient thermal isolation between adjacent reaction zones.[34] During insertion of the fluidic cartridge into the instrument, it was pressed gently against the Cu heating blocks surface covered with conductive tap to provide good thermal contact. The Cu heating blocks provided the necessary temperatures for the CF PCR and CF LDR. All pumps and valve actuators were aligned with the corresponding valves and pumps and all external fluidic connections were made through the FDB to external bulk reservoirs. This process occurred simultaneously for all elements so after a single-loading step, the system was ready for operation. All active fluidic and heating elements were under microprocessor control so that once started, the process did not require operator intervention.

The modular system was designed to perform the following processing steps: (1) cell lysis; (2) DNA purification; (3) ethanol wash and air dry of the SPE bed; (4) DNA release from the SPE bed with PCR buffer; (5) CF PCR; (6) mixing the PCR products with LDR buffer; (7) CF LDR; (8) DNA microarray incubation and wash; and (9) array readout and data analysis. The thermally lysed bacterial cells (see Sample Load chamber, **Figure 3.1A**) were suspended in an SPE immobilization buffer consisting of 3% PEG, 0.5 M NaCl and 63% ethanol. Other regents, including the PCR and LDR reaction mixtures, were loaded into individual storage channels. Once the fluidic cartridge was inserted into the instrument, on-chip processing was initiated with running the sample suspended in the SPE extraction buffer through a thermal zone (95 ℃) to lyse the cells and then, the SPE bed. The SPE bed was washed with 85% ethanol to remove other cellular components and dried with air. Finally, the purified gDNA was released using 30 µL of the PCR mixture and pumped through the PCR CF thermal reactor at a volumetric flow rate of 1 µL/min.

Once the PCR was completed, 30 µL of an LDR reaction mixture was pumped through the cartridge at the appropriate volumetric flow rate. The resultant PCR amplicons were sequentially mixed with the LDR mixture via a passive Y-shaped micromixer possessing 40 µm wide and 100 µm deep inlet and outlet channels (aspect ratio 3); the mixing ratio of PCR amplicons with the LDR mixture was 1 to 1. The resultant LDR products were directly pumped through the array module with the LDR products subjected to hybridization to surface-tethered zip-code probes. Following array wash with buffer (2x SSC, 0.1% SDS), fluorescence images of the arrays were collected using the optical reader consisting of a laser diode and CCD imaging sensor with a 12 mm x 3 mm field-of-view using an integration time of 20 s.

3.3 Results and Discussion

3.3.1 Architecture of Modular System

The fluidic cartridge was fabricated using double-sided hot embossing with many of the molecular processing functional components generated during the embossing step, which produced not only the fluidic network, but the solid-phase extraction bed (micropillars), micromixer, thermal reactors (continuous flow) and waveguide. The only post-molding steps required for chip finishing were, UV activation of the appropriate areas of the chip, spotting DNA probes onto the waveguide surface and thermal assembly of the cover plate to the substrate.

The modular design approach adopted herein offered some attractive advantages. For example, the module and motherboard were made from a particular thermoplastic material selected to optimize processing step(s) performance and meet manufacturing requirements. The motherboard was made from PC and used for SPE and thermal cycling units, cell lysis, PCR and LDR, while the array module was made from PMMA and contained an air-embedded planar waveguide. We chose PC as the material for the motherboard due to its unique characteristics to allow for the specific condensation of nucleic acids to its photo-activated surface.[29] PC also has a relatively high Tg to allow it to withstand the sustained high operating temperatures required for the thermal reactions. On the other hand, the material for construction of the array module was PMMA because PMMA has significantly lower amounts of autofluorescence compared to PC[42] as well as minimal non-specific adsorption artifacts.[43]

The modular fluidic cartridge consisted of five micro-devices with different functions (see **Figure 3.1**). (1) A cell lysis unit that lysed cells thermally. The sample was placed in the SPE extraction buffer and shuttled through a channel to allow thermal lysis. (2) A

solid-phase extraction device for the purification of gDNA from a whole cell lysate using an extraction bed composed of UV activated micropillars. SPE purification of gDNA is critical because it removes material from the sample that may interfere with downstream molecular processing, which in this work involved a duplexed PCR and multiplexed LDR. The SPE device was populated with an array of 3,600 50 μm diameter pillars. The SPE bed possessed a total surface area of 33.6 mm^2, and the DNA load capacity was estimated to be ~242 ng. Nucleic acids were selectively immobilized onto the photoactivated PC surface, which contained carboxylate groups generated via UV irradiation using an immobilization buffer containing PEG, NaCl and ethanol. After cleanup using ethanol, purified and concentrated nucleic acids were eluted from the PC surface using water or a PCR buffer. The PC-SPE method did not require magnetic beads or the loading of microchannels with beads. We have shown that photoactivated PC-SPE methods can be used for the purification of gDNA, DNA sequencing fragments and total RNA from cell lysates and blood.[29, 30, 44]

(3) CF thermal reactors. The format we adopted for two thermal reactors was a continuous flow format, which is based on flowing a reaction mixture through a microchannel with different isothermal zones. Compared to batch-type thermal reactors, the CF format offers some unique advantages: (1) Better thermal management because the system is brought to thermal equilibrium prior to the start of the reactions; (2) the speed of the thermal cycling reactions (PCR and LDR) are limited only by enzyme kinetics not by heating-cooling rates,[32, 40] providing extremely short reaction times; (3) dynamic transport of the fluid through the thermal reaction zone, which obviates the need for containment valves; and (4) the number of cycles or the time of the thermal reaction can be controlled by the length of the reaction channel and the linear transport

rate through the reaction zone.[41] In addition, several thermal management strategies were utilized to give a uniform temperature distribution throughout a particular thermal zone. For example, insulating grooves between temperature zones on the backside of the fluidic motherboard were designed to increase the thermal resistance to lateral heat conduction between zones.[34] Heating of the thermal reaction domains was carried out by placing a high thermal conductivity material, such as Cu blocks, between the heating elements and the motherboard for precise temperature control. A thin PC substrate was used to minimize the thermal capacitance of the heated area. To prolong residence time in the extension or ligation zones and reduce thermal reactor footprint, a dual-depth serpentine channel geometry (200 µm and 100 µm) was included in both CF PCR and CF LDR devices. The larger channel cross section in the extension/ligation zones provided a longer residence time in these zones without the need for changing the volumetric flow rate.

(4) Universal array device. An air-embedded waveguide associated with a laser-coupling prism for laser-induced fluorescence evanescent excitation of the universal array were integrated into a single microfluidic module.[31] Optical detection of the array elements was achieved with a home-built fluorescence reader consisting of a laser diode and a high sensitivity CCD camera. The evanescent excitation offered high spatial resolution and a broad field-of-view (12 mm x 3 mm), allowing for imaging of the entire array without requiring scanning, which made the data acquisition process simple and very fast, as well as simplifying the optomechanical design of the system. Additionally, the shallow microfluidic channel (100 µm) was designed inside this PMMA module for fast flow-through hybridization. Our group has demonstrated that arrays constructed in microfluidic channels have fast hybridization kinetics.[28] Other groups have also reported

reduced non-specific signal and background in microfluidically addressed arrays.[45]

The PC motherboard and the PMMA module were assembled in a 3-dimensional architecture using a simple and robust fluidic interconnect, which consisted of two conically-shaped holes placed on the backsides of both the motherboard and the waveguide module with connecting tubes made of a semi-rigid polymeric material (*e.g.,* Tefzel™, see **Figure 3.1B**). Following compression sealing, the semi-rigid connecting tubing conformed to the shape of the conical holes and provided an unswept volume of ~20 nL. This interconnect was successfully tested for pressures up to 600 psi. As compared to our previous studies utilizing a PDMS elastomer as an O-ring gasket between two chips, which produced unswept volumes to 200 nL,[32] the reported interconnect provided several beneficial characteristics; (1) It was a press fit connection, which allowed for quick connection and disconnection of the chips; (2) no gaskets were needed, which eliminated material-sample compatibility issues; and (3) the interconnect was easy to fabricate and self-aligning with minimal unswept volume.

3.3.2 Characterization of the Waveguide Module

A protocol that allowed for end-point attachment of amine-terminated oligonucleotides to a PMMA surface was utilized herein. Briefly, PMMA microchannels, which measured 10.9 mm x 1.2 mm x 100 μm, were irradiated with oxygen plasma and activated with EDC/NHS. After activation, the oligonucleotide zip-code probes were dispensed onto the PMMA surface using a noncontact spotting instrument, which eliminated any potential damage that could incur on the waveguide surface if using contact printing.

In the literature, different methods of bonding plastic microfluidic devices to form an enclosed channel network have been reported, including solvent assisted bonding,[46, 47]

thermal bonding,[48, 49] adhesive boning,[50, 51] laser welding,[52] or surface modifications.[53-55] In this study, the PMMA module was assembled using thermal fusion bonding at 107 ℃ for 20 min following spotting of the arrays. When PMMA is heated to near its Tg, it approaches a viscoelastic state,[56] which could potentially damage the oligonucleotide probes. Therefore, the stability of these DNA probes was evaluated to determine whether the thermal fusion bonding process would affect the integrity of these probes.

We carried out experiments in which oligonucleotide probes (zip-code 1 and zip-code 3, see **Table 3.1**) were tethered to sheet PMMA using the aforementioned protocol and then, one of the PMMA sheets was heated to 107 ℃ for 20 min while the other was not. Complementary DNAs that were fluorescently labeled were dispensed onto both PMMA sheets and subjected to hybridization to the surface-tethered probes. The results of this evaluation are shown in **Figure 3.3**, which indicated no discernible decrease in fluorescence intensity after heat treatment indicating little if any chemical degradation of the spotted probes during thermal processing.

In our system, the PMMA module was poised on the CF LDR device. The hybridization of LDR products bearing zip-code complements to their surface-tethered zip-code probes is a thermally sensitive event. Due to the thermal conductivity of both plastics, heat from the CF LDR device, which includes zones poised at 95 ℃ for denaturation and 65 ℃ for ligation, can propagate to the hybridization chamber of the PMMA module affecting the number of hybridions formed. To evaluate the effects of different temperatures on the fluorescence signals obtained following hybridization, different temperatures were tested including 40, 50 and 60 ℃. Experiments were performed in which complementary targets were pumped at a volumetric flow rate of 0.5

μL/min for 5 min through the hybridization chamber. The results indicated no noticeable decrease in fluorescence intensity at temperatures ranging from 40 – 60 ℃ (data not

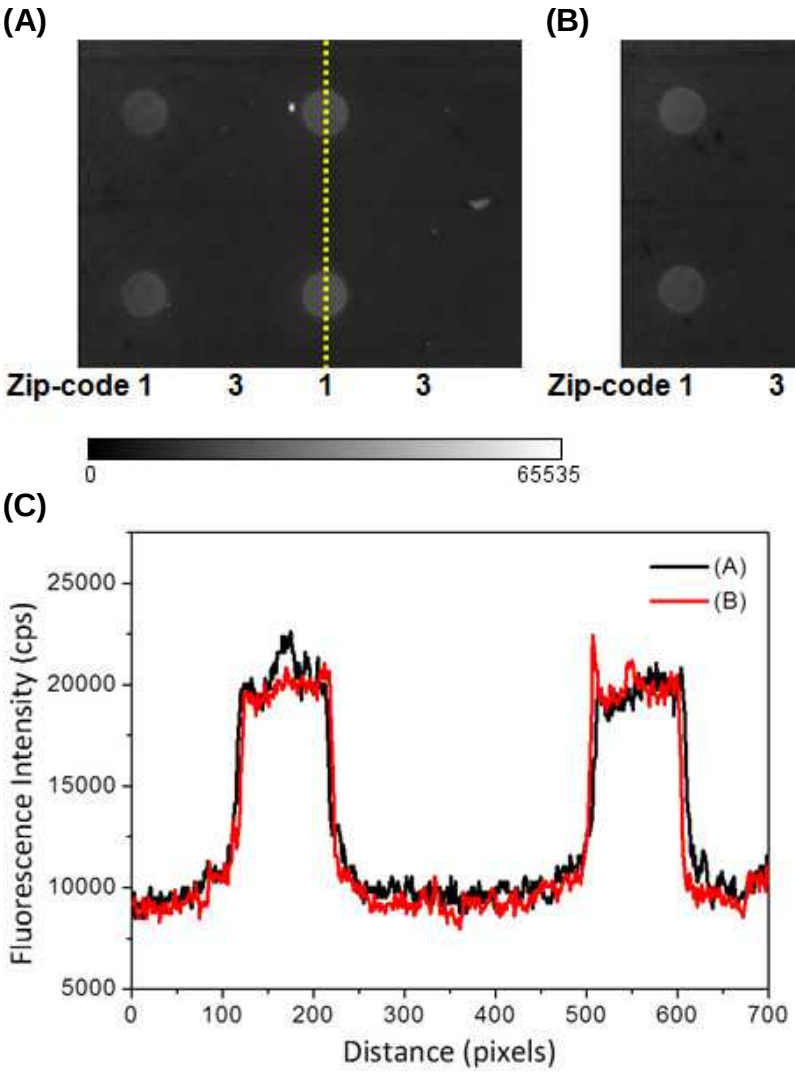

Figure 3.3 Effects of the thermal fusion bonding process on the stability of the zip-code probes. After 3'-amine-modified oligonucleotide probes (zip-code 1 and zip-code 3) were spotted onto the activated PMMA surface, PMMA sheets were either (A) heated to 107 ºC for 20 min or (B) not heated. The LDR was carried out using a conventional thermal cycler for a sample containing *E. coli* K12 only. The LDR products were dispensed onto both PMMA sheets followed by array hybridization, buffer wash and fluorescence imaging. The fluorescence intensity profiles from a vertical section of the middle two spots (see dotted yellow line) in (A) and (B) are shown in (C). Zip-code probe 3 served as the negative control and zip-code 1 probed for the target, *E. coli* K12. The spot size of the universal array was ~150 μm in diameter.

shown); any temperature leakage from the CF LDR device to the universal array sitting atop this thermal processor would not affect hybridization yield. This is a consequence of the fact that we are using a universal array in this example. The zip-code probes and zip-code complements appended to the LDR primers can be designed to have a relatively high T_m; we have decoupled the mutation detection step from the hybridization process relaxing the need for strict hybridization stringency.

3.3.3 Detection of Pathogens Using the Integrated System

To demonstrate the utility of the modular system and the assay for the detection of bacterial pathogens, the analysis of *E. coli* O157:H7 and *Salmonella*, which are among the most problematic food/water pathogens,[2, 4] was used as a model. The highly conserved single nucleotide alternation in the *uidA* gene of the O157:H7 serotype (T93G) was used to differentiate *E. coli* O157:H7 from other *E coli* strains.[57-60] For the PCR/LDR/universal array assay, a pair of *uidA*-specific primers was used to amplify a 168-bp *uidA* gene of *E. coli* O157:H7 and *E. coli* K12 as well as a pair of *sipB/C*-specific primers to amplify a 250-bp *sipB/C* gene of *Salmonella*.

Following PCR amplification of the appropriate gene fragments, which contained the identification loci, the amplicons were mixed with two sets of LDR primers, common primers and discriminating primers. The discriminating primer contained a complementary zip-code sequence (cZip) at its 5'-end and a target-specific sequence at its 3'-end. In this work, the allele-specific discriminating primers for *E. coli* O157:H7 contained a G nucleotide at its 3'-terminus (cZip5-uidA-Mt, **Table 3.1**), while the discriminating primer for *E. coli* K12 had a 3'-terminus with a T nucleotide (cZip1-uidA-Wt, **Table 3.1**). The common primer was phosphorylated at its 5'-end and possessed a fluorescent dye at its 3'-end. If there was a perfect match between the locus containing

the unique signature sequence of the target and the sequence at the 3'-end of the discriminating primer, the ligase enzyme would ligate the common and the discriminating primers. The LDR product was then directed by the cZip to a specific location of the universal array, which used probes serving as zip-codes (24-mer with similar T_m values, **Table 3.1**) that contained sequences not found in the target DNA. The fluorescence signal detected at the specific zip-code position of the universal array indicated the presence of the corresponding pathogen in the sample. The advantages of the PCR/LDR/universal array assay include: (1) LDR and universal array hybridization can be configured to detect a variety of targets by simply appending the correct cZips to the discriminating primers used in the LDR step, which allows for a highly multiplexed assay in a single reaction mixture. (2) LDR combined with the universal array readout decouples the mutation discrimination step from the hybridization step, which allows for higher specificity to detect the intended sequence variation, even in a high excess of DNA not harboring the intended sequence variation. (3) PCR coupled with LDR gives two rounds of target amplification, which provides better signal-to-noise in the measurement.

Figure 3.4 shows the results of CF LDR products hybridized to zip-code probes 1, 3, 5 and 11 using the PMMA waveguide module. Zip-code probe 3 was set as the negative control, which was complementary to neither *E. coli* K12, *E. coli* O157:H7 or *Salmonella* zip-code complement sequences appended to their LDR primers and thus, no fluorescence was seen from the zip-code 3 probes. Zip-code probes 1, 5 and 11 were designed to target *E. coli* K12, *E. coli* O157:H7 and *Salmonella*, respectively. Our results indicated that when only *E. coli* O157:H7 was present in the sample, zip-code probe 5 produced a positive signal (**Figure 3.4A**). When both *E. coli* O157:H7 and

Salmonella were present in the sample, both zip-code probes 5 and 11 gave successful hybridization events as shown in the fluorescence image of **Figure 3.4B**. When both *E. coli* O157:H7 and *E. coli* K12 were added into the sample, zip-code probes 1 and 5 generated successful hybridization signals as shown in **Figure 3.4C**. A sample containing a mixture of *E. coli* K12, *E. coli* O157:H7 and *Salmonella* was also evaluated

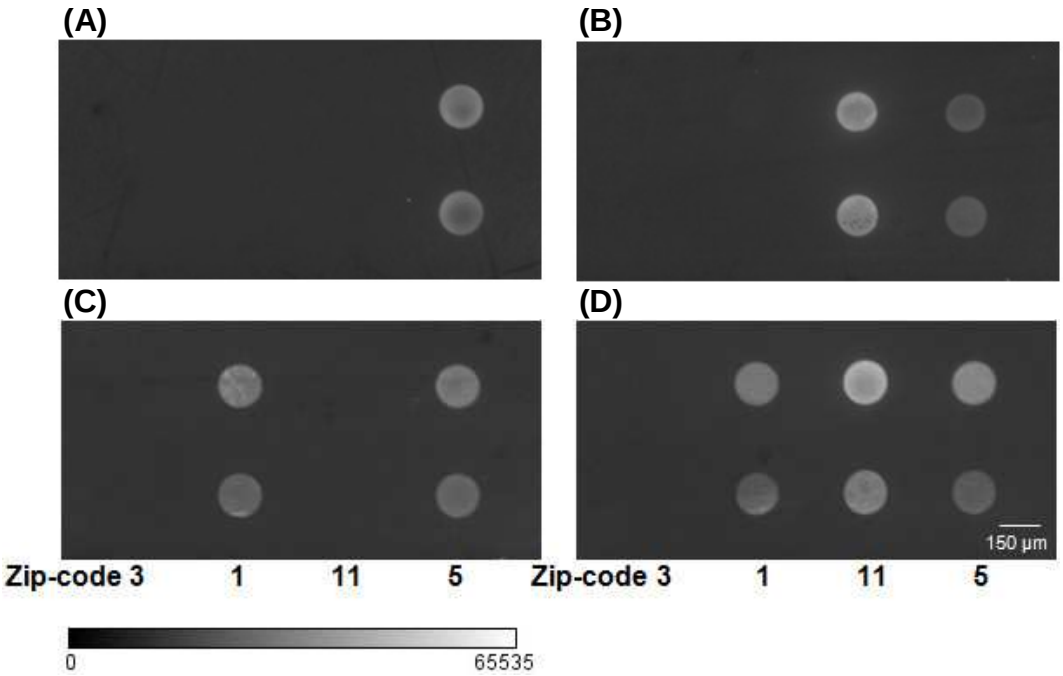

Figure 3.4 Detection of bacterial pathogens using the integrated and modular system. Fluorescence images of the universal array following CF PCR and CF LDR for a sample containing (A) *E. coli* O157:H7, (B) *Salmonella* and *E. coli* O157:H7, (C) *E. coli* K12 and *E. coli* O157:H7 and (D) *E. coli* K12, *Salmonella* and *E. coli* O157:H7. The sample flowed through the system using a volumetric flow rate of 1 µL/min for PCR and 2 µL/min for LDR and then, the arrays were imaged using the fluorescence reader with a 20 s integration time. Zip-code probe 3 was the negative control and zip-code 1, 5 and 11 probed for *E. coli* K12, *E. coli* O157:H7 and *Salmonella*, respectively.

and each zip-code probe (1, 5 and 11) produced fluorescence signals as shown in **Figure 3.4D**. The specificity of each zip-code to detect the appropriate target was evident from this data. For example, ligation products bearing the appropriate zip code complement sequence generated from *E. coli* O157:H7 or *E. coli* K12 did not hybridize to zip-code probe 11, which was targeted for the detection of *Salmonella*. Even when a

single nucleotide variation was required to be discerned, *E. coli* O157:H7 versus *E. coli* K12, no cross-hybridization was observed due to the high degree of dissimilarity between the zip-code probe sequences.

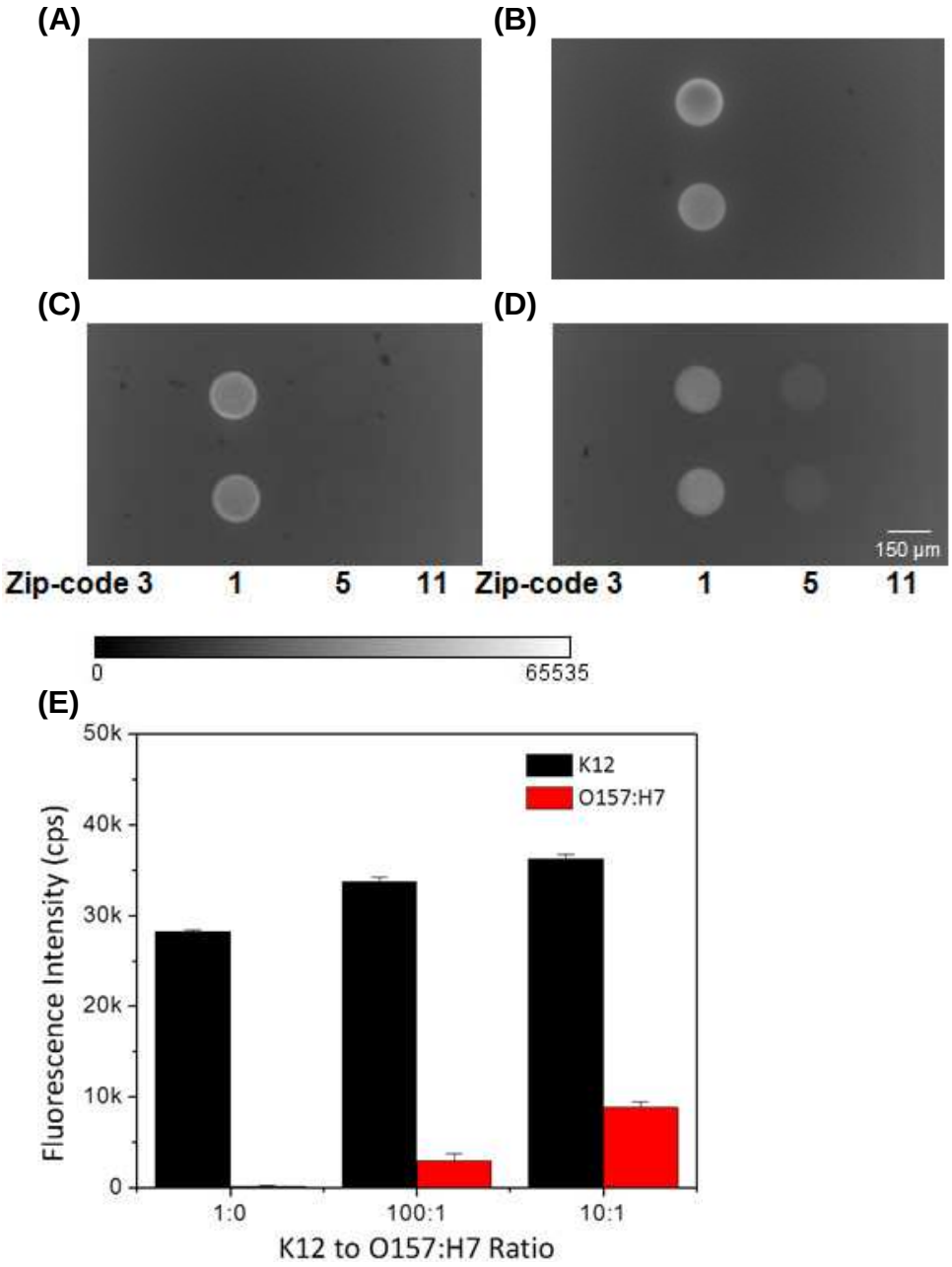

Figure 3.5 Identification of *E. coli* O157:H7 in the presence of background *E. coli* K12 with various amounts of O157:H7: (A) No DNA templates; (B) K12 only; (C) K12 to O157:H7 ratio of 100:1 and (D) K12 to O157:H7 ratio of 10:1. The fluorescence intensity profiles from (B), (C) and (D) are shown in (E). The error bars represent one standard deviation, which was determined from two measurements.

We further tested the ability of our system for detecting the *E. coli* O157:H7 strain in the presence of large amounts of background *E. coli* K12. This is particularly important for screening O157:H7 serotypes in a high background of commensal *E. coli* because this situation is commonly found in *E. coli* O157:H7 or other pathogenic *E. coli* infections.[16] In this study, *E. coli* O157:H7 was mixed with *E. coli* K12 at ratios of 0:1, 1:10, 1:100 and 1:250. The *E. coli* O157:H7 and *E. coli* K12 cells containing the *uidA* gene were concurrently PCR amplified and appropriate strains identified using LDR consisting of two discriminating primers (cZip1-uidA-Wt and cZip5-uidA-Mt) and one common primer (uidA-com). In the presence of *E. coli* O157:H7 or *E. coli* K12, matched LDR products were generated and hybridized at the appropriate locations of the universal array. **Figure 3.5** shows LDR products generated from *E. coli* O157:H7 and *E. coli* K12 with different mixing ratios. When no *E. coli* cells were present in the sample, neither zip-code probe 1 or 5 produced hybridization signals as shown in **Figure 3.5A**. When only *E. coli* K12 was present in the sample, a ligation product was generated and detected at zip-code probe 1 (**Figure 3.5B**). Universal array signals produced from *E. coli* O157:H7 were distinguished from *E. coli* K12 at the signal-to-background ratio ≥2 with an O157:H7 to K12 ratio of 1:100.

3.3.4 Detection Limit (LOD) of *E. coli* O157:H7

We also were interested in evaluating the LOD in terms of the number of pathogenic cells we could detect using our assay and integrated system. To determine the LOD, the molecular assay was conducted using *E. coli* O157:H7 as a target. **Figure 3.6** presents a calibration plot of the fluorescence signal as a function of the starting *E. coli* O157:H7 cell number. The lowest cell number that produced a positive signal at a signal-to-noise ratio ≥2 was 100 cfu (colony forming units) of *E. coli* O157:H7. This LOD

could be improved through employing any of the following strategies: (1) generation of an SPE bed with smaller micropillars and a smaller edge-to-edge spacing that would improve DNA recovery and preconcentration factor;[61] (2) increasing the number of PCR and/or LDR thermal cycles; (3) improve the capture efficiency of the LDR products by the zip-code probes by using a shallower (<100 µm) microfluidic channel;[28] and/or (4) increasing the numerical aperture of the relay microscope objective, which would improve the amount of fluorescence collected, but at the expense of reducing the field-of-view during universal array imaging.

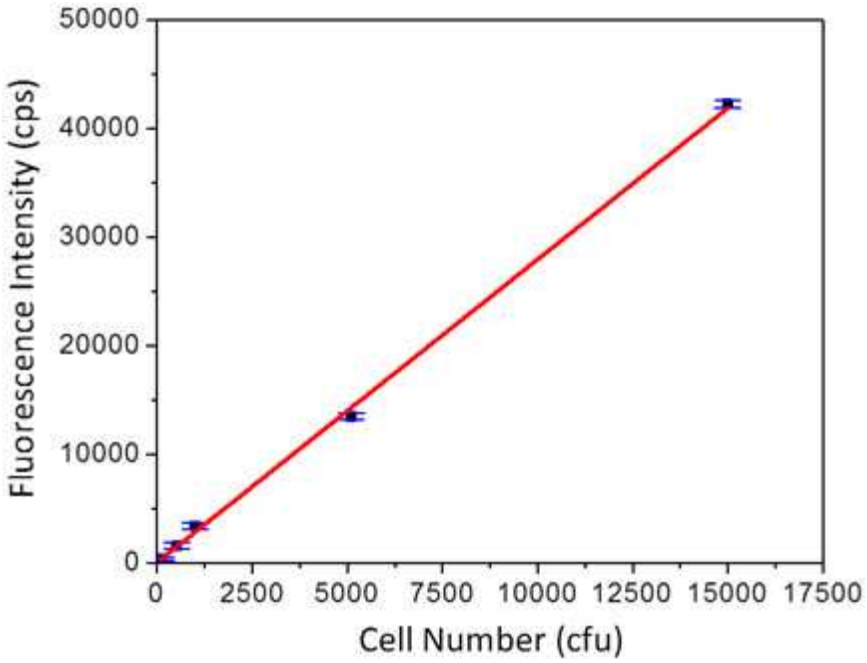

Figure 3.6 Standard curves consisting of fluorescence signals from various cell numbers of *E. coli* O157:H7 cells. The data points represent the mean of two measurements with the error bars showing ±1 standard deviation unit. The linear regression analysis yielded: $y = 2.791x + 50.11$ ($r^2 = 0.998$)

3.3.5 Analysis of *E. coli* O157:H7 in a Water Sample

In many cases, enrichment of the target cell type is required prior to molecular analysis due to the extremely low-abundance of the target pathogenic cells.[62] The US EPA allowable levels of *E. coli* are 0, 200 and 1,000 cfu per 100 mL of drinking,

swimming and recreational waters, respectively, and the minimum infectious dose is ~10 cells. Therefore, pre-enrichment of the target cells is often required, especially in drinking and recreational waters.

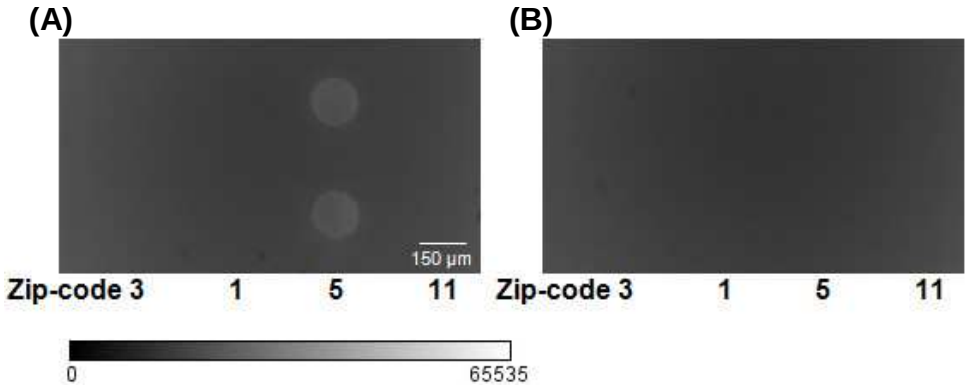

Figure 3.7 Analysis of *E. coli* O157:H7 in a water sample. The fluorescence image of the array was accomplished using evanescent excitation with an integration time of 20 s following microarray hybridization for the waste-water sample containing (A) *E. coli* O157:H7 and (B) no cells. The water sample was filtered and enriched using a PMMA microfluidic device consisting of curvilinear channels decorated with polyclonal anti-O157 antibodies. After cell enrichment, cells were released and analyzed using the integrated system targeting the gene which effectively discriminated the O157:H7 serotype from other types of *E. coli*.

We evaluated the ability of our modular system coupled with a cell enrichment device to analyze the *E. coli* O157:H7 serotype in a waste-water sample. The microchip enrichment procedure has been detailed elsewhere.[62] Briefly, sewer water (1 mL) was obtained from a purification plant in Baton Rouge and was filtered using a PCTE membrane with a 10 µm pore size to remove large particulates (*e.g.,* solid particulates and debris) from the sample. The effluent was then processed for *E. coli* using a PMMA microfluidic chip, which was equipped with 16 curvilinear high aspect ratio microchannels covalently decorated with polyclonal anti-O157 antibodies. O-157 serotypes of *E. coli* were then released from the channel surface using 5 µL of a cell-stripper solution and transferred into the integrated system for molecular analysis. After the waste-water sample was processed using the microfluidic chip, those *E. coli*

serotypes expressing O157 antigens, including O157:H7, O157:H12, O157:H42, O157:H29, O157:H19 and O157:H45, were enriched by a factor of 2 x 10^2 with the specific serotype confirmed via PCR/LDR/universal array processing.

Figure 3.7 presents results showing the analysis of *E. coli* O157:H7 in a waste-water sample using our modular system. The results indicated LDR products generated and fluorescence signals produced at zip-code probe 5, which specifically interrogated for the *E. coli* O157:H7 strain (see **Figure 3.7A**). No fluorescence signal was seen for *E. coli* K12. A negative control sample was also performed and no *E. coli* O157:H7 signal was detected as shown in **Figure 3.7B**. In the waste-water sample analyzed, the level of *E. coli* O157:H7 determined from the calibration plot was 9.5 ±0.3 x10^3 cfu/10 µL.

3.4 Conclusions

We have developed an integrated and modular microfluidic system that consisted of a module made from PMMA and a fluidic motherboard made from PC with the material selected based on optimizing the processing step(s) poised onto the module or motherboard. The motherboard was made from PC and used for cell lysis, SPE, CF PCR and CF LDR due to the specific condensation of DNA to UV-activated PC and the high Tg of PC. On the other hand, the array module was made from PMMA due to its lower fluorescence background and minimal non-specific DNA adsorption demonstrated by PMMA. The integrated platform was realized by implementing a CF PCR/CF LDR/universal array molecular assay into a disposable fluidic cartridge. The use of off-chip active components reduced the complexity of fluidic cartridge fabrication and simplified operation, making it appropriate for one-time use applications. Specifically, the use of double-sided embossing and the passive elements, such as micropillars for the SPE, micromixers and air-embedded waveguides, formed during the embossing

process allowed for minimizing the number of finishing steps required to produce the final cartridge, which can in many cases dominate chip cost.

We demonstrated the utility of the integrated system by analyzing *E. coli* O157:H7 and *Salmonella* bacterial pathogens in a total processing time <40 min (10 min for sample preparation, 24 min for PCR, 4 min for LDR and 20 s for image readout). The assay utilized by the system provided the ability to differentiate strains based on single nucleotide variations; discrimination between *E. coli* K12 and *E. coli* O157:H7 were demonstrated even for one O157:H7 sequence in 100 K12 sequences.

The integrated system was further evaluated by detecting *E. coli* O157:H7 in a waste-water sample. Enrichment was first carried out using another microfluidic device consisting of serpentine channels with polyclonal anti-O157 antibodies immobilized onto their surfaces.

While the system was demonstrated for the analysis of *E. coli* O157:H7 or *Salmonella*, simple reprogramming of the primer sequences used for the PCR and LDR would allow the system to be used for the detection of any pathogenic species without requiring hardware reconfiguration, especially when used in conjunction with the universal array; the same array can be used for any bacterial species when the correct zip-code complements are appended to the LDR primers used for detecting specific sequence variations. For example, by adding PCR primers and LDR primers targeting *stx2* and *eaeA* genes and corresponding zip-code probes, this system can easily identify the Shiga toxin 2 (*stx2*)-positive, intimin (*eae*)-negative STEC serotype O104:H4.[6]

3.5 References

1. D. L. Archer and J. E. Kvenberg, *Journal of Food Protection*, 1985, **48**, 887-894.

2. P. S. Mead, L. Slutsker, V. Dietz, L. F. McCaig, J. S. Bresee, C. Shapiro, P. M. Griffin and R. V. Tauxe, *Emerging Infectious Diseases*, 1999, **5**, 607-625.

3. M. L. Cohen, *Nature*, 2000, **406**, 762-767.

4. E. C. D. Todd, *International Journal of Food Microbiology*, 1989, **9**, 313-326.

5. T. Roberts, *American Journal of Agricultural Economics*, 1989, **71**, 468-474.

6. M. Askar, M. S. Faber, C. Frank, H. Bernard, A. Gilsdorf, A. Fruth, R. Prager, M. Hohle, T. Suess, M. Wadl, G. Krause, K. Stark and D. Werber, *Eurosurveillance*, 2011, **16**, 2-4.

7. http://www.euro.who.int/en/home.

8. B. Swaminathan and P. Feng, *Annual Review of Microbiology*, 1994, **48**, 401-426.

9. S. Rodriguez-Mozaz, M. P. Marco, M. J. L. de Alda and D. Barcelo, *Pure and Applied Chemistry*, 2004, **76**, 723-752.

10. Y. Hu, Q. Zhang and J. C. Meitzler, *Journal of Applied Microbiology*, 1999, **87**, 867-876.

11. A. M. Ibekwe, P. M. Watt, C. M. Grieve, V. K. Sharma and S. R. Lyons, *Applied and Environmental Microbiology*, 2002, **68**, 4853-4862.

12. V. Chizhikov, A. Rasooly, K. Chumakov and D. D. Levy, *Applied and Environmental Microbiology*, 2001, **67**, 3258-3263.

13. J. R. E. Shepard, Y. Danin-Poleg, Y. Kashi and D. R. Walt, *Analytical Chemistry*, 2005, **77**, 319-326.

14. M. Kostrzynska and A. Bachand, *Canadian Journal of Microbiology*, 2006, **52**, 1-8.

15. M. A. Burns, B. N. Johnson, S. N. Brahmasandra, K. Handique, J. R. Webster, M. Krishnan, T. S. Sammarco, P. M. Man, D. Jones, D. Heldsinger, C. H. Mastrangelo and D. T. Burke, *Science*, 1998, **282**, 484-487.

16. E. T. Lagally, J. R. Scherer, R. G. Blazej, N. M. Toriello, B. A. Diep, M. Ramchandani, G. F. Sensabaugh, L. W. Riley and R. A. Mathies, *Analytical Chemistry*, 2004, **76**, 3162-3170.

17. R. G. Blazej, P. Kumaresan and R. A. Mathies, *Proceedings of the National Academy of Sciences of the United States of America*, 2006, **103**, 7240-7245.

18. C. J. Easley, J. M. Karlinsey, J. M. Bienvenue, L. A. Legendre, M. G. Roper, S. H. Feldman, M. A. Hughes, E. L. Hewlett, T. J. Merkel, J. P. Ferrance and J. P.

Landers, *Proceedings of the National Academy of Sciences of the United States of America*, 2006, **103**, 19272-19277.

19. H. Becker and C. Gartner, *Anal. Bioanal. Chem.*, 2008, **390**, 89-111.

20. S. A. Soper, S. M. Ford, S. Qi, R. L. McCarley, K. Kelly and M. C. Murphy, *Analytical Chemistry*, 2000, **72**, 642A-651A.

21. A. de Mello, *Lab on a Chip*, 2002, **2**, 31N-36N.

22. Y. J. Liu, C. B. Rauch, R. L. Stevens, R. Lenigk, J. N. Yang, D. B. Rhine and P. Grodzinski, *Analytical Chemistry*, 2002, **74**, 3063-3070.

23. R. H. Liu, J. N. Yang, R. Lenigk, J. Bonanno and P. Grodzinski, *Analytical Chemistry*, 2004, **76**, 1824-1831.

24. C. G. Koh, W. Tan, M. Zhao, A. J. Ricco and Z. H. Fan, *Analytical Chemistry*, 2003, **75**, 4591-4598.

25. A. F. Sauer-Budge, P. Mirer, A. Chatterjee, C. M. Klapperich, D. Chargin and A. Sharon, *Lab on a Chip*, 2009, **9**, 2803-2810.

26. H. Shadpour, H. Musyimi, J. F. Chen and S. A. Soper, *Journal of Chromatography A*, 2006, **1111**, 238-251.

27. G. A. Thomas, Farquar, H.D., Sutton, S., Hammer, R.P., Soper, S.A., *Molecular Review Diagnostics*, 2002, **2**, 429-447.

28. Y. Wang, B. Vaidya, H. D. Farquar, W. Stryjewski, R. P. Hammer, R. L. McCarley, S. A. Soper, Y. W. Cheng and F. Barany, *Analytical Chemistry*, 2003, **75**, 1130-1140.

29. M. A. Witek, S. Llopis, A. Wheatley, R. McCarley and S. A. Soper, *Nucleic Acids Research*, 2006, **34**, e74.

30. M. A. Witek, M. L. Hupert, D. S. W. Park, K. Fears, M. C. Murphy and S. A. Soper, *Analytical Chemistry*, 2008, **80**, 3483-3491.

31. F. Xu, P. Datta, H. Wang, S. Gurung, M. Hashimoto, S. Wei, J. Goettert, R. L. McCarley and S. A. Soper, *Analytical Chemistry*, 2007, **79**, 9007-9013.

32. M. Hashimoto, M. L. Hupert, M. C. Murphy, S. A. Soper, Y. W. Cheng and F. Barany, *Analytical Chemistry*, 2005, **77**, 3243-3255.

33. M. Hashimoto, F. Barany and S. A. Soper, *Biosensors & Bioelectronics*, 2006, **21**, 1915-1923.

34. P. C. Chen, D. Nikitopoulos, S. A. Soper and M. C. Murphy, *Biomedical Microdevices*, 2008, **10**, 141-152.

35. M. L. Hupert, W. J. Guy, S. D. Llopis, H. Shadpour, S. Rani, D. E. Nikitopoulos and S. A. Soper, *Microfluidics and Nanofluidics*, 2007, **3**, 1-11.

36. C. Situma, Y. Wang, M. Hupert, F. Barany, R. L. McCarley and S. A. Soper, *Analytical Biochemistry*, 2005, **340**, 123-135.

37. S. A. Soper, M. Hashimoto, C. Situma, M. C. Murphy, R. L. McCarley, Y. W. Cheng and F. Barany, *Methods*, 2005, **37**, 103-113.

38. V. K. Sharma, E. A. Dean-Nystrom and T. A. Casey, *Molecular and Cellular Probes*, 1999, **13**, 291-302.

39. J. L. E. Ellingson, J. L. Anderson, S. A. Carlson and V. K. Sharma, *Molecular and Cellular Probes*, 2004, **18**, 51-57.

40. M. Hashimoto, P. C. Chen, M. W. Mitchell, D. E. Nikitopoulos, S. A. Soper and M. C. Murphy, *Lab on a Chip*, 2004, **4**, 638-645.

41. J. F. Chen, M. Wabuyele, H. W. Chen, D. Patterson, M. Hupert, H. Shadpour, D. Nikitopoulos and S. A. Soper, *Analytical Chemistry*, 2005, **77**, 658-666.

42. M. B. Wabuyele, S. M. Ford, W. Stryjewski, J. Barrow and S. A. Soper, *Electrophoresis*, 2001, **22**, 3939-3948.

43. Y. C. Xu, B. Vaidya, A. B. Patel, S. M. Ford, R. L. McCarley and S. A. Soper, *Analytical Chemistry*, 2003, **75**, 2975-2984.

44. H. Wang, J. F. Chen, L. Zhu, H. Shadpour, M. L. Hupert and S. A. Soper, *Analytical Chemistry*, 2006, **78**, 6223-6231.

45. D. Erickson, X. Z. Liu, U. Krull and D. Q. Li, *Analytical Chemistry*, 2004, **76**, 7269-7277.

46. L. Brown, T. Koerner, J. H. Horton and R. D. Oleschuk, *Lab on a Chip*, 2006, **6**, 66-73.

47. C. H. Lin, C. H. Chao and C. W. Lan, *Sensors and Actuators B-Chemical*, 2007, **121**, 698-705.

48. Y. Sun, Y. C. Kwok and N. T. Nguyen, *Journal of Micromechanics and Microengineering*, 2006, **16**, 1681-1688.

49. X. L. Zhu, G. Liu, Y. H. Guo and Y. C. Tian, *Microsystem Technologies-Micro-and Nanosystems-Information Storage and Processing Systems*, 2007, **13**, 403-407.

50. F. J. Blanco, M. Agirregabiria, J. Garcia, J. Berganzo, M. Tijero, M. T. Arroyo, J. M. Ruano, I. Aramburu and K. Mayora, *Journal of Micromechanics and Microengineering*, 2004, **14**, 1047-1056.

51. Y. J. Pan and R. J. Yang, *Journal of Micromechanics and Microengineering*, 2006, **16**, 2666-2672.

52. T. Ussing, L. V. Petersen, C. B. Nielsen, B. Helbo and L. Hojslet, *International Journal of Advanced Manufacturing Technology*, 2007, **33**, 198-205.

53. C. W. Tsao, L. Hromada, J. Liu, P. Kumar and D. L. DeVoe, *Lab on a Chip*, 2007, **7**, 499-505.

54. M. E. Vlachopoulou, A. Tserepi, P. Pavli, P. Argitis, M. Sanopoulou and K. Misiakos, *Journal of Micromechanics and Microengineering*, 2009, **19**.

55. Y. H. Tennico, M. T. Koesdjojo, S. Kondo, D. T. Mandrell and V. T. Remcho, *Sensors and Actuators B-Chemical*, 2010, **143**, 799-804.

56. S. J. Park, K. S. Cho and C. G. Choi, *Journal of Colloid and Interface Science*, 2003, **258**, 424-426.

57. P. Feng and K. A. Lampel, *Microbiology-Sgm*, 1994, **140**, 2101-2107.

58. T. A. Cebula, W. L. Payne and P. Feng, *Journal of Clinical Microbiology*, 1995, **33**, 248-250.

59. S. R. Monday, T. S. Whittam and P. C. H. Feng, *Journal of Infectious Diseases*, 2001, **184**, 918-921.

60. K. J. Yoshitomi, K. C. Jinneman and S. D. Weagant, *Molecular and Cellular Probes*, 2003, **17**, 275-280.

61. M. Witek, D. Park, M. Hupert, R. L. McCarley, M. C. Murphy and S. A. Soper, *Analytical Chemistry*, 2008, **80**, 3483-3491.

62. U. Dharmasiri, M. A. Witek, A. A. Adams, J. K. Osiri, M. L. Hupert, T. S. Bianchi, D. L. Roelke and S. A. Soper, *Anal. Chem.*, 2010, **82**, 2844-2849.

CHAPTER 4 FULLY INTEGRATED AND SELF-CONTAINED THERMOPLASTIC GENOSENSOR FOR THE DIAGNOSIS OF MULTI-DRUG RESISTANT TUBERCULOSIS (MDR-TB)

4.1 Introduction

Infectious diseases are a major global health burden, accounting for approximately 15 million deaths annually with a significant number occurring in developing countries.[1-4] The recently accelerated evolution and spread of drug resistant pathogenic agents pose two daunting challenges for the prevention, diagnosis and treatment of infectious diseases:[4-7] How to accurately and rapidly diagnose drug-resistant infections and how to deliver these diagnostic technologies and tools to resource-limited settings?

In particular, the resurgence of tuberculosis (TB) is accompanied by rapid spreading of multi-drug resistant TB (MDR-TB) resulting from *Mycobacterium tuberculosis* (Mtb) strains that fail to respond to the first-line drugs rifampin and isoniazid. MDR-TB cannot be differentiated from drug susceptible TB from clinical symptoms, chest X-ray examinations or sputum smears.[8] Currently, only less than 5% of approximately 1/2 million MDR-TB cases estimated globally are appropriately diagnosed and treated due to the vastly inadequate laboratory infrastructure for conventional drug susceptibility testing (DST) by cell culturing in high burden countries.[9] Even if available, it may take up to 8 – 12 weeks to complete culturing tests during which time patients are ineffectively treated and thus, drug resistant strains continue to spread creating a formidable obstacle in formulating global plans to eradicate this disease.

Several commercialized or home-brewed nucleic acid amplification tests (NAATs), such as line probe assays or quantitative PCRs, have recently been demonstrated to identify MDR-TB in a timeframe of 1-2 days. Although these tests are a significant improvement over DSTs in assay turnaround time, sophisticated laboratory settings and

extensively trained personnel must be in place to ensure accuracy, reliability, and reproducibility of test results. The cost is prohibitive as well for the widespread implementation of these assays to referral laboratories let alone to remote clinical facilities, which are in urgent need for fast and reliable assays that are easy to implement for MDR-TB testing. In addition, the performance of these assays is usually compromised when a mixed subpopulation of drug resistance and susceptible strains (hetero-resistance) are simultaneously presented in the clinical sample.[10-12]

To address the aforementioned challenges, we have developed a diagnostic tool package consisting of a novel multistep molecular assay implemented in a fully-integrated genosensor system. The molecular assay could interrogate single base mutations (codon 516, 526, and 531) in the rifampin-resistance determining region (RRDR) of the *rpo*B gene as surrogate markers for MDR-TB.[13, 14] The multi-step process included Mtb cell lysis, solid-phase DNA extraction and purification, duplex PCR for amplifying a 193 bp fragment containing the RRDR and a positive control fragment, multiplexed LDR (ligase detection reaction) for discrimination/identification of single base mutations and universal array hybridization. All of the aforementioned processing steps were carried out within a disposable fluidic cartridge operated by accompanying peripherals packaged into a small footprint instrument. No operator intervention was required once the clinical sample (sputum) was loaded into the fluidic cartridge. This diagnostic tool package offered advantages including short analysis times, automated operation (*i.e.,* sample in – answer out), reduced possibility of cross-contamination, improved health-worker protection and lower overall cost of the analysis. It's a significant step in translating a highly specific molecular assay strategy and lab-on-a-chip enabling technologies to a diagnostic tool package tackling a global health crisis.

4.2 Methods

4.2.1 Fabrication of Fluidic Cartridge

The fluidic cartridge consists of three plastic manufacturing modules (**Figure 4.1A-C**) including a solid phase DNA extraction (SPE) module, a thermal reactor module for cell lysis, PCR and LDR, and a waveguide module for universal array hybridization and fluorescence readout. Short pieces of Tefzel^{TM} tubing (OD = 1/16", ID = 250 µm, Upchurch) were inserted into the conical holes on the backsides of fluidic modules to provide fluidic transport between them (**Figure 4.1D** and **4.1E**).

4.2.1.1 Fabrication of UV-activated SPE Module

The SPE beds were replicated by one-step aligned double-sided hot-embossing from a nickel mold insert and a brass mold insert mounted opposite to each other in a JENOPTIK HEX-02 hot embossing system (Jena, Germany). The nickel mold insert for molding twenty-four (3 x 8) extraction beds was fabricated by UV-LIGA process. The brass mold insert for molding backside conical interconnectors was fabricated by high-precision micro-milling, as described elsewhere.[15] After hot-embossing, the extraction bed and a 250 µm thick PC coverslip were exposed to 254 nm UV radiation (15 mW/cm^2) for 20 min. The SPE module was assembled by thermal fusion bonding at 147 ℃ for 20 min.

4.2.1.2 Fabrication of Thermal Reactor Module

The PC substrate (**Figure 4.3A**) containing microchannels for cell lysis, PCR and LDR on the frontside and micro-valve seats, thermal isolation grooves and fluidic interconnecting ports on the backside was replicated by double-sided hot-embossing using two micro-milled brass mold inserts. The PC module was assembled by thermal

fusion bonding of the PC substrate and a 250 µm thick PC coverslip at 150 ℃ for 20 min.

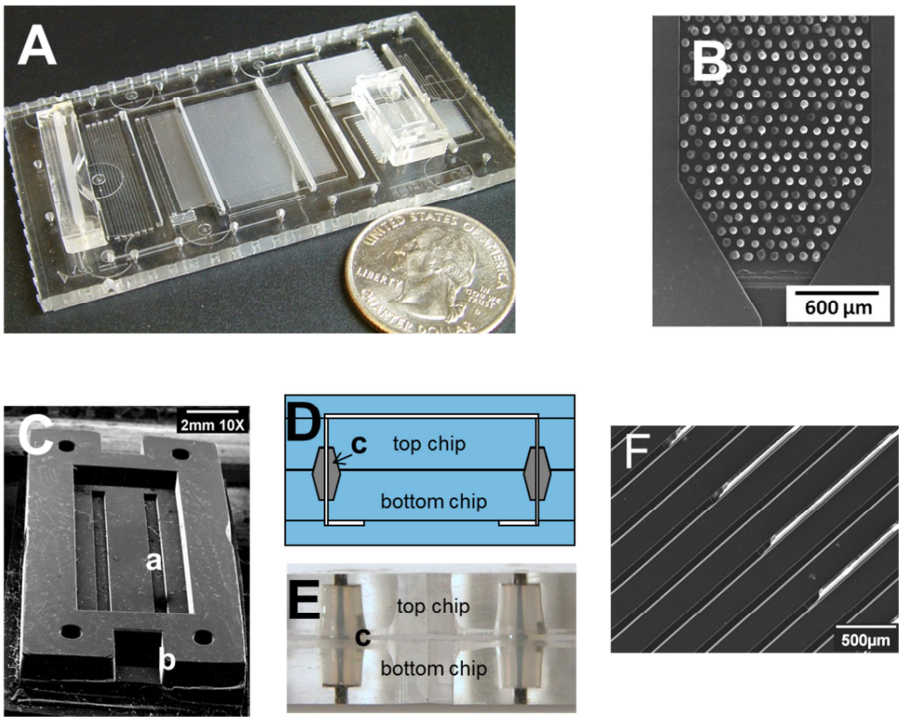

Figure 4.1 (A) Assembled modular microfluidic stack. (B) SEM of DNA-SPE bed. (C) SEM of the universal array module with integrated waveguide (a) and coupling prism (b). (D, E) Schematic and optical micrograph of chip-to-chip fluidic interconnects; c – connecting tube inside a cone-shaped port; channels were filled with black dye for visualization. (F) Cross-section of dual depth thermal reactor.

4.2.1.3 Fabrication, Spotting and Assembly of Fluorescence Readout Module

The fluorescence readout module was assembled from two hot-embossed PMMA parts: a waveguide part and an interconnecting part containing conical ports for fluidic connection to PC thermocycling module as described above. The waveguide part has a 1.2 mm x 10 mm recess (100 µm in depth) for zip-code probe immobilization and hybridization on the front side and an air-embedded planar waveguide along with an integrated laser-coupling prism on the backside. Twenty-four (4 by 6) of waveguide parts were replicated on one piece of PMMA substrate by an aforementioned double-

sided hot-embossing process. Followed oxygen plasma activation, EDC-NHS chemistry was used to functionalize the surface of the PMMA substrate. The freshly prepared PMMA substrates were mounted onto the vacuum holder of a Piezorray® non-contact microarraying system (PerkinElmer Inc.) through custom made adapters. With the aid of visual positioning camera, the zip-code oligonucleotide probes were dispensed onto the bottom of the recess. By carefully programming, the universal zip-code arrays were spotted onto five pieces of PMMA substrates, each containing twenty-four waveguide parts, in a single run. After four hours incubation in a humid box at room temperature, the waveguide parts were thoroughly cleaned to remove the excess zip-code probes. After drying, the waveguide and interconnection parts were assembled together using UV curable optical adhesive (NOA 68, Norland) to form functional fluorescent readout module.

4.2.2 Instrumentation

The field-deployable instrument has been developed to perform the molecular assay in the disposable fluidic cartridge. The physical dimensions of this prototype instrument are 12” (length) x 12” (depth) x 12” (height) and include the Instrument Control Unit (ICU) board, solenoids, actuators, pumps, solenoid valves, heating stage and on-board solution reservoirs. After the sample, PCR and LDR cocktail were manually loaded with a pipette; the fluidic cartridge was inserted into the instrument and gently held between the heater surface and the self-alignment pins located on a fluid distribution motherboard. The cooper heating blocks are covered by thermal conductive tape providing good thermal contact. The self-alignment pins made from stainless steel tubing also serve as fluidic connection between the disposable fluidic cartridge and the external valves, pumps and bulk reservoirs through the fluidic distribution motherboard.

Once the fluidic cartridge was loaded, the complete analysis process, including the cell lysis, DNA extraction, PCR, LDR and universal array hybridization, was automatically controlled by the ICU and no further user intervention was required.

The fluorescence images were collected by a compact optical system consisting of a laser diode and a CCD image sensor. The 635 nm emission from the laser diode (HL6320G, 10 mW, Hitachi) was collimated using a laser collimation package (LT220P-B, ThorLabs) and injected into the waveguide through an integrated prism (**Figure 4.3E**). The evanescent wave excited fluorescence image was collected by a CCD image sensor (S7030-0907; 512 x 58 pixels; 24 x 24 µm/pixel; Hamamatsu) through a compact optics composed of two of 2x objective lens (Olympus) and filter sets (3RD660LP long pass filter and 3RD660-680 band pass filter, Omega Optics.).

4.2.3 *Mycobacterium tuberculosis* (Mtb) Samples

Drug susceptible Mtb strain H37Rv (ATCC 27294) and rifampin resistant Mtb strain (ATCC) were cultured in BSL-3 laboratory in Hansen's Disease Center in LSU. 10-fold serial dilutions from 10^7 to 10^0 of Mtb strain H37Rv were prepared for evaluation of the limit of detection. Samples containing mixed drug susceptible and resistant Mtb sub-population were prepared by mixing drug resistant and drug susceptible strains at the ratio of 0%, 1%, 2%, 5%, 10%, 50% and 100%. All cultured Mtb samples were fixed in 70% ethanol for 24 h prior to removal from the BSL-3 facility.[16]

4.2.4 Construction of Positive Control

A 124 bp fragment of the IS6110 gene was amplified using the following pair of primers: CCT GCG AGC GTA GGC GTC GG (forward) and TCT CGT CCA GCG CCG CTT CGG (reverse).[17] PCR was then performed as follows: 2 min at 94 ℃; 20 cycles of 1 min at 94 ℃, 1 min at 56 ℃, and 1 min at 72 ℃; and a final extension of 15 min at

72 ℃. The PCR product was purified using a QIAquic k spin column PCR purification kit (QIAGEN, Cat. no. 28104). The purified amplicon was cloned into pCR®4-TOPO® plasmid using TOPO TA cloning kit for sequencing (Invitrogen, Cat. no. K4575-J10).

Two mutations were introduced into the amplified DNA using a GeneTailor site-directed mutagenesis system (Invitrogen, Cat. no. 12397-014) according to the manufacturer's instructions. Briefly, the aforementioned plasmid was methylated with DNA methylase at 37 ℃ for 1 h. Two mutations, incl uding a 3-base mutation of TCA → AGT at the center of the LDR discriminating primer location and a single-base deletion of T at the ligation site of the LDR, were introduced by amplifying the methylated plasmid using two overlapping primers: TGT GGG TAG CAG ACC AGT CCT ATG TG(T)C GAC CTG GGC AG (forward) and GGT CTG CTA CCC ACA GCC GGT TAG GTG CTG (reverse), and Platinum®*Pfx* DNA Polymerase (Invitrogen, Cat. no. 11708-013). Amplification began with a denaturation step of 2 min at 94 ℃, followed by 20 cycles of 30 s at 94 ℃, 30 s at 55 ℃, 5 min at 68 ℃; and a final extension step of 10 min at 68 ℃. The mutagenic mixture was then transf ormed into One-Shot® MAX Efficiency® DH5α™-T1R competent cells (Invitrogen, Cat. no.12297-016). The methylated plasmid was digested by MrcBC endonuclease in the host cell while the methylated and mutated DNA from the above amplification was circularized by the host cell. Finally, the plasmid was purified using a QIAgen plasmid Midi kit (Cat. no. 12143) and the mutations were confirmed by DNA sequencing using T3 and T7 primers. The plasmid containing the two mutations (designated as PC) was used as a positive control for the molecular analysis of clinical samples. The plasmid concentration was quantified by measuring the absorption at 260 nm.

Table 4.1 Sequences of oligonucleotides used in the PCR/LDR/universal zip-code hybridization assay for MDR-TB

PCR product size (bp)	Oligos	Sequence (5'→3')	T_m (℃) [e]
124	IS6110-forward	CCTGCGAGCGTAGGCGTCGG	65.4
	IS6110-reverse	TCTCGTCCAGCGCCGCTTCGG	66.7
	cZip51-PC	**GGCTCAAGTTGCGTCCCAGACCGT**GTGGGTAGCAGACCAGTCCTATGTG	65.4
	cZip43-IS6110	**CCGTCAGACAAGGGCTTTGCGTCC**GGGTAGCAGACCTCACCTATGTGT	64.3
	IS6110/PC-com	[a]pCGACCTGGGCAGGGTTCGC-Cy5[b]	64.0
193	rpoB-forward	CGTGGAGGCGATCACACCGCAGACGTT	67.7
	rpoB-reverse	ACCTCCAGCCCGGCACGCTCACGTG	70.8
	cZip13-rpoB516wt	**CGCACGATAGGTGGTCTACCGCTG**CAGCTGAGCCAATTCATGGA	63.1
	cZip21-rpoB516mt	**GGTCAGGTTACCGCTGCGATCGCA**CAGCTGAGCCAATTCATGGT	65.3
	rpoB516-com	[a]pCCAGAACAACCCGCTGTC-Cy5[b]	56.3
	cZip1-rpoB531wt	**GCTGAGGTCGATGCTGAGGTCGCA**CCACAAGCGCCGACTGTC	64.9
	cZip5-rpoB531mt	**GCTGTACCCGATCGCAAGGTGGTC**CCACAAGCGCCGACTGTT	63.7
	rpoB531-com	[a]pGGCGCTGGGGCCCGGC-Cy5[b]	70.2
	cZip11-rpoB526wt	**CGCAAGGTAGGTGCTGTACCCGCA**CGCTGTCGGGGTTGACCC	65.2
	cZip23-rpoB526mt	**GGTCCGATTACCGGTCCGATGCTG**CGCTGTCGGGGTTGACCT	63.3
	rpoB526-com	[a]pACAAGCGCCGACTGTCGG-Cy5[b]	61.0
	Zip-code 1	TGCGACCTCAGCATCGACCTCAGC-sp-NH_2[d]	64.9
	Zip-code 3	CAGCACCTGACCATCGATCGCAGC-sp-NH_2[d]	64.1
	Zip-code 5	GACCACCTTGCGATCGGGTACAGC-sp-NH_2[d]	63.7
	Zip-code 11	TGCGGGTACAGCACCTACCTTGCG-sp-NH_2[d]	65.2
	Zip-code 13	CGCACGATAGGTGGTCTACCGCTG-sp-NH_2[d]	63.1
	Zip-code 15	GACCGGTATGCGACCTGGTATGCG-sp-NH_2[d]	63.5
	Zip-code 21	TGCGATCGCAGCGGTAACCTGACC-sp-NH_2[d]	65.3
	Zip-code 23	CAGCATCGGACCGGTAATCGGACC-sp-NH_2[d]	63.3
	Zip-code 25	GACCATCGTGCGGGTAGGTAGACC-sp-NH_2[d]	62.7
	Zip-code 43	GGACGCAAAGCCCTTGTCTGACGG-sp-NH_2[d]	64.3
	Zip-code 51	ACGGTCTGGGACGCAACTTGAGCC-sp-NH_2[d]	65.4

[a] p: phosphorylated.
[b] Cy5: λ_{ex} = 649 nm, λ_{em} = 670 nm.
[c] The bold sequences are complementary to the sequences of zip-code probes.
[d] sp-NH_2: $(CH_2CH_2O)_6PO_4$-NH_2.
[e] Conditions: oligo concentration, 1 μM; Na^+ concentration, 50 mM.

4.2.5 Sample and Reagent Loading

Cell cultures in 70% ethanol and decontaminated clinical samples were briefly centrifuged at 12,000g and the supernatants were removed. The sediments were re-suspended in 20 µL SPE binding buffer and manually loaded to the cell lysis unit in the fluidic cartridge (**Figure 4.3**). The SPE binding buffer contained 1.2 M NaCl and 6% polyethylene glycol (PEG, M_w = 8000) and 80 fg (~2000 copies) of PC plasmid.

1x PCR cocktail consisted of 10 mM Tris-HCl buffer (pH = 8.3), 50 mM KCl, 1.5 mM $MgCl_2$, 200 µM dNTPs, 0.5 U/µL *Taq* polymerase, 0.5 µg/µL ultra-pure BSA, 500 nM forward and reverse primers and the DNA extracted from the SPE unit. Duplex PCR was performed to amplify 193 bp fragment containing RRDR in *rpo*B gene and 124 bp fragment of IS6110 gene and PC. PCR primers are listed in **Table 4.1**. The temperature zones were set at 95 ℃, 62 ℃ and 72 ℃ for denatu ration, annealing and extension, respectively. 1 x PCR cocktail was loaded in the PCR buffer storage zone (**Figure 4.3A**).

1x LDR cocktail consisted of 20 mM Tris-HCl buffer (pH = 7.6), 25 mM KCl, 5 mM $MgCl_2$, 1 mM NAD^+, 5 mM DTT, 0.1 % Triton X-100, 2 U/µL *Taq* ligase, 0.5 µg/µL ultra-pure BSA, LDR primer sets and the PCR products from PCR unit. 25 nM of the discriminating primers and 50 nM of the common primers for codon 516, and 50 nM of the discriminating primers and 100 nM of the common primers for codon 526 and 531, respectively, were used. The LDR primers sequences are listed in **Table 4.1**. 2x LDR cocktail was loaded in the LDR buffer storage zone (**Figure 4.3A**).

4.2.6 Colorimetric Line DNA Probe Assay

A PDMS stencil containing a microchannel network was cast using a mold master made from PMMA and consisted of 250 µm wide and 30 µm deep microchannels

spaced by 1 mm. After a brief treatment with the oxygen plasma, the PDMS stencil was physically sealed to an EDC-NHS functionalized PMMA sheet by conformal contact.[18, 19] Then, 50 µM of zip-code oligonucleotide probes in pH 9.0 carbonate buffer were flowed through the PDMS microchannels. After 1 h of incubation, the PDMS stencil was removed. The PMMA sheet was thoroughly cleaned and cut into 5 mm wide strips for the line DNA probe assays (see **Figure 4.6B**).

Mono-maleimido functionalized Nanogold (Nanoprobes Inc.) particles (1.4 nm) were conjugated to LDR common primers functionalized with a sulfhydryl group (-SH) at their 5' ends and a phosphate group (PO_4) at the 3' terminus.[20] Then, 10 µM common primers were reduced by 100 µM Tris(2-Carboxyethyl) phosphine Hydrochloride (TCEP·HCl, Pierce) in 1x TE buffer for 30 min at room temperature. Following the disulfide cleavage, a 10-fold excess of the mono-maleimido Nanogold particles were added and incubated at room temperature for 2 h. The LDR common primer-Au conjugates were then purified twice using Bio-Spin 6 chromatography columns (Bio-Rad) according to the manufacturer's instructions. The labeling efficiency and the concentration of the common primer-Au conjugate were determined by measuring the absorbance of the oligonucleotide at 260 nm and the absorbance of the Nanogold particle at its absorbance maximum of 420 nm.

Twenty µL of the ligation products generated from a fast thermal cycling (15 cycles of 95 ℃ for 5 s and 60 ℃ for 15 s) protocol was a pplied to the line DNA probe strips and incubated for 10 min at 50 ℃. Silver enhanceme nt was performed by applying a mixture of 20 µL of initiator and enhancer from a Li enhancer kit (Nanoprobes, Inc) to the PMMA surface. After 15 min of incubation, the hybridization pattern was visible to the naked eye and could be recorded by a digital camera (see **Figure 4.6C**).

4.3 Results

It is estimated more than 90% of rifampin resistant Mtb strains are also resistant to isoniazid, which makes rifampin resistance a reliable surrogate marker for MDR-TB. Collectively, more than 95% of resistance to rifampin is associated with mis-sense, insertion, and deletion mutations in the rifampin resistance-determining region (RRDR) of the *rpo*B gene, especially single base mutations in codons 516, 526 and 531. Rapid identification of these mutations is critical in MDR-TB case management and minimizing the spread of drug resistant Mtb strains.[13, 14, 21]

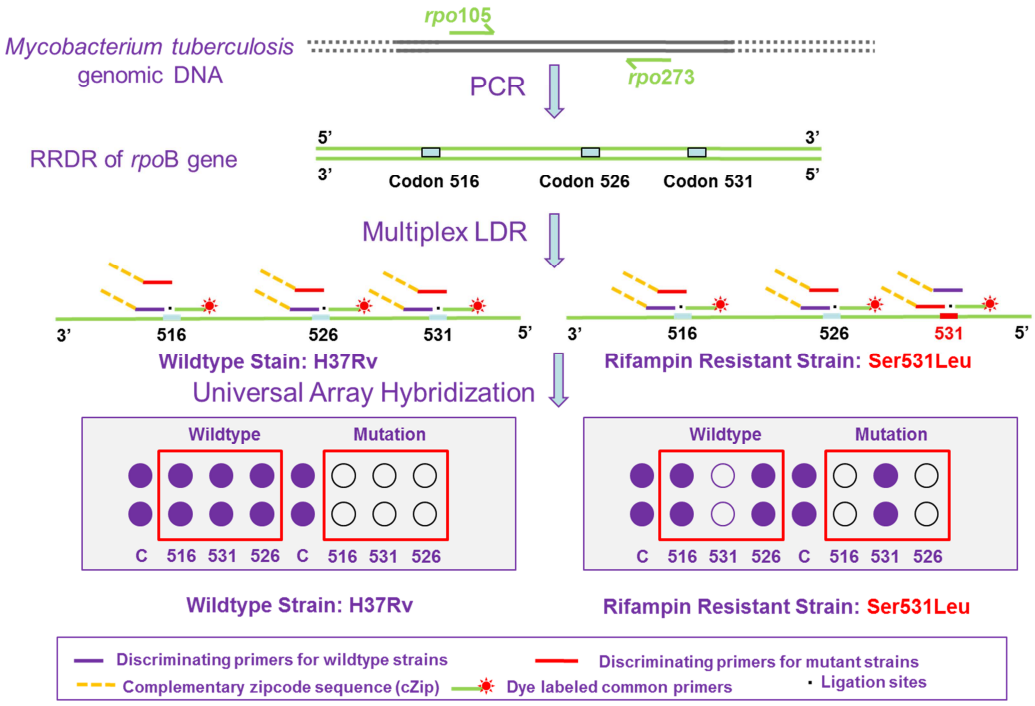

Figure 4.2 Schematic representation of the molecular assay for detection of single base variations in codons 516, 526 and 531. The left panel and the right panel demonstrate the processes when wild-type Mtb stain H37Rv and rifampin resistant Mtb strain (Ser531Leu) are subjected to the molecular assay, respectively.

4.3.1 MDR-TB Molecular Assay

A multi-step molecular assay, PCR/LDR/universal array hybridization, was successfully applied for single base mutation determinations as described elsewhere.[22]

A schematic representation of the molecular assay for detecting single base mutations in codons 516, 526 and 531 in the RRDR is shown in **Figure 4.2**. Briefly, following PCR amplification of a 193 bp *rpo*B gene fragment containing RRDR region, 3 sets of LDR primers (mutation specific discriminating primers and common primers) were used for interrogating the most frequent single base mutations in codons 516, 526 and 531 of the *rpoB* gene. The discriminating primer was flanked by a complementary zip-code sequence (cZip) at its 5'-end and a discriminating base for either wild-type or mutation discrimination at its 3'-end. The common primer was phosphorylated at its 5'-end and contained a fluorescence dye, Cy5, at its 3'-end. A perfect match at the 3'-end of the discriminating primer would initiate a ligation reaction by a thermally stable ligase enzyme, which also carried a specific cZip sequence to direct the product to a specific location of a two-dimensional array. The genotype at the particular locus can be subsequently decoded by zip-code array hybridization and read out by fluorescence or colorimetric imaging of a universal array.

4.3.2 Fluidic Cartridge Design

The fluidic cartridge shown in **Figure 4.1** and **Figure 4.3** could carry out five different processing steps including cell lysis, solid phase DNA extraction (SPE), PCR, LDR and universal array hybridization, which were distributed on two different modules and the fluidic motherboard according to the material and manufacturing requirements. For example, the SPE module was made from PC that was photoactivated (PPC) due to its unique characteristics allowing for the specific condensation of nucleic acids to its UV-activated surface.[23] In addition, to avoid packing the SPE bed with beads to increase the available surface area to provide a high DNA load, high aspect ratio micropillars were embossed into the bed during fabrication of the fluidic network. PC also has a

relatively high glass transition temperature, which makes it a suitable material for the substrate used for the thermal reactors and thus was used for the fluidic motherboard. In addition, the fluidic control elements, in this case several membrane microvalves, also benefitted from the use of PC, because PC has a relatively large elongation at break threshold. Thus, it can be used for fabrication of both the valve seat and the valve

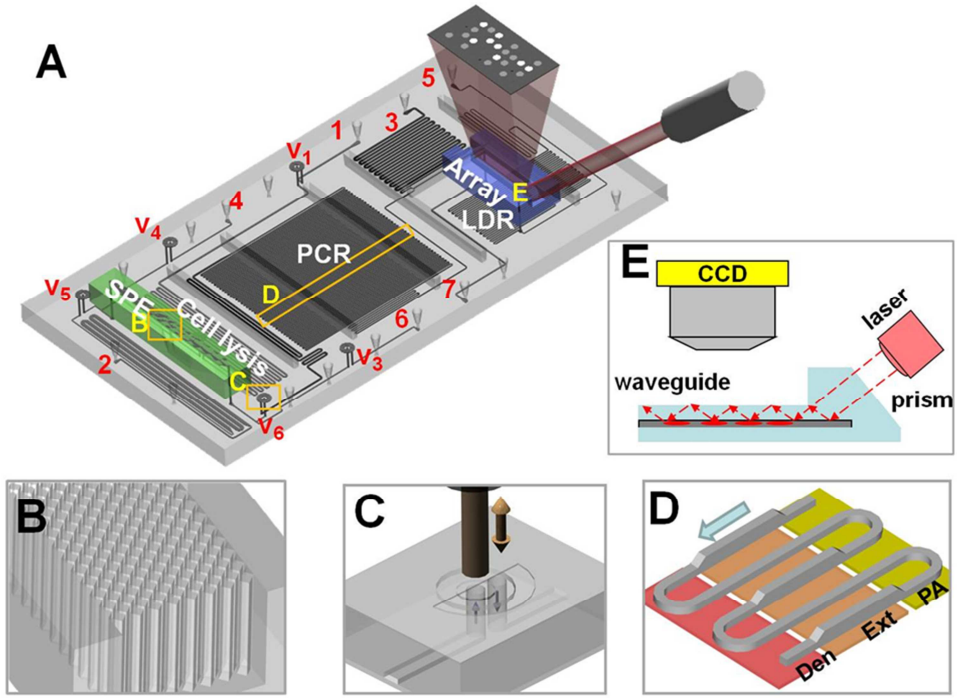

Figure 4.3 Integrated, modular microfluidic chip for TB analysis. (A) 3D rendering of the chip and the detection method. 1-7 – fluidic inlets and outlets: 1 – sample inlet, 2 – PCR cocktail inlet, 3 – LDR cocktail inlet, 4 – ethanol and air inlet, 5 – array wash inlet, 6 – vacuum connection and 7 – waste. V_1-V_6 – on-chip membrane valves (note that V_2 is positioned next to SPE module on the cell lysis microchannel and is not visible in current view). (B) Close-up of the SPE bed showing DNA capture bed filled with an array of high-aspect ratio pillars. (C) Schematic operation of the on-chip membrane valve with direct mechanical actuation – electrically actuated solenoid presses on the center of the polymer membrane closing the passage of fluid from the bottom layer through the valve and back to bottom layer. (D) Geometry of the continuous flow PCR reactor with dual-depth microchannels for extended residence time the extension-zone; Den – denaturation, Ext – extension and PA – primer annealing. (E) Schematic representation the detection mode. Laser excitation is coupled to the waveguide through integrated prism. Light travelling through the waveguide excites the labeled LDR products hybridized to zip code array spotted at the bottom of the waveguide. Resulting fluorescence signal is imaged with CCD camera.

membrane, which allows for monolithic valve construction and simplifies assembly processes as the valve membranes can be attached in the same lamination step as the fluidic cover plate. Unfortunately, PC is not compatible with ultra-sensitive fluorescence detection because of its relatively high background. On the other hand, PMMA demonstrates good optical clarity and minimal non-specific adsorption characteristics making it an optimal material for construction of the waveguide module of the universal array.[24] In addition, printing DNA arrays on the surface of the waveguide module can be done in a single run making the manufacturing process easier and more efficient with the probes tethered to the surface using robust chemistry.

Figure 4.1B and **Figure 4.3B** presents schematic drawings and SEM images of the SPE module. Each SPE extraction bed had a footprint of 20 mm x 1 mm and a 50 µm depth populated with an array of 11,000 of 20 µm x 20 µm micropillars spaced by a 40 µm center-to-center distance.[25] The total surface area of the immobilization bed was 74 mm^2 and the DNA load was estimated to be ~600 ng,[26] which is equivalent to genomic material extracted from ~10^8 bacteria cells assuming a typical bacterial genome size of 5 Mbp. **Figure 4.1C** shows a schematic and operation of the PC membrane valves with direct solenoid actuation. The thermal reactors poised on the fluidic motherboard (**Figure 4.1A** and **Figure 4.3A**) incorporated a continuous flow format, which provided PCR results that are limited by the kinetic constraints of the polymerase and not thermal management issues.[27] In addition, several thermal management technologies were included to improve amplification efficiency, such as backside thermal isolation grooves, thin PC substrates and copper plate thermal stages to give a more uniform temperature distribution throughout the particular thermal zone.[28] To achieve faster continuous flow

thermal cycling in a limited footprint, a dual-depth channel (200 µm and 100 µm) was designed to extend the resident time in the extension zone (**Figure 4.1F** and **Figure 4.3D**).

Figures 4.3E shows the PMMA module with an integrated air-embedded waveguide and a laser-coupling prism for laser-induced fluorescence (LIF) evanescent wave excitation of the universal array. The trapezoid prism had an entrance angle of 64°, which exceeded the critical angle of 63.2° between the PMMA (n = 1.49 @ 635 nm) and the buffer solution (n = 1.33) and the critical angle of 42° between PMMA and air (n = 1.0). The total surface area of the planar waveguide was 1.2 mm x 10 mm and could accommodate about 100 probe spots (diameter ~100 µm, center-to-center spacing = 300 µm). The entire array could be imaged in a single exposure using evanescent field excitation and a highly sensitive rectangular CCD camera, which alleviated the need for additional optical mechanics to permit scanning of the array. The field-of-view of the optical setup was 12 mm x 3 mm.

4.3.3 Operation of the Fluidic Cartridge

Prior to analysis, PCR and LDR reaction cocktails were dispensed into the corresponding on-chip storage channels followed by loading sample suspended in the SPE immobilization buffer into the lysis channel. The fluidic cartridge was then connected to the control hardware through a fluidic interface bus. This bus allowed for all fluidic connections to be made in one step and at the same time, aligned the cartridge with the heaters used for thermal processing and solenoid plungers used for actuation of the on-chip membrane valves. During operation, the membrane valves were opened and closed according to a pre-programmed sequence of events to achieve the desired flow path of the sample and reagents through the fluidic network.

Processing sequence started with thermal lysis of the Mtb cells at 95 ℃ for 3 min followed by extraction of released gDNA using PPC-SPE module. After washing of the SPE bed with 70% ethanol and drying with air, extracted gDNA was released directly into a PCR cocktail and pumped through a continuous flow thermal reactor at an optimized flow rate, which allowed the sample to be processed through the PCR reactor in ~5 min after which time, the LDR cocktail was pumped out from its storage channel and mixed with the PCR product. Continuous mixing was achieved with a Y-type diffusional mixer consisting of 80 µm wide and 200 µm deep inlet and outlet channels (aspect ratio = 2.5). This mixer geometry provided complete mixing between PCR product and LDR reagents in 10 s at room temperature with a mixing rate limited by diffusion of the ligase enzyme (40 $\mu m^2/s$). This mixing time corresponds to ~10 mm channel length at a combined flow rate of 1 µL/min. In order to accommodate higher processing speeds for future applications, we can incorporate an additional length of microfluidic channel into the flow path prior to the continuous flow LDR reactor and place it within the 95 ℃ temperature zone, which would increase the diffusion coefficient of the components by a factor of ~3.5 as compared to room temperature. The reaction mixture was then processed through the continuous flow LDR reactor and finally, through the universal array chip and to waste. The array was washed (2x SSC and 0.1% SDS) in order to elute any nonspecifically adsorbed fluorescent dye-labeled products and interrogated using a CCD camera at 635 nm excitation.

4.3.4 Identification of Drug Susceptible and Resistant Strains

Figure 4.4 shows results from a series of molecular assays using five different positive and negative control samples. The layout of the universal array is shown in **Figure 4.4A**. Spots C were amino and Cy5 double labeled oligonucleotide probes used

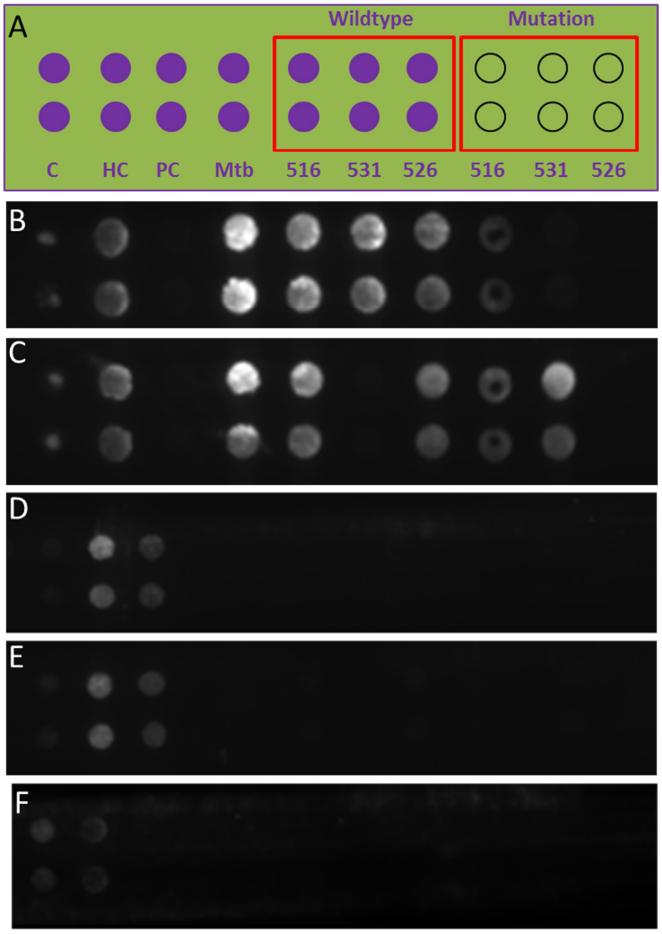

Figure 4.4 Universal array layout (A) and hybridization results from different input samples (B-E). C: Cy5 (5' end) and amino (3' end) double labeled oligonucleotide probes used as spotting control and markers; HC: zip3 probes used as hybridization controls; PC: positive controls targeted spiked positive control plasmid sequence; Mtb: Mtb-specific probed for the IS6110 insertion fragment. 516WT, 531WT and 526WT: probes targeted rifampin susceptible Mtb strains; 516MT, 531MT and 526MT: probes targeted rifampin resistant Mtb strains. Molecular assay results from rifampin susceptible Mtb strain (B), rifampin resistant strain (C), *E. coli* (D) and human genomic DNA (E). (F) shows molecular assay results when the thermal stage was turned off to simulate the hardware failure.

as spotting quality control and mark spots. Spots HC were zip3 probes used as the hybridization control. Spots PC were used as positive control targeting spiked positive control plasmids in cell lysis buffer. PC were used to distinguish true negative samples (no TB infection) from the failure of DNA extraction, amplification or hybridization, either

a result from degraded bio-reagents, enzymatic inhibitors, or failed fluidic/thermal control. Spots Mtb were Mtb complex specific probes targeting the IS6110 insertion fragment. Wild-type spots, 516, 531 and 526, were used to target rifampin susceptible strains while mutation spots, 516, 531 and 526 used to target rifampin resistant strains. **Figure 4.4B** shows results from a cultured drug susceptible Mtb stain (H37Rv), while **Figure 4.4C** shows results from a cultured rifampin resistant strain (S531L) carrying a TCG → TTG mutation at codon 531 in the *rpo*B gene. Successful identification of the drug susceptible and resistant samples was demonstrated by the high fluorescence intensities from spots 531WT in **Figure 4.4B** and from spots 531MT in **Figure 4.4C**. The fluorescence intensities from the spots 531MT in **Figure 4.4B** and from the spots 531WT in **Figure 4.4C**, respectively, were close to the background, which demonstrated excellent single base discrimination capabilities of the diagnostic tool package. In both **Figures 4.4B** and **4.4C**, spots C, HC and PC showed high fluorescence intensities as expected. **Figures 4.4D** and **4.4E** present negative control results run with a cultured *E. coli* sample and human genomic DNA, respectively. **Figure 4.4F** shows results obtained from a cultured drug susceptible Mtb strain (H37Rv); however, the heater at the PCR denaturation zone (95 ℃) was intentionally turned off. The PC spots showed strong fluorescence signals in both **Figure 4.4D** and **4.4E** but no fluorescence signal in **Figure 4.4F**, demonstrating that the PC spots were successfully used as a positive control circumventing the false negative diagnostic results.

We were also interested in evaluating the minimum number of Mtb cells required to provide reasonable signal-to-noise ratios using our system and whether results could meet the need for clinical diagnosis. To determine the limit-of-detection, molecular assays were conducted using a 10-fold serial dilution of cultured H37Hv cells as inputs.

As few as 50 Mtb cells could be successfully detected, representing a 100-fold sensitivity improvement compared to current clinical smear tests, which require 5,000 – 10,000 bacilli in 1 mL of sputum.

4.3.5 Identification of Hetero-resistance of Mtb Strains

Hetero-resistance of Mtb is defined as the coexistence of mixed subpopulations of drug susceptible and resistant Mtb strains in the same patient, which is considered as a preliminary stage to full resistance. It is typically a result of super-infection arising under the selection pressure during antibiotic treatment. The occurrence rate of hetero-resistance could be as high as 20% as reported in recent studies.[11, 12] To evaluate the ability of our diagnostic tool for the identification of drug resistant Mtb strains in the presence of an excessive amount of drug susceptible strains, a series of artificial hetero-resistance samples containing a certain percentage of rifampin resistant strains, ranging from 0%, 1%, 2%, 5%, 10%, 50% and 100%, in drug susceptible stains of H37Rv were prepared and analyzed. The results are shown in **Figure 4.5**. The fluorescence signals from the 531MT spots increased with an increased percentage of the rifampin resistant strains present in the sample. The fluorescence signals from the spots 531MT were discernible when the rifampin resistant strains only constitute as little as 1% of the total population (see **Figure 4.5**). After background subtraction, the fluorescence signals from the spots 531MT run with samples containing 1% of rifampin resistant strains were calculated to be ~10-fold higher than fluorescence signals from those spots run with samples containing 0% of rifampin resistant strains (100% of drug susceptible strains). Therefore, less than 1% of the drug resistant strains can be discriminated when 3-times the standard deviation from nonspecific signals are used to determine the limit of specificity detection. Very low fluorescence signals from the 531M

spots were run with 100% of drug susceptible strains, which could be attributed to mis-ligation and nonspecific hybridization. It has been noted that a T-G mismatch as used herein has the lowest fidelity for the *Taq* ligase.[29] For other types of mismatches or a single-plex LDR assay, a lower percentage of drug resistant strains are expected to be discriminated.

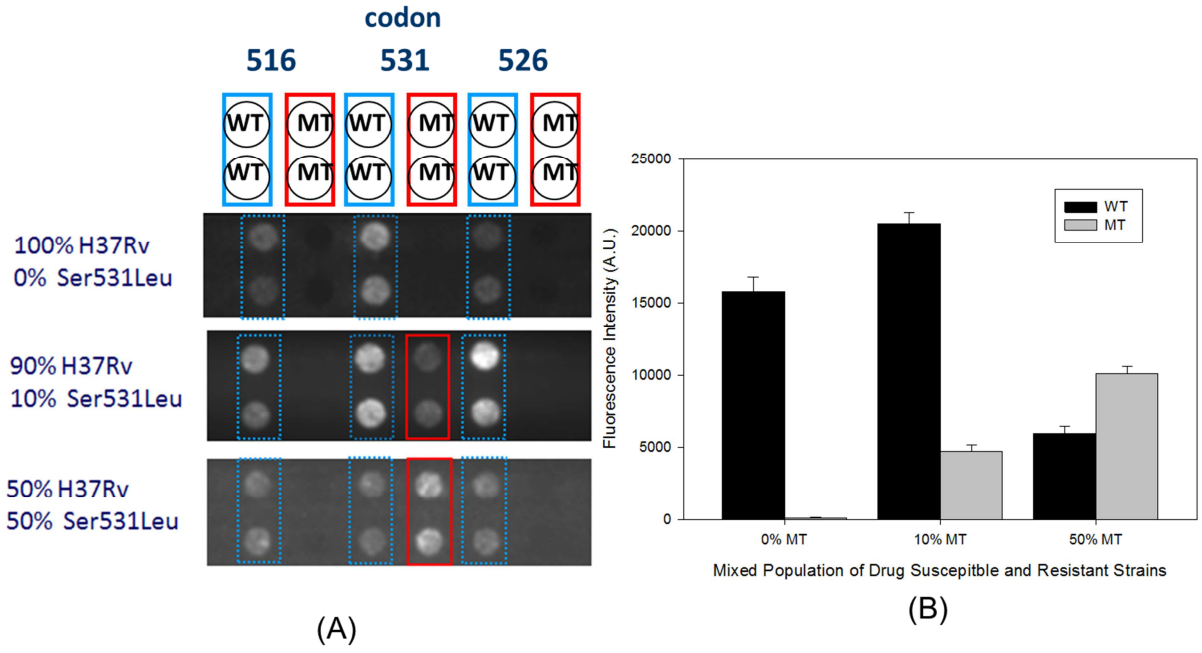

Figure 4.5 Identification of mixed population of drug susceptible and drug resistant Mtb strains. (A) Hybridization image; (B) fluorescence intensities.

4.3.6 Colorimetric Module

A colorimetric line probe assay was developed as detailed in section 4.2.6. Briefly, PMMA strips immobilized with zip-code line probes were prepared using a PDMS stencil containing a microchannel network (**Figure 4.6B**). 1.4 nm Nanogold labeled common primers replaced fluorescence dye labeled common primers as shown in **Figure 4.6A**. After LDR and hybridization, the nanogold acted as a catalytic site and resulted in large amounts of silver deposition, which was visible to the naked eyes and could be recorded by a digital camera. A drug susceptible Mtb stain (H37Rv) and a

rifampin resistant strain (S531L) were tested and the results are shown in **Figure 4.6C**. The successful development of the colorimetric line probe assay provides a cost-effective and robust alternative to fluorescence readout.

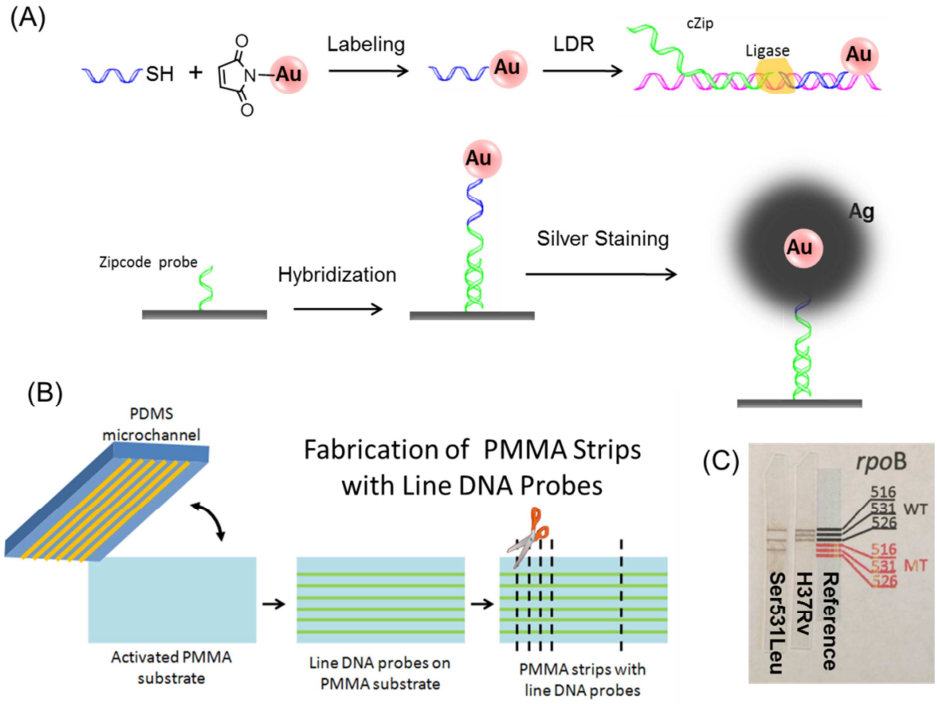

Figure 4.6 Schematic drawing and preliminary results of low cost colorimetric readout. (A) Schematic drawing of labeling, LDR and hybridization, silver developing chemistry. 1.4 nm monomaleimido-functionalized Nanogold particles were covalently linked to a 3' sulfhydryl-labeled LDR common primer. Ligation products were flanked by cZip sequences and nanogold particles, which can hybridize to the immobilized zip-code probes. The hybridization results were visible to the naked eyes after silver staining enhancement. (B) Fabrication of PMMA strips with line DNA probes. A PDMS sheet containing microchannel network of 250 µm wide and 1 mm spacing was physically sealed with a piece of oxygen plasma activated and EDC-NHS functionalized PMMA sheet by conformal contact. 50 µM zip-code oligonucleotide probes in pH 9.0 carbonate buffer were filled the microchannel. After one hour incubation, the PMMA sheet was cleaned and cut to 5 mm wide strips. (C) Preliminary results of colorimetric readout. A fast thermal cycling (15 cycles of 95 ℃ for 5 s and 60 ℃ for 15 s using a bench-top thermocycler) in a modified LDR buffer was carried out for minimizing the possible degradation of the Nanogold-conjugated common primer. Drug susceptible and resistant Mtb strains were successfully identified by bare eyes and the image shown was recorded by a digital camera. WT: drug susceptible wild-type Mtb stains; MT: rifampin resistant Mtb strains.

4.4 Discussion

Developing and implementing rapid and accurate MDR-TB diagnostic tools to high burden developing countries are of paramount importance to the Stop TB Strategy by the World Health Organization (WHO). NAATs that can identify MDR-TB by interrogating drug resistant related signature genetic mutations present a promising opportunity for rapid drug resistance assays. The WHO expert group recently recommended two line probe assays, *INNO-LiPA Rif.TB* from Innogenetics and MTBDR*plus* from Hain Lifescience, both of which employ multiplexed PCR reverse hybridization approach, for rapid screening of MDR-TB. However, the performance of line probe assays is compromised when a mixed population of drug resistant and susceptible bacterial subpopulations exists.[10] This is because the conventional sequence-specific array hybridization is unable to detect low abundance single base mutations due to cross hybridization, especially in high GC content regions where secondary structures are prevalent, e.g. RRDR in rpoB gene. Quantitative PCR (qPCR) using molecular beacons or Taqman probes is another NAAT approach used by Cepheid's GeneXpert MDR-TB assay and several other home-brew assays. However, there are several intrinsic limitations: first, only limited number of mutations can be interrogated in a single assay; second, hetero-resistant infection may lead to false-negative results; third, silent mutations, which do not confer drug resistance, may lead to inaccurate interpretations and false-positive results.

We have developed a NAAT using PCR-LDR-universal array hybridization approach, which decouples the mutation discrimination step from the hybridization step and employs a high fidelity *Taq* ligase. It has several attractive advantages for developing MDR-TB assays: (1) The closely clustered drug resistance mutations of

MDR-TB can be effectively interrogated. (2) Only the specific drug resistance mutations will generate positive results. Silent mutations not conferring drug resistance won't generate false positive results using this assay strategy. (3) Hetero-resistance Mtb containing low abundance of drug resistant strains (<1%) in a patient with emerging drug resistance can be easily detected, which enables timely treatment strategy adjustments.

After developing this highly specific molecular assay, the next challenge was how to implement this assay to low resource settings. Similar to line probe assays and qPCRs, the NAAT we developed is based on PCR amplification, which could detect the pathogen biomarkers from just a few DNA molecules, making it very sensitive contamination. Carryover contamination could be a serious problem in a clinical laboratory because a large amount of same types are carried out on a daily basis. Therefore, sophisticated laboratory infrastructure, such as segregated, controlled environment rooms for uni-directional work flow of DNA extraction, pre-PCR, PCR amplification, and post-PCR hybridization and extensively trained personnel must be enforced to ensure reliable results, which hampers the wide implementation of NAATs and creates a gap between advanced diagnostic technology and healthcare needs in developing countries. This gap has been acknowledged by a panel of global healthcare experts and they ranked "modified molecular technologies for affordable, simple diagnostics of infectious diseases" as the highest priority in biotechnologies directed for improving health in developing countries in the next 5 to 10 years.[30] Fully-integrated point-of-care (POC) genosensor systems using the lab-on-a-chip concept that can accept crude biological samples and automatically perform multi-step molecular assays

in an enclosed, disposable format is one of the most promising enabling technologies to bridge the gap.

Significant progress has recently been made in the development of partially or fully integrated systems,[31-36] which represent the summit of technologists' capabilities in fabrication and manufacturing. However, the disconnections between these delicate and comprehensive proof-of-concept devices and the desired robust end-user diagnostic tools are also apparent. Several issues need to be taken into consideration in designing real world diagnostic tools.[36] For example, the economic conditions in the developing countries rule out the use of expensive silicon/glass materials and clean room manufacturing procedures. The transportation cost for the fragile silicon/glass material may be prohibitive. The regeneration and/or reassembling of the microfluidic chip[32] are an unachievable task for under trained health workers. After carefully evaluating these constrains, we developed a disposable fluidic cartridge and a control instrument for delivering the NAAT to resource limited settings. First, the fluidic cartridge used a hybrid modular architecture, which combined several task-specific modules interconnected to a fluidic motherboard with the material selected to optimize performance. These modules included a UV-photoactivated polycarbonate (PPC) module containing micropillars for solid phase DNA extraction and purification and another module made from poly(methylmethacrylate), PMMA, consisting of a planar waveguide array. The solid phase extraction module was made from PC due to its high specificity for the condensation of nucleic acids to its surface when photoactivated and PMMA was used for the array module because of its excellent optical properties, simple surface activation protocols and robust attachment chemistry of oligonucleotides to its surface.

The thermal reactions were carried out on a fluidic motherboard also made from PC due to its high glass transition temperature to withstand thermal processing without experiencing structure deformation. In addition, the fluidic control system was also poised on this motherboard and consisted of several on-chip valves made from a PC membrane serving as the cover plate for the fluidic network, which has a large elongation at break point to allow reversible operation of the valves even when employing traditional non-elastomeric materials. The fluidic cartridge can also be easily reconfigured, for example, the fluorescence universal array readout module can be reconfigured to a colorimetric readout module to further reduce instrument cost. As opposed to a monolithic approach[31-35] or a LEGO approach[37, 38] already reported in the literature, the hybrid modular structure balanced the efficiency and flexibility in fluidic cartridge design. Second, robust and low-cost manufacturing processes have been developed. The disposable fluidic cartridge presented in this paper was fabricated by a one-step replication process from a metal mold insert containing multi-scale and complex structures (e.g. micropillar bed, waveguide prism, etc.). In addition, the number of active components on the disposable fluidic cartridge was minimized and designed to be compatible with mass production processes, e.g. on chip membrane valves. Thermal management (e.g. heaters, temperature sensors, etc.), optical detection and most of the fluidic manipulation (e.g. pumps) are operated by off-chip supporting peripherals packaged in a cubic foot sized box. Finally, minimal end-user operation is required. Tedious pre- and post- processing steps, such as loading silica beads for DNA purification or regeneration/reassembly of the fluidic cartridge,[31, 32] are difficult tasks for untrained healthcare workers in resource-limited settings. The operator only needs to load the patient sample and push a run button to use the diagnostic tool presented in

this paper. On chip storage of dried bio-reagents is under investigation, which will further reduce the work load of the end-user to sample loading only.

In summary, the development of the accurate, fast and affordable diagnostic tool package presented here demonstrates a unique modular concept consisting of task specific modules interfaced to a fluidic motherboard. The performance of the diagnostic tool has been validated by cultured drug susceptible and drug resistant Mtb strains. As little as 1% of rifampin resistant Mtb strain could be discriminated from artificial hetero-resistance samples containing a mixed subpopulation of drug susceptible and resistant Mtb strains. When challenged with smear positive clinical sputum samples, the results from our diagnostic tool were consistent with the clinical records. Compared to the turnaround time of 8 – 12 weeks for DST and 1-2 days for line probe assays available in centralized laboratories, our system was able to identify MDR-TB in less than 40 min, which will contribute significantly to the MDR-TB case treatment and management. The total cost of the diagnostic tool package with fluorescence detection is around $15,000, with the disposable of <$10 per test. Lower cost systems (<$8,000) using colorimetric hybridization readout or conductivity hybridization readout are under development. Recently, a variety of mutations closely related to XDR-TB have been reported. By incorporating multiplex PCR and additional LDR primers, the diagnostic tool we presented here can also be expended to detect gene mutations responsible for second line drugs resistant Mtb (XDR-TB). It also holds the potential to be a universal platform for identifying genetic signature sequences and mutations in a variety of disseminated applications, including clinical diagnosis, forensic test and bioterrorism detection, in both developing and developed countries.

4.5 References

1. WHO, *World Health Organization. Report on infectious diseases: Removing Obstacles to Healthy Development.* , 1999.

2. WHO, *World Health Organization. The world health report 2002 - Reducing Risks, Promoting Healthy Life* 2002.

3. WHO, *World Health Organization. Scaling up the response to infectious diseases: A way out of poverty.* , 2002.

4. M. D. Perkins, G. Roscigno and A. Zumla, *Lancet*, 2006, **367**, 942-943.

5. I. N. Okeke, K. P. Klugman, Z. A. Bhutta, A. G. Duse, P. Jenkins, T. F. O'Brien, A. Pablos-Mendez and R. Laxminarayan, *Lancet Infect. Dis.*, 2005, **5**, 568-580.

6. I. N. Okeke, R. Laxminarayan, Z. A. Bhutta, A. G. Duse, P. Jenkins, T. F. O'Brien, A. Pablos-Mendez and K. P. Klugman, *Lancet Infect. Dis.*, 2005, **5**, 481-493.

7. D. M. Morens, G. K. Folkers and A. S. Fauci, *Nature*, 2004, **430**, 242-249.

8. E. Marris, *Nature Medicine*, 2007, **13**, 267-267.

9. WHO, *Policy guidance on drug-susceptibility testing (DST) of second-line antituberculosis drugs*, 2008.

10. WHO, *World Health Organization Expert Group Report. Molecular Line Probe Assays for Rapid Screening of Patients at Risk of Multi-Drug Resistant Tuberculosis(MDR-TB).* (http://www.who.int/tb/features_archive/expert_group_report_june08.pdf), 2008.

11. S. Hofmann-Thiel, J. van Ingen, K. Feldmann, L. Turaev, G. T. Uzakova, G. Murmusaeva, D. van Soolingen and H. Hoffmann, *Eur. Respir. J.*, 2009, **33**, 368-374.

12. H. Rinder, K. T. Mieskes and T. Loscher, *Int. J. Tuberc. Lung Dis.*, 2001, **5**, 339-345.

13. D. L. Williams, L. Spring, L. Collins, L. P. Miller, L. B. Heifets, P. R. J. Gangadharam and T. P. Gillis, *Antimicrobial Agents and Chemotherapy*, 1998, **42**, 1853-1857.

14. D. L. Williams, C. Waguespack, K. Eisenach, J. T. Crawford, F. Portaels, M. Salfinger, C. M. Nolan, C. Abe, V. Stichtgroh and T. P. Gillis, *Antimicrobial Agents and Chemotherapy*, 1994, **38**, 2380-2386.

15. M. L. Hupert, W. J. Guy, S. D. Llopis, H. Shadpour, S. Rani, D. E. Nikitopoulos and S. A. Soper, *Microfluid. Nanofluid.*, 2007, **3**, 1-11.

16. D. L. Williams, T. P. Gillis and W. G. Dupree, *J. Clin. Microbiol.*, 1995, **33**, 1558-1561.

17. R. C. Anderson, X. Su, G. J. Bogdan and J. Fenton, *Nucleic Acids Res.*, 2000, **28**.

18. E. Delamarche, A. Bernard, H. Schmid, B. Michel and H. Biebuyck, *Science*, 1997, **276**, 779-781.

19. C. Situma, Y. Wang, M. Hupert, F. Barany, R. L. McCarley and S. A. Soper, *Anal. Biochem.*, 2005, **340**, 123-135.

20. A. P. Alivisatos, K. P. Johnsson, X. G. Peng, T. E. Wilson, C. J. Loweth, M. P. Bruchez and P. G. Schultz, *Nature*, 1996, **382**, 609-611.

21. J. M. Musser, *Clin. Microbiol. Rev.*, 1995, **8**, 496-&.

22. N. P. Gerry, N. E. Witowski, J. Day, R. P. Hammer, G. Barany and F. Barany, *Journal of Molecular Biology*, 1999, **292**, 251-262.

23. M. A. Witek, S. D. Llopis, A. Wheatley, R. L. McCarley and S. A. Soper, *Nucleic Acids Research*, 2006, **34**.

24. F. Xu, P. Datta, H. Wang, S. Gurung, M. Hashimoto, S. Wei, J. Goettert, R. L. McCarley and S. A. Soper, *Analytical Chemistry*, 2007, **79**, 9007-9013.

25. D. S. W. Park, M. L. Hupert, M. A. Witek, B. H. You, P. Datta, J. Guy, J. B. Lee, S. A. Soper, D. E. Nikitopoulos and M. C. Murphy, *Biomed. Microdevices*, 2008, **10**, 21-33.

26. M. A. Witek, M. L. Hupert, D. S. W. Park, K. Fears, M. C. Murphy and S. A. Soper, *Analytical Chemistry*, 2008, **80**, 3483-3491.

27. M. Hashimoto, P. C. Chen, M. W. Mitchell, D. E. Nikitopoulos, S. A. Soper and M. C. Murphy, *Lab Chip*, 2004, **4**, 638-645.

28. P. C. Chen, D. E. Nikitopoulos, S. A. Soper and M. C. Murphy, *Biomed. Microdevices*, 2008, **10**, 141-152.

29. J. Y. Luo, D. E. Bergstrom and F. Barany, *Nucleic Acids Research*, 1996, **24**, 3071-3078.

30. A. S. Daar, H. Thorsteinsdottir, D. K. Martin, A. C. Smith, S. Nast and P. A. Singer, *Nat. Genet.*, 2002, **32**, 229-232.

31. A. F. Sauer-Budge, P. Mirer, A. Chatterjee, C. M. Klapperich, D. Chargin and A. Sharon, *Lab Chip*, 2009, **9**, 2803-2810.

32. C. J. Easley, J. M. Karlinsey, J. M. Bienvenue, L. A. Legendre, M. G. Roper, S. H. Feldman, M. A. Hughes, E. L. Hewlett, T. J. Merkel, J. P. Ferrance and J. P. Landers, *Proc. Natl. Acad. Sci. U. S. A.*, 2006, **103**, 19272-19277.

33. R. H. Liu, J. N. Yang, R. Lenigk, J. Bonanno and P. Grodzinski, *Analytical Chemistry*, 2004, **76**, 1824-1831.

34. R. Pal, M. Yang, R. Lin, B. N. Johnson, N. Srivastava, S. Z. Razzacki, K. J. Chomistek, D. C. Heldsinger, R. M. Haque, V. M. Ugaz, P. K. Thwar, Z. Chen, K. Alfano, M. B. Yim, M. Krishnan, A. O. Fuller, R. G. Larson, D. T. Burke and M. A. Burns, *Lab Chip*, 2005, **5**, 1024-1032.

35. R. G. Blazej, P. Kumaresan and R. A. Mathies, *Proc. Natl. Acad. Sci. U. S. A.*, 2006, **103**, 7240-7245.

36. P. Yager, T. Edwards, E. Fu, K. Helton, K. Nelson, M. R. Tam and B. H. Weigl, *Nature*, 2006, **442**, 412-418.

37. M. Rhee and M. A. Burns, *Lab on a Chip*, 2008, **8**, 1365-1373.

38. K. A. Shaikh, K. S. Ryu, E. D. Goluch, J. M. Nam, J. W. Liu, S. Thaxton, T. N. Chiesl, A. E. Barron, Y. Lu, C. A. Mirkin and C. Liu, *Proc. Natl. Acad. Sci. U. S. A.*, 2005, **102**, 9745-9750.

CHAPTER 5 CONCLUSIONS AND FUTURE WORK

5.1 Conclusions

"One could argue that miniaturized chemical analysis systems are just a fashionable craze. However, it is difficult to foresee the impact a new technological concept will have, when it is in its early stages of development." (Manz *et al.* "Miniaturization of chemical-analysis systems – a look into next century technology or just a fashionable craze?" *Chimia* 1991, **45**, 103-105).[1]

The last twenty years have witnessed microfluidics evolve from a concept first proposed by Manz *et al.*[2] to one of the hottest research frontiers. A variety of single functional microfluidic devices and fluidic manipulation components have been developed. However, these more and more sophisticated single functional devices are more of "fashionable crazes" than impactful technologies. The gap between microfluidics and the real world needs is still significant. The ultimate question, what is the "killer application" of microfluidics, is yet to answer.

An integrated and modular microfluidic cartridge and a fully automated instrumentation in this dissertation present our efforts to explore the "killer application" aiming to bridge the gap between the microfluidic system and the diagnostic needs in the resource limited settings. Fully integrated microfluidic systems are designed to automatically perform all of the molecular processing steps in a single platform to provide sample in/answer out capabilities. A series of discrete microdevices carrying out specific molecular functions such as cell lysis, nucleic acid extraction and/or purification, PCR amplification, and analysis techniques for reading successful PCRs are interconnected to process the sample volume at the picoliter to nanoliter scale. In chapter 1, we reviewed the various microdevices that have been fabricated to handle

functional steps in the processing of nucleic acids, followed by several significant examples of integrated microfluidic systems with DNA microarrays used as the terminal readout. The applications of these systems, as well as future challenges were discussed.

In chapter 2, an integrated modular-based microfluidic system for rapid and specific identification of methicillin-resistant *Staphylococcus aureus* (MRSA) was demonstrated. MRSA is a major cause of hospital-acquired (HA-MRSA) infection worldwide. In recent years, community acquired-MRSA (CA-MRSA) strains, which cause severe infections, are emerging as a serious problem. A multiplexed PCR/LDR coupled with the universal array allowed for simultaneous detection of five genes that encode for 16S ribosomal RNA (SG16S), the protein A (*spa*), the femA protein of *S. epidermidis* (*femA*), the virulence factor of Panton-Valentine leukocidin (PVL) and confer methicillin resistance (*mecA*). The multi-step assay included continuous flow PCR (CF PCR) amplification of the *mecA* gene harboring methicillin resistance loci that can provide information on drug susceptibility, continuous flow ligase detection reaction (CF LDR) to generate fluorescent ligation products containing a zip-code complement that directed the ligation product to a particular address on a universal array containing zip-code probes and universal DNA array readout, which consisted of a planar waveguide for evanescent excitation. Each of these processing steps was optimized individually before they were streamlined. The fluidic cartridge design was based on a modular format, in which certain steps of the molecular processing pipeline were poised on modules made from a thermoplastic selected for the particular processing step. In addition, to minimize the post-processing steps for finishing the fluidic cartridge, many of the functional components were produced during the polymer molding process, enabling low-cost

manufacture for one-time use applications. The cartridge was comprised of one module interconnected to a fluidic motherboard configured in a 3-dimensional network; the motherboard was made from polycarbonate, PC, and used for PCR and LDR, while the module was made from poly(methylmethacrylate), PMMA, and contained an air-embedded waveguide and the DNA array. Fluidic handling, thermal management and optical readout hardware were located off-chip and configured into a small footprint instrument. Results indicated that this modular system could differentiate CA-MRSA from HA-MRSA based on the presence/absence of the PVL gene as well as *S. aureus* from other *Staphylococcal* species using the sequence content in the *femA* gene. This system can identify several strains of bacteria in <40 min and detect MRSA directly from a mixture of *Staphylococci*.

In chapter 3, the fluidic system for bacterial genotyping was further integrated with a micro-solid phase extraction (micro-SPE) device. The sequence of sample processing steps performed within the fluidic cartridge including cell lysis, SPE of genomic DNA (gDNA) from the whole cell lysate, CF PCR amplification of specific gene fragments, CF LDR to detect single-base sequence variations and universal zip-code array readout. The fluidic cartridge was composed of a PMMA module situated on a PC motherboard; the PC motherboard was used for cell lysis, SPE, PCR and LDR, while the PMMA module contained an air-embedded planar waveguide in which a DNA microarray was spotted. The utility of the modular system was demonstrated by performing pathogen detection directly from whole *E. coli* O157:H7 and *Salmonella* cells using a duplexed PCR followed by multiplexed LDR with readout via a low-density universal array. The presence of two genes, *uidA* and *sipB/C*, that discriminate between *E. coli* and *Salmonella*, was evaluated as a model system. Results showed that the fluidic system

could successfully identify several strains of bacteria in <40 min and also perform strain identification, even from a mixed population with the target a minority. We further demonstrated the ability to analyze the *E. coli* O157:H7 strain directly from a waste-water sample with high specificity using the integrated system.

In chapter 4, a fully integrated and field deployable system for identifying multi-drug resistant tuberculosis (MDR-TB) was presented. The worldwide concern of MDR-TB resulting from *Mycobacterium tuberculosis* (Mtb) strains that fail to respond to the first-line drugs, rifampin and isoniazid, creates a formidable challenge in formulating global plans to eradicate this disease. Less than 5% of new MDR-TB cases occurring each year are diagnosed and treated in a timely fashion due to the length (8 – 12 weeks) and complexity of traditional cell culture *in vitro* diagnostic methods. In response to WHO's call for fast and accurate MDR-TB diagnostic tools, especially those that can be operated by under-trained healthcare workers in resource limited settings, in chapter 4 the modular system was adapted for interrogating single nucleotide variations in the *rpo*B gene associated with rifampin-resistant Mtb strains. All steps of the multi-step molecular assay, including Mtb cell lysis, SPE of gDNA, PCR amplification, ligation-based discrimination/identification of single nucleotide variations and universal array readout were incorporated into a disposable plastic fluidic cartridge. The cartridge was comprised of two modules, the SPE module and the waveguide module, which were interconnected to a fluidic motherboard that consisted of devices for cell lysis, PCR and LDR. The integrated system could identify MDR-TB strains directly from clinical sputum samples in <40 min with minimal risk of human errors or cross-contamination. This diagnostic tool will revolutionize MDR-TB and other infectious disease diagnostic testing

in both developed and developing countries due to its ease of implementation and highly automated format.

5.2 Future Work

Generally, an integrated microfluidic system that streamlined several critical steps in genetic-based analyses, including cell lysis, SPE of nucleic acids, their amplification, determination sequence variations and readout has been demonstrated in this dissertation. It can be easily reconfigured according to requirements of the specific application need. The next challenge is to analysis trace or low-abundance samples that are critical in clinical and other applications. In most cases, cells or targets of interest in real-world samples, such as tissue, blood, soil, water or food samples are trace or low-abundant and complex and thus, need to undergo careful sample preparation for sensitive detection.[3] Also, raw samples are often large in volume for microfluidic analysis, and this discrepancy in volumes makes pre-concentration necessary due to time constraints and the need for rapid detection. A typical example is the detection of *E. coli* O157:H7 where as few as 10 cells must be detected from a large sample volume and complex sample background. Therefore, the next critical step is the integration of cell isolation and pre-concentration process through a variety of cell separation and capture techniques onto the current microfluidic platform. Several approaches, such as affinity-based selection,[4, 5] physical properties,[6, 7] dielectrophoresis,[8-10] immunomagnetic interactions[11] and fluorescence-activated cell sorting,[12, 13] have been reported to sort and to collect target cells from raw samples and can be integrated into microfluidic-based systems. One of the most attractive applications of this system is to analysis circulating tumor cells (CTCs). CTCs present an exciting new biomarker for various cancers, such as breast, colon, lung, prostate, ovarian, pancreas and bladder cancer.

The attractive feature associated with these biomarkers is that they can be secured from a simple blood draw, alleviating the need for biopsies. The analytical challenge with finding these biomarkers is they appear at only about 1 cell per 10^9 erythrocytes (red blood cells). Such studies have already begun by colleagues within the Soper research group for front-end cell capture using target-specific antibodies[14, 15] or aptamers[16] immobilized onto a miniaturized microfluidic device.

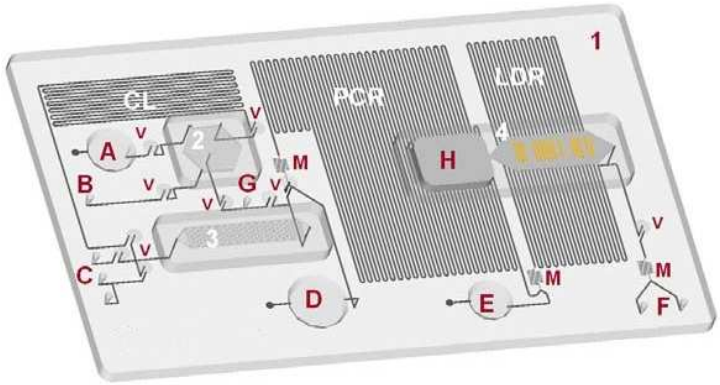

Figure 5.1 Schematic of the modular fluidic cartridge. The fluidic cartridge has 3 modules: cell selection (2), gDNA SPE isolation/purification (3) and universal array readout (4). These modules are interconnected into a fluidic mother board (1) that contains thermal domains for performing cell lysis, PCR and LDR. Heating of the thermal reaction domains is carried out by placing the fluidic cartridge on Cu heating blocks set at the necessary temperatures. Also shown are locations of on-chip valves (V), pumps (A, D and E) and high-aspect ratio mixers (M). A – sample input; B – lysing and SPE buffer; C – SPE (elution buffer, ethanol and air); D – PCR cocktail; E – LDR cocktail; G – vacuum pump; H – waste.

The fluidic cartridge (see **Figure 5.1**) is composed of 3 modules that are used for cell selection (2), gDNA SPE isolation/purification (3) and universal array readout (4). These modules are interconnected into a fluidic motherboard that contains processing steps for cell lysis, PCR and LDR. In this work, the cell sorting module is fabricated in PMMA due to its tendency to display minimal cell non-specific adsorption artifacts.[14]

Crude biological samples are introduced and driven through the cell selection bed. Following isolation of the target cells, they are lysed and the gDNAs are purified via SPE. The purified DNAs are subjected to PCR amplification and LDR. Finally, the LDR products are directed to a specific location of the universal array and hybridization events are detected using evanescent excited fluorescence. The system provides a cost-effective solution to direct sample-to-answer genetic analysis and thus, has a potential impact in the fields of gene expression analysis, pathogen and infectious disease detection and low-abundant DNA point mutation diagnostics, environmental testing and biological warfare agent detection. In addition to PCR/LDR/universal zip-code array assay platform, the modular fluidic cartridge could be reconfigured for use with other assay formats, such as PCR-μCE.

5.3 References

1. A. Manz, D. J. Harrison, E. M. J. Verpoorte, J. C. Fettinger, H. Ludi and H. M. Widmer, *Chimia*, 1991, **45**, 103-105.

2. A. Manz, N. Graber and H. M. Widmer, *Sens. Actuator B-Chem.*, 1990, **1**, 244-248.

3. C. Lui, N. C. Cady and C. A. Batt, *Sensors*, 2009, **9**, 3713-3744.

4. S. Nagrath, L. V. Sequist, S. Maheswaran, D. W. Bell, D. Irimia, L. Ulkus, M. R. Smith, E. L. Kwak, S. Digumarthy, A. Muzikansky, P. Ryan, U. J. Balis, R. G. Tompkins, D. A. Haber and M. Toner, *Nature*, 2007, **450**, 1235-U1210.

5. B. C. Heinze, J. Y. Song, C. H. Lee, A. Najam and J. Y. Yoon, *Sens. Actuator B-Chem.*, 2009, **138**, 491-496.

6. H. Mohamed, L. D. McCurdy, D. H. Szarowski, S. Duva, J. N. Turner and M. Caggana, *Ieee Transactions on Nanobioscience*, 2004, **3**, 251-256.

7. H. Mohamed, J. N. Turner and M. Caggana, *J. Chromatogr. A*, 2007, **1162**, 187-192.

8. F. F. Becker, X. B. Wang, Y. Huang, R. Pethig, J. Vykoukal and P. R. C. Gascoyne, *Proc. Natl. Acad. Sci. U. S. A.*, 1995, **92**, 860-864.

9. P. Gascoyne, C. Mahidol, M. Ruchirawat, J. Satayavivad, P. Watcharasit and F. F. Becker, *Lab Chip*, 2002, **2**, 70-75.

10. J. Vykoukal, D. M. Vykoukal, S. Freyberg, E. U. Alt and P. R. C. Gascoyne, *Lab Chip*, 2008, **8**, 1386-1393.

11. N. Beyor, T. S. Seo, P. Liu and R. A. Mathies, *Biomed. Microdevices*, 2008, **10**, 909-917.

12. A. Y. Fu, H. P. Chou, C. Spence, F. H. Arnold and S. R. Quake, *Analytical Chemistry*, 2002, **74**, 2451-2457.

13. C. Simonnet and A. Groisman, *Analytical Chemistry*, 2006, **78**, 5653-5663.

14. A. A. Adams, P. I. Okagbare, J. Feng, M. L. Hupert, D. Patterson, J. Gottert, R. L. McCarley, D. Nikitopoulos, M. C. Murphy and S. A. Soper, *J. Am. Chem. Soc.*, 2008, **130**, 8633-8641.

15. U. Dharmasiri, S. K. Njoroge, M. A. Witek, M. G. Adebiyi, J. W. Kamande, M. L. Hupert, F. Barany and S. A. Soper, *Analytical Chemistry*, 2011, **83**, 2301-2309.

16. U. Dharmasiri, S. Balamurugan, A. A. Adams, P. I. Okagbare, A. Obubuafo and S. A. Soper, *Electrophoresis*, 2009, **30**, 3289-3300.

APPENDIX: PERMISSIONS

SPRINGER LICENSE
TERMS AND CONDITIONS

Aug 19, 2011

This is a License Agreement between Hui-Wen Chen ("You") and Springer ("Springer") provided by Copyright Clearance Center ("CCC"). The license consists of your order details, the terms and conditions provided by Springer, and the payment terms and conditions.

All payments must be made in full to CCC. For payment instructions, please see information listed at the bottom of this form.

License Number	2732610608771
License date	Aug 19, 2011
Licensed content publisher	Springer
Licensed content publication	Springer eBook
Licensed content title	Integrated Microfluidic Systems for DNA Analysis
Licensed content author	Samuel K. Njoroge
Licensed content date	May 23, 2011
Type of Use	Thesis/Dissertation
Portion	Full text
Number of copies	1
Author of this Springer article	Yes and you are a contributor of the new work
Order reference number	
Title of your thesis / dissertation	FULLY INTEGRATED MICROSYSTEM FOR BACTERIAL GENOTYPING
Expected completion date	Dec 2011
Estimated size(pages)	200
Total	**0.00 USD**

Terms and Conditions

Introduction

The publisher for this copyrighted material is Springer Science + Business Media. By clicking "accept" in connection with completing this licensing transaction, you agree that the following terms and conditions apply to this transaction (along with the Billing and Payment terms and conditions established by Copyright Clearance Center, Inc. ("CCC"), at the time that you opened your Rightslink account and that are available at any time at http://myaccount.copyright.com).

Limited License

With reference to your request to reprint in your thesis material on which Springer Science and Business Media control the copyright, permission is granted, free of charge, for the use indicated in your enquiry. Licenses are for one-time use only with a maximum distribution equal to the number that you identified in the licensing process.

This License includes use in an electronic form, provided it is password protected or on the university's intranet, destined to microfilming by UMI and University repository. For any other electronic use, please contact Springer at (permissions.dordrecht@springer.com or permissions.heidelberg@springer.com)

The material can only be used for the purpose of defending your thesis, and with a maximum of 100 extra copies in paper. Although Springer holds copyright to the material and is entitled to negotiate on rights, this license is only valid, provided permission is also obtained from the (co) author (address is given with the article/chapter) and provided it concerns original material which does not carry references to other sources (if material in question appears with credit to another source, authorization from that source is required as well). Permission free of charge on this occasion does not prejudice any rights we might have to charge for reproduction of our copyrighted material in the future.

Altering/Modifying Material: Not Permitted
However figures and illustrations may be altered minimally to serve your work. Any other abbreviations, additions, deletions and/or any other alterations shall be made only with prior written authorization of the author(s) and/or Springer Science + Business Media. (Please contact Springer at permissions.dordrecht@springer.com or permissions.heidelberg@springer.com)
Reservation of Rights
Springer Science + Business Media reserves all rights not specifically granted in the combination of (i) the license details provided by you and accepted in the course of this licensing transaction, (ii) these terms and conditions and (iii) CCC's Billing and Payment terms and conditions.
Copyright Notice:
Please include the following copyright citation referencing the publication in which the material was originally published. Where wording is within brackets, please include verbatim.
"With kind permission from Springer Science+Business Media: <book/journal title, chapter/article title, volume, year of publication, page, name(s) of author(s), figure number(s), and any original (first) copyright notice displayed with material>."
Warranties: Springer Science + Business Media makes no representations or warranties with respect to the licensed material.
Indemnity
You hereby indemnify and agree to hold harmless Springer Science + Business Media and CCC, and their respective officers, directors, employees and agents, from and against any and all claims arising out of your use of the licensed material other than as specifically authorized pursuant to this license.
No Transfer of License
This license is personal to you and may not be sublicensed, assigned, or transferred by you to any other person without Springer Science + Business Media's written permission.
No Amendment Except in Writing
This license may not be amended except in a writing signed by both parties (or, in the case of Springer Science + Business Media, by CCC on Springer Science + Business Media's behalf).
Objection to Contrary Terms
Springer Science + Business Media hereby objects to any terms contained in any purchase order, acknowledgment, check endorsement or other writing prepared by you, which terms are inconsistent with these terms and conditions or CCC's Billing and Payment terms and conditions. These terms and conditions, together with CCC's Billing and Payment terms and conditions (which are incorporated herein), comprise the entire agreement between you and Springer Science + Business Media (and CCC) concerning this licensing transaction. In the event of any conflict between your obligations established by these terms and conditions and those established by CCC's Billing and Payment terms and conditions, these terms and conditions shall control.
Jurisdiction
All disputes that may arise in connection with this present License, or the breach thereof, shall be settled exclusively by the country's law in which the work was originally published.
Other terms and conditions:
v1.2

Gratis licenses (referencing $0 in the Total field) are free. Please retain this printable license for your reference. No payment is required.

If you would like to pay for this license now, please remit this license along with your payment made payable to "COPYRIGHT CLEARANCE CENTER" otherwise you will be invoiced within 48 hours of the license date. Payment should be in the form of a check or money order referencing your account number and this invoice number RLNK0. Once you receive your invoice for this order, you may pay your invoice by credit card. Please follow instructions provided at that time.

Make Payment To:
Copyright Clearance Center
Dept 001
P.O. Box 843006
Boston, MA 02284-3006

For suggestions or comments regarding this order, contact Rightslink Customer Support:
customercare@copyright.com **or +1-877-622-5543 (toll free in the US) or +1-978-646-2777.**

VITA

Hui-Wen Chen was born in May of 1976 in Yilan, Taiwan. She graduated with a Bachelor of Science degree in chemistry from Chung Yuang Christian University, Taiwan, in 1998. Following her graduation, she extended her study in analytical chemistry with her advisor Prof. Jyh-Myng Zen and received a Master of Science degree from National of Chung-Hsing University, Taiwan, in 2000. Her graduate thesis dealt with the research of preparation and analytical application of cinder based chemical modified electrode, and the thesis won the 6th Chung Hsing Science Award.

After receiving her master degree, she worked for the Center for Measurement Standards/Industrial Technology Research Institute (CMS/ITRI) in Taiwan, where she served as an associate researcher for both the institute and the National Measurement Laboratory (NML). She was involved in various research projects to establish, maintain and improve national measurement standards in humidity and chemistry and to counsel on transfer of measurement technology to enable the domestic standards to achieve consistency with international standards. During that time, she and coworkers obtained a UK patent in the title of Humidity Sensor Element, Device and Method for Manufacturing Thereof. In the fall of 2006, she started her graduate work at Louisiana State University in Baton Rouge, Louisiana with her advisor Prof. Steven A. Soper. During her doctoral program, the main focus of her research was the development of fully integrated microsystem for bacterial genotyping. She is currently a candidate for the degree of Doctor of Philosophy in analytical chemistry, which will be awarded at the December 2011 commencement.